NTNU – Trondheim
Norwegian University of
Science and Technology

Control and Simulation of a Thruster-Assisted Moored Offshore Vessel in Sea-ice

Ivar Aleksander Gjessing

Master of Science in Engineering and ICT
Submission date: Januar 2015
Supervisor: Roger Skjetne, IMT
Co-supervisor: Øivind K. Kjerstad, IMT
Hans-Martin Heyn, IMT

Norwegian University of Science and Technology
Department of Marine Technology

NTNU Trondheim
Norwegian University of Science and Technology
Department of Marine Technology

PROJECT DESCRIPTION SHEET

Name of the candidate: Ivar Gjessing

Field of study: Marine control engineering

Thesis title (Norwegian): Regulering og simulering av eit thruster-assistert forankra fartøy i sjøis.

Thesis title (English): Control and simulation of a thruster-assisted moored offshore vessel in sea-ice.

Background

The Norwegian offshore industry is experiencing an increased demand for integrated offshore operations in Arctic ice-covered waters. Such operations are technically and physically more challenging than conventional open-water operations due to low temperatures, remoteness, darkness, and the presence of sea ice and icebergs, which raises many interesting research questions. Stationkeeping operations by position mooring (PM) or dynamic positioning (DP) are challenging since ice forces are much larger and rapidly varying compared to conventional open-water environmental forces.

In this project the focus is on control and simulation of a thruster-assisted position mooring (TAPM) vessel in sea-ice. Open water TAPM control modes such as heading control, surge-sway damping, and setpoint chasing positioning strategies shall be considered for operation in drifting sea-ice. One problem in sea-ice is that ice loads are very large and rapidly varying. Hence, conventional integral action for open water, which often has a convergence time of 20 minutes or more, is not applicable for the rapid correction needed to compensate ice loads. Newly developed methods that use hybrid control theory to reset the integral state during steps in the external bias forces will therefore be investigated in this project.

Work description

1. Perform a literature review to provide background and relevant references on:
   - Sea-ice statistics and ice types for relevant Arctic geographic locations.
   - DP and TAPM control systems for open water and for operations in sea-ice.
   - Ice management systems for stationkeeping operations in ice infested areas.
   - Ice-structure simulators for floating vessels in sea-ice.
   - Hybrid control methods related to resetting of estimated states or integral state.

   Write a list with abbreviations and definitions of terms and concepts, explaining relevant concepts related arctic offshore stationkeeping operations.
2. Develop a low-fidelity design model and a high-fidelity simulation model of the mooring system with connection to the vessel through a rotatable turret.
3. Implement the simulation model for the NTNU Numerical Ice Tank simulator. Consider to improve the online signal trending functionality, and other relevant functionality, of the simulator to enhance its run-time user friendliness.
4. Propose and present a control law from relevant literature for heading control, surge-sway damping, and setpoint chasing for open water. Implement the control law in your simulator and test its performance in relevant scenarios and environmental conditions.
5. Analyze and explain the setpoint chasing guidance strategy for open water, and investigate and discuss the basic stability properties of the closed-loop system. Incorporate the setpoint chasing method for TAPM in drifting sea-ice, implement it into your simulator, and discuss its performance in various test scenarios.
6. Propose a set of simulation scenarios for your Arctic TAPM control system. Test your simulation model for these scenarios, and present the results in a systematic and well-arranged manner.

Tentatively:

7. Develop a hybrid observer for the TAPM control system with resetting of its state estimates to better handle steps in ice loads. Implement it together with a TAPM control law to control the heading and position of the vessel in drifting sea-ice. Simulate and analyze the performance.

Guidelines

The scope of work may prove to be larger than initially anticipated. By the approval from the supervisor, described topics may be deleted or reduced in extent without consequences with regard to grading.

The candidate shall present his personal contribution to the resolution of problems within the scope of work. Theories and conclusions should be based on mathematical derivations and logic reasoning identifying the various steps in the deduction.

The report shall be organized in a rational manner to give a clear exposition of results, assessments, and conclusions. The text should be brief and to the point, with a clear language. The report shall be written in English (preferably US) and contain the following elements: Abstract, acknowledgements, table of contents, main body, conclusions with recommendations for further work, list of symbols and acronyms, references, and optional appendices. All figures, tables, and equations shall be numerated. The original contribution of the candidate and material taken from other sources shall be clearly identified. Work from other sources shall be properly acknowledged using quotations and a Harvard citation style (preferably the *natbib* Latex package). The work is expected to be conducted in an honest and ethical manner, without any sort of plagiarism and misconduct. Such practice is taken very seriously by the university and will have consequences. NTNU can use the results freely in research and teaching by proper referencing, unless otherwise agreed upon.

The thesis shall be submitted with two printed and electronic copies to 1) the main supervisor and 2) the archive, each copy signed by the candidate. The final revised version of this thesis description must be included. The report must appear in a bound volume or a binder according to the NTNU standard template. Computer code and a PDF version of the report shall be included electronically.

Start date:	1 September, 2014	**Due date:**	As specified by the administration.

Supervisor: Professor Roger Skjetne
Co-advisors: PhD cand. Øivind K. Kjerstad
PhD cand. Hans-Martin Heyn

Trondheim, 15.01.2015

Roger Skjetne
Supervisor

Sammendrag

Utforskingen av nordlige havområder gir stadig mulighet for nye og interessante forskningsområder i forhold til å tilpasse allerede eksisterende teknologi til å takle de harde omgivelsene i nord. Mørke, kulde, hardt vær, lang avstand til sivilisasjonen og ikke minst islagt hav og drivende isfjell sørger for at konvensjonelt utstyr til bruk på sørlige breddegrader ikke kan brukes. Islaster er sterkt forskjellige fra belastninger på åpent vann, i tillegg til at de tøffe omgivelsene og avstanden til folk stiller enda større krav til sikkerhet.

Arktiske forhold er vanskelige å gjenskape andre steder blant annet grunnet den store uforutsigbarheten og de store variasjonene det innebærer. Å transportere utstyr til Arktis og foreta undersøkelser og forsøk der er både tidkrevende og dyrt. Det er mulig å gjenskape isforhold i modellbasseng, men det tar en del tid og innsats i forhold til forsøk med åpent vann.

Dette er motivasjonen for å ta i bruk numeriske datasimuleringer. Denne oppgaven vil gå nærmere inn på egenskapene til den numeriske istank-simulatoren (Numerical Ice Tank, NIT) utviklet ved NTNU for å implementere en simuleringsmodell for et turret-ankringssystem i denne. En ankersystem-modell basert på elementmetoden vil bli implementert og testet i istank-simulatoren. Kontrollstrategier i forhold til tilpasning av eksisterende systemer til islagte områder vil bli omtalt og testet i simulatoren.

Det vil også bli gjennomgått teoretisk bakgrunnsstoff rundt dynamisk posisionering, position mooring, kontrolldesig, arktiske forhold og matematisk modellering.

Abstract

The exploration of the northern seas is constantly raising new and interesting research topics in order to adapt our technology to handle this extraordinary harsh climate. Darkness, remoteness, cold and harsh weather, and not at least, drifting ice and icebergs, are making the conventional equipment used further south useless. The ice loads are largely different from open water sea loads, while remoteness and the harsh environment makes safety an even more important issue.

The Arctic conditions are difficult to recreate due to the unpredictability and large variations in ice features, and going up there with all the needed equipment is particularly expensive. It is possible to create realistic ice features in a model basin, but it takes time and effort compared to open water.

This is why a numerical computer simulator is an attractive option. This thesis is investigating the properties of the Numerical Ice Tank (NIT) simulator developed at NTNU in order to implement a high fidelity turret mooring model into it. A finite element based mooring model is implemented and tested in the NIT. Controller strategies for adaption into ice infested areas are discussed and tested in the simulator.

A theoretical background on dynamic positioning (DP), position mooring (PM), controller design, arctic conditions and mathematical modelling is provided.

Acknowledgements

This masters thesis is marking the end of several good years in Trondheim and at NTNU.

First of all I want to thank my supervisor, Roger Skjetne, for providing me with the help and support I needed, and for the S-function template that worked well for implementing the mooring cable FEM model in Simulink. I want to thank my co-advisors, Øivind Kjerstad and Hans-Martin Heyn for being supportive when I needed it. Special thanks to Øivind Kjerstad for helping me troubleshooting the simulator software and reviewing my thesis.

Finally I want to thank my family for long distance support, my coffee mug for short distance support, my flatmates for taking out the garbage, Trekassa for doing all the simulations, the guys at my office for keeping quiet, Trondheim Kommune for providing slippery roads for biking, Accenture for waiting, Trondheim Parkering for taking care of my finances and Samfundet for taking care of the rest.

January 25, 2015

Ivar A. Gjessing

Table of Contents

List of Tables

List of Figures

List of Symbols and Acronyms

A_{thr}	Thruster dynamics time constants matrix
AUV	Autonomous Underwater Vehicle
$\boldsymbol{b}$	Bias vector in NED frame
C++	Programming language
$\boldsymbol{C}_A(\boldsymbol{\nu})$	Added mass Coriolis and centripetal force matrix
$\boldsymbol{C}_{RB}(\boldsymbol{\nu})$	Rigid body Coriolis and centripetal force matrix
COT	Center of Turret
d_{moor}	Linear damping coefficient
$\boldsymbol{D}(\boldsymbol{\nu})$	Damping force matrix
$\boldsymbol{D}$	Linear damping force matrix
$\boldsymbol{D}_{moor}$	Linear mooring damping force matrix
$\boldsymbol{D}_{tot}$	Linear total damping force matrix, including mooring
DOF	Degrees of Freedom
DP	Dynamic Positioning
DYPIC	Dynamic Positioning in Ice (project)
$\boldsymbol{E}_b$	Input noise scaling matrix
FEM	Finite Element Modelling
$\boldsymbol{G}(\boldsymbol{\eta})$	Restoring force matrix
HF	High frequency
$\boldsymbol{H}_m(s)$	Acceleration control transfer function
$\boldsymbol{K}$	Linear mooring force matrix
k_{moor}	Linear mooring coefficient
$\boldsymbol{K}_d$	Derivative control gain matrix
$\boldsymbol{K}_i$	Integral control gain matrix
$\boldsymbol{K}_m$	Acceleration control gain matrix
$\boldsymbol{K}_p$	Proportional control gain matrix
l_t	Distance from center of turret to vessel mass center
LF	Low frequency
$\boldsymbol{M}_A$	Added mass matrix
$\boldsymbol{M}_{RB}$	Rigid body mass matrix
$\boldsymbol{M}$	Combined mass matrix

MSS	Marine Systems Simulator - Matlab/Simulink library
NED	North-East-Down reference frame
NIT	Numerical Ice Tank
NTNU	The Norwegian University of Science and Technology
PID	Proportional-Integrator-Derivative (controller)
PM	Position Mooring
p	Angular velocity about the x axis (Roll)
q	Angular velocity about the y axis (Pitch)
r	Angular velocity about the z axis (Yaw)
r_t	Moment generated in mooring turret
$\boldsymbol{R}(\boldsymbol{\eta})$	Rotation matrix
SAR	Synthetic Aperture Radar
t_M	Model scale time
t_S	Full scale time
TAPM	Thruster Assisted Position Mooring
$\boldsymbol{T}_b$	Bias time constant matrix
T_n	Natural period
u	Velocity in surge
v	Velocity in sway
V_M	Model scale velocity
V_S	Full scale velocity
VIV	Vortex Induced Vibrations
w	Velocity in heave
WF	Wave frequency
$\boldsymbol{w}_b$	White noise vector
XML	Extensible Markup Language - standard for structured data storage
x	Position in x (north) direction
X_t	Surge force from turret
y	Position in y (east) direction
Y_t	Sway force from turret
z	Position in z (down) direction
Z_t	Heave force from turret
$\boldsymbol{\eta}$	Vessel position in NED frame
$\boldsymbol{\eta}_r$	Setpoint position in NED frame
$\boldsymbol{\eta}_t$	Turret position in NED frame

λ	Scaling factor
θ	Pitch angle; angle about the y axis
$\boldsymbol{\nu}$	Vessel velocities in body frame
$\boldsymbol{\nu}_r$	Relative (to surrounding water) vessel velocities in body frame
$\boldsymbol{\tau}_c$	Commanded thrust
$\boldsymbol{\tau}_{ice}$	Ice forces
$\boldsymbol{\tau}_{moor}$	Mooring forces
$\boldsymbol{\tau}_{thr}$	Thruster forces
$\boldsymbol{\tau}_{waves}$	Wave forces
$\boldsymbol{\tau}_{wind}$	Wind forces
$\boldsymbol{\tau}_{PID}$	PID controller force output
ϕ	Roll angle; angle about the x axis
ψ	Yaw angle; angle about the z axis
ω_n	Natural frequency

Chapter 1

Introduction

1.1 Background

1.1.1 Offshore Operations and Station Keeping

When discussing offshore operations, it is usually thought of as the various tasks related to oil production and exploration taking place at sea. However, there are a lot of other tasks to be done at sea, including rescue operations, research work, pipelaying or fishing. Oil production is probably one of the more technologically advanced and challenging operations at sea, which is why this is where most of the development and research is taking place.

A combination of the need of a large amount of big and heavy machinery, the distances it has to be moved, and the need to keep it out there for an extended period of time is creating challenges. The large variety of conditions these tasks must be performed in when it comes to variations in depth, variations in duration of the mission, and weather conditions are creating a need to develop a large variety of solutions to fill the need.

Depending on the type of operation, a structure might need to stay at the same place at sea for everything from shorter day missions, a few months of exploration to a several year long production period (Faÿ, 1990).

For long lasting operations on relatively small water depths a common solution is to build a solid structure standing on the seabed, like a jacket structure. This will keep the platform steady without any energy consumption, but it is less flexible and requires more time to get in place.

For larger water depths it is necessary to have a floating structure. This is also an advantage in general during shorter lasting operations due to the less

amount of effort needed to get it in place. These can be kept in place by the use of anchors and mooring lines. The drawback of this solution is the vulnerability when it comes to waves and other periodical loads on the structure, leading to potentially large oscillations due to the spring effect from the mooring lines and the relatively low damping of the system.

By introducing a control system and thrusters, the vessel can be kept in place automatically while active damping can be used in order to prevent large oscillations. This led to the introduction of dynamic positioning (DP), making it possible to stay in place without any time consuming external installations, and with no need of seabed installations. This was first implemented on the ship *Cuss 1* in California in 1961, with manual control of the thrusters. But already later the same year another ship was equipped with automatic thruster control (Faÿ, 1990).

Dynamic positioning can be defined as the following, according to Faÿ (1990):

A process involving the actions of thrusters which, commanded by a controller and opposing the environmental forces, maintain a ship or any floating vessel in the vicinity of a reference point and stabilize its heading. The position is known at all times from the data transmitted by a position reference system.

1.1.2 Dynamic Positioning and Position Mooring Systems

Mooring Solutions

A mooring system refers to a set of mooring lines connecting a floating vessel to the seabed in order to keep it in position (Faÿ, 1990). Traditionally, anchoring of a ship consists of a single mooring line connecting the ship to the seabed. This solution is not optimal since the ship is free to move around the anchor point, and will oscillate in yaw when subject to winds and current.

A better solution is spread mooring, when several anchor lines are connected to different sides of the ship. This makes the ship stay in the same direction, but on the other hand it is not very flexible when it comes to for instance change of heading.

A useful and common solution for position mooring (PM) systems is turret mooring. All mooring lines meet in what is called a turret, located inside or outside the hull (see Figure 1.1). It is most common to position the turret somewhere within the front half of the ship. The lines are then spread in all directions (see Figure 1.2), providing similar restoring behavior in surge and sway. The turret is usually free to rotate, making the vessel able to change yaw angle. This is particularly useful for ships, since they have very different properties for handling

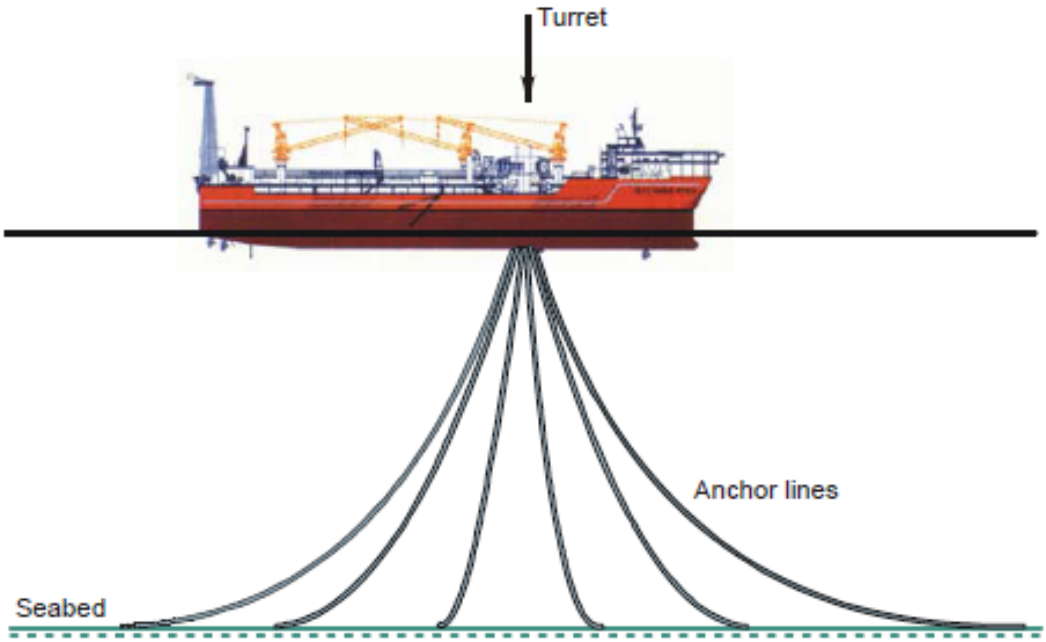

Figure 1.1: Turret moored vessel. From Sørensen (2012).

environmental loads depending on which directions they come from. Being able to turn the ship in order to minimize forces, referred to as weathervaning, is therefore an advantage. This is made possible by using turret mooring (Fossen, 2011).

Mooring systems for position keeping were first used in offshore operations in 1953 outside the California coastline (Faÿ, 1990). A challenge when using mooring is that the elasticity of the mooring system creates a mass-spring-system with natural frequencies not far from the loads a vessel at sea can be exposed to. This combined with the relatively low hydrodynamical damping of the mooring lines can lead to large, low frequency oscillations.

This, combined with the water depth limitations of a mooring system, motivated the idea of replacing the passive mooring with active compensation by a thruster system (Faÿ, 1990). However, since this requires a large amount of energy, the conventional mooring systems still has some advantages. The idea behind thruster-assisted position mooring (TAPM) systems is to combine the advantages from both worlds by having the mooring system taking the mean loads while the thrusters contribute to improve the performance of the system beyond what the mooring system is capable of. More on this in the next section.

For more on mooring systems, see for instance Strand et al. (1998).

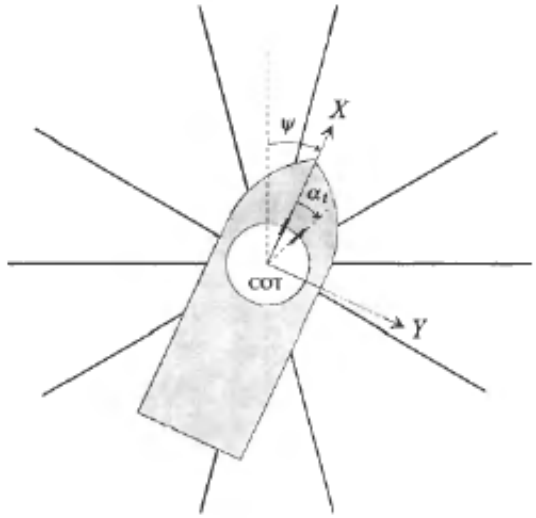

Figure 1.2: The mooring lines are spread out in every direction from the turret. From Strand et al. (1998).

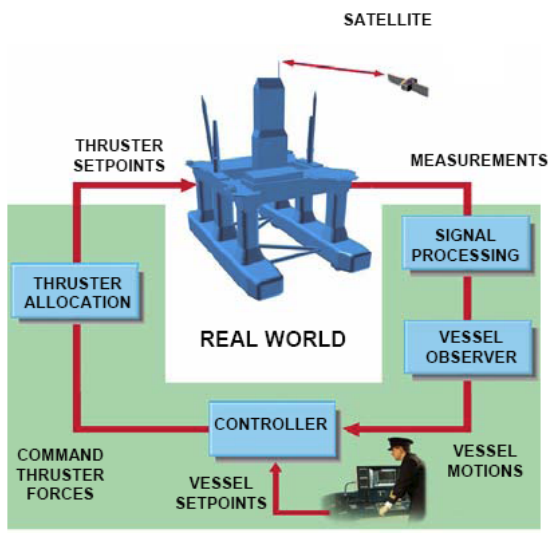

Figure 1.3: The structure of a DP system control architecture. From Sørensen (2012).

DP and PM Control Systems

A DP or PM system relies on a large system of components in order to work. The core of the system is the controller, generating a desired thrust vector given the various input it is provided. The most vital controller input is the vessel position and heading, but in most cases it also takes a variety of other inputs in order to improve performance, like velocities, wind measurements, accelerometer

data and gyroscope readings. The desired thrust is then provided to a thrust allocation system, converting it into separate thrust commands to each thruster. The thrusters then have their own control system, making sure the right power is applied to the thruster. The power system then has to be able to generate the required power.

In order to achieve a good estimate of the its position the vessel is equipped with a number of position reference systems, depending on the DP class requirement, meaning the level of security needed. These reference systems is then evaluated in order to find the most accurate position estimate.

Due to sensor noise and other factors causing inaccuracy, it is necessary to filter the signals in order to get a smooth position reference to provide to the controller. This is ensured by an observer, which can be for instance a Kalman filter or a nonlinear passive observer (Fossen, 2011).

If provided with accelerometer or wind measurements, the controller can take advantage of these by applying them as feed forward terms, meaning it can predict future position offsets by knowing something about the forces acting on the vessel at the present time. These techniques are however limited by inaccuracy and sensor disturbances, especially the wind sensors which are not known for being terribly accurate, much due to the significant local variations of the wind.

In addition to the filtered sensor measurements the controller is provided with a reference position from the DP operator. This is the desired position for the vessel, meaning the position the controller is supposed to keep the vessel as close as possible to.

The architecture of DP systems is shown in Figure 1.3.

For PM systems the position is determined by the mooring, and the control objectives can be a bit different. For more on that, keep reading.

For more on marine control systems design, see for instance Sørensen (2012), Fossen (2011) or Fossen (2002).

Control Objectives

For a DP system, the main objective is to keep the ship within a certain radius of a fixed point. This might be in order to prevent breaking of risers and other drilling equipment, stay close to where an operation is performed, for instance lifting operations, or just to prevent from drifting away when idling. Depending on the kind of operations different security requirements is present, as well as different control objectives.

Apart from staying in place, it is desired to use the control system to provide additional damping forces. This could compensate for low frequency wave loads, oscillations due to wind, etc.

For PM systems, the damping action is a primary part of the control system functionality. Here, the mooring system will take the mean loads in surge and sway. The behavior of the mooring system is similar to a spring, and this can therefore be considered as a proportional controller. There might therefore be a need for a derivative term, which can be provided by the control system.

In addition to this, the control system will in most cases be used to control heading, since stiffness in yaw is usually not provided by the mooring system. This is useful for instance when the operation requires the vessel to stay in the same direction, or just to prevent unnecessary accelerations back and forth in yaw. It can also be used for keeping an optimal heading angle with respect to weather forces. Especially for ships there will be a significant difference in resulting forces from wind and current depending on which direction it is acting from. The stresses on the mooring system can therefore be reduced by keeping the optimal angle for handling the weather.

Another useful feature for a PM system is line-break detection and compensation. This refers to using the thrusters to prevent further damage in the case of one of the mooring lines breaking. Sensors on the mooring system can detect if one line breaks, and when this information is sent to the control system the thrusters can be activated immediately to generate force in the right direction. In this way another line-break may be prevented, the position will be kept and the operation can be aborted in a safe and controlled manner. Line break can also be prevented by using the thrusters to compensate when the mooring line stresses become too high in the case of extreme conditions.

The most common control objectives for a TAPM system can be summarized as:

- Damping action (surge and sway)
- Heading control
- Line-break compensation
- Line-break prevention

1.1.3 Control Plant Model and Process Plant Model

In control theory there are two common ways of modelling a dynamic system, depending on what the model is used for.

The goal of the process plant model is to describe the system dynamics as accurately as possible. This would include different nonlinear phenomena, disturbances and sensor noise. This model is used for numerical simulations and stability- and performance analysis as an alternative to physical model tests (Nguyen and Sørensen, 2009a).

In order to create a good description of how a dynamic system behaves under any condition, it is in most cases necessary to develop a relatively large and complex model. There are most likely several nonlinear phenomena that needs to be considered, and a lot of complicated, computationally intensive equations.

A process plant model is therefore not suited for real time running or analytical calculations, meaning it can not be used as part of controller design. This is where a control planet model is used, which is a simplified version of the process plant model. It is less computationally intensive, and is easier to work with both numerically and analytically (Sørensen, 2012).

1.1.4 The Motivation for Going Further North

Due to an increasing demand for oil in the world lately, it is of high interest for the oil companies to investigate the possibilities of going further north than before to look for petroleum resources.

However, the oil price has been reduced lately from 115 dollars per barrel last summer to around 50 dollars per barrel (oil-price.net, 2015), which is currently making oil production in the Arctic less likely to be cost effective. This is pointed out in Teknisk Ukeblad (2015), stating that the oil price must be at least around 70 dollars per barrel in order to make oil production in the Barents sea cost-efficient.

Still it is not unlikely that it will rise again later, making Arctic oil operations worth the cost. Also, the amount of ice in the Arctic has been reducing during the previous years, meaning the conditions for offshore operations might be more attractive in the future.

Since the need of going further north is likely to increase in the future, it is of high interest to investigate the possibilities and limitations of northern areas in order to develop robust systems that can handle these conditions in a safe manner.

1.1.5 The Arctic Environment

Ice Conditions and Types

The challenges of operating in Arctic conditions are many. Cold temperatures, harsh weather, remote locations and lack of daylight during winter are some of them. The probably most significant of them all when it comes to station keeping are sea ice and icebergs, causing large and unpredictable forces on the structures, and sometimes forcing abortion of operations.

Ice in the Arctic areas can occur in a wide range of different forms, depending on the area, weather conditions, climate, time of year and a large amount of other factors. Understanding what types of ice that is likely to interact with a vessel, and which properties that are connected to which type can help us estimating the behavior of the forces on the vessel.

These are some of the most relevant terms regarding the description and definition of different ice properties, as covered in Bushuyev (year unknown).

Ice types

Age The properties of ice is largely depending on if the ice is newly created or if it has been frozen for several years. The following list states the main categories of ice age.

- **New ice:** Ice which has just been formed. This is again divided into subcategories depending on the age and how it is made. Some of these are frazil ice, which is thin plates of new ice, and slush, which is floating snow soon to become ice.
- **Nilas:** A thin, elastic ice crust up to ten centimeters thick. Its thickness can be determined by the color; dark nilas is thinner.
- **Young ice:** Older than nilas and less elastic. Breaks due to swell.
- **First-year ice:** Next stage after young ice. Not more than one winter old.
- **Old ice:** Ice that has survived at least one summer. It is divided into residual first-year ice, second year ice and multi-year ice.

Origin Ice can be categorized from the location where it was formed. The ice properties can for instance change significantly depending on if the ice consists of freshwater or saltwater.

- **Sea ice:** Ice formed from sea water. This is (naturally) the most common type of floating ice at sea.

- **Ice of land origin:** Ice formed on land which has eventually ended up in the sea. This could for instance be icebergs that was earlier a part of a glacier.

- **River and lake ice:** Ice formed at a lake or river, then transported into the sea.

Stages of melting Depending on how the ice is melting it can take several different forms which can have largely varying properties. Below are some terms related to melting.

- **Puddle:** An accumulation of water on ice due to melting of snow and ice from above.

- **Flooded ice:** Sea ice flooded with water, either due to melting or because of a river floating onto it.

- **Thaw holes:** Vertical holes in sea ice. Formed by puddles which has melted its way through the ice.

- **Dried ice:** Occurs when water disappears from flooded ice. It can happen due to draining through thaw holes or when the ice cracks.

- **Rotten ice:** Late state of melting.

Types of ice areas

- **Bergy water:** A large area where icebergs are floating, but the area is still navigable. It does not have a clearly defined boundary.

- **Level ice:** Flat sea ice that has not been subject to any deformation.

- **Deformed ice:** Ice that has been deformed due to interactions with the surrounding ice.

- **Snow-covered ice.**

- **Bare ice.** Ice without snow on it.

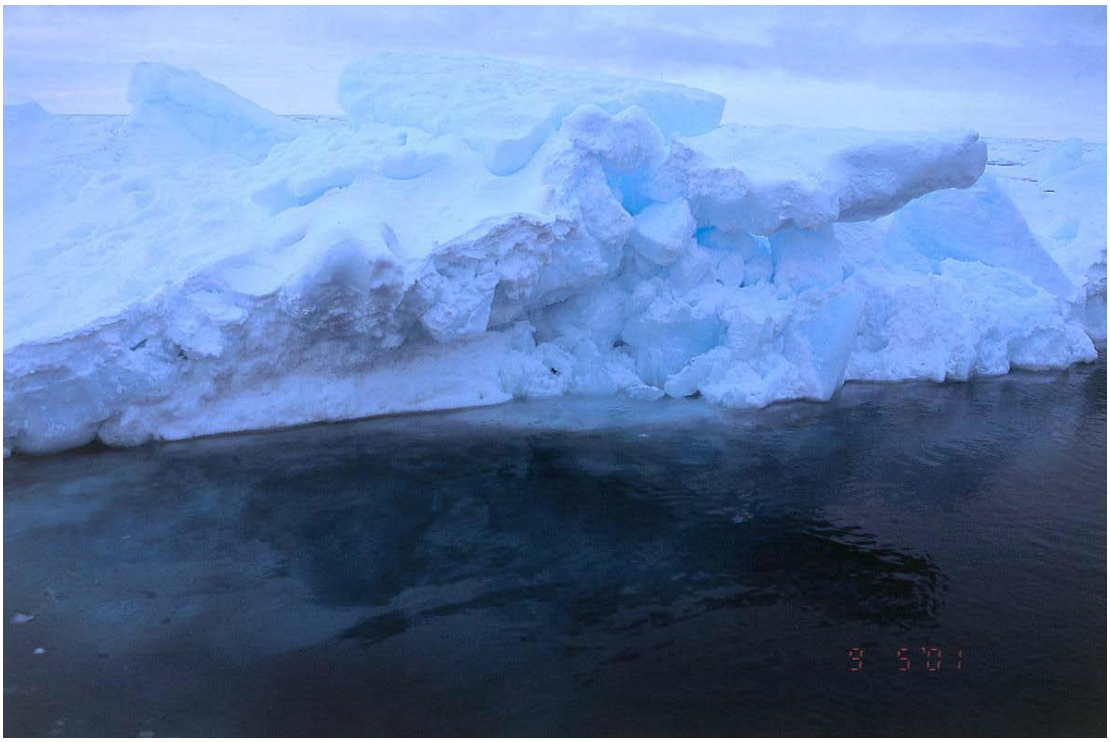

Figure 1.4: Ice ridge. From Løset

Other terms

- **Ridge:** A thick accumulation of ice occurring due to pressure in the boundary between different ice floes or in cracks. See Figure 1.4. Can be challenging for ships to pass through.
- **Ram:** A part of an iceberg or ice wall sticking out under water. Can be especially dangerous since it is difficult to see.
- **Fast ice:** Solid ice connected to the shore or to an ice wall.
- **Pack ice:** Any type of ice, except fast ice and grounded ice, in other words ice that is able to drift.
- **Floe:** A general term for any kind of relatively flat piece of ice. Have a horizontal size from 20 meters and up.

Icebergs Icebergs are causing a large threat on structures in Arctic areas. An iceberg colliding into an operating vessel can be fatal, and must be avoided, either by moving the vessel away from the iceberg or by towing the iceberg away from

the vessel. When performing station keeping operations the option of moving the vessel can be expensive and should be avoided.

The large variation of iceberg sizes, shapes, as well as the unpredictability of their motions makes iceberg management a challenging task.

See Figure 1.5 for a size comparison of the different icebergs.

Sea Ice and Iceberg Statistics

Compared to other seas in the Arctic areas the Barents sea has a relatively low percentage of ice covering. At most the ice is only covering between 55 and 60 percent of the surface area (International Organization for Standardization, 2010). This occurs during the spring and late winter; around March to April.

The ice thickness varies from 1,5 to 3 meters, depending on whether it is first-year or multi-year ice. The latter is thicker, and occurs mostly at the east coast of the Svalbard Archipelago and Franz Josef Land (International Organization for Standardization, 2010).

Icebergs can occur all year, frequency ranging from 10 to 40 per year, mass up to 10 000 000 tonnes. They originate from the glaciers of Svalbard, Franz Josef Land and Novaya Zemlya (International Organization for Standardization, 2010).

Standards Norway (2007) provides some data on the risks of colliding with an iceberg, as shown in Figure 1.6. By the Norwegian coastline there are almost no risk of encountering an iceberg, while the closer it gets towards Svalbard, the higher the risk of icebergs.

While icebergs might be floating around during all times of year, sea ice is naturally a greater challenge during winter and spring than in the summer and fall. As can be seen from Figure 1.7, the sea ice is almost surrounding Svalbard at winter times, while in summer it retracts leaving open water also north of Svalbard. This means ice management in the form of ice breakers is necessary when going far enough north.

During winter the ice pressure can be strong, creating ridges ranging up to 5 meters above sea, and up to 20 meters keel depth. This is naturally a challenge to arctic offshore operations. It is most commonly observed in the northwestern and southeastern areas due to onshore drifting of the ice (International Organization for Standardization, 2010).

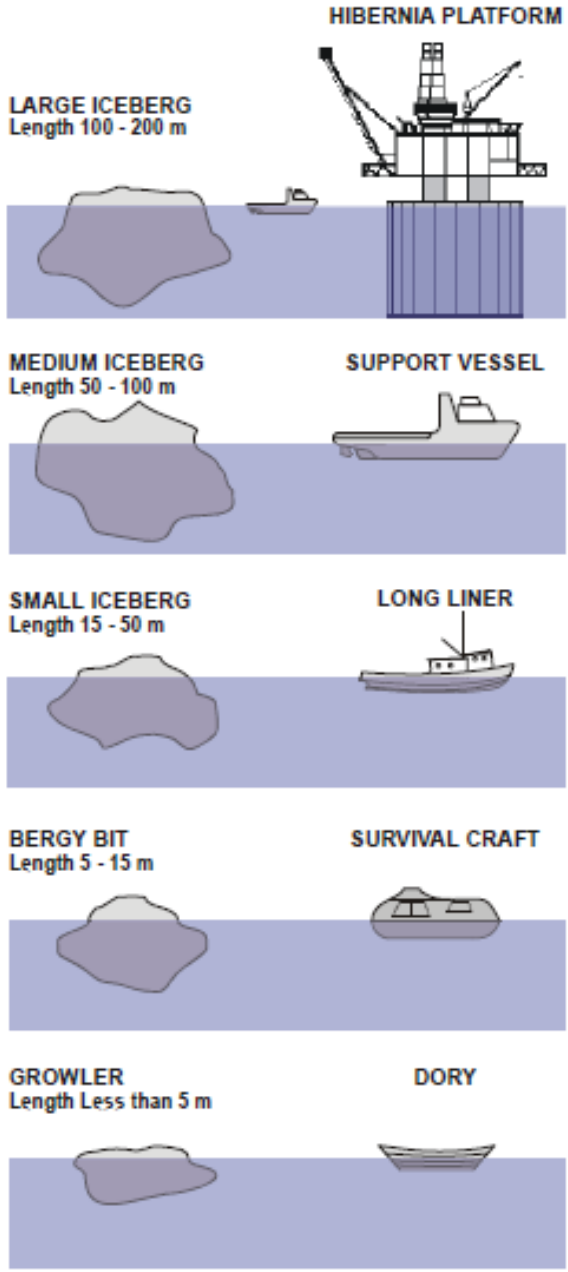

Figure 1.5: Comparison of iceberg sizes. From McClintock et al. (2007)

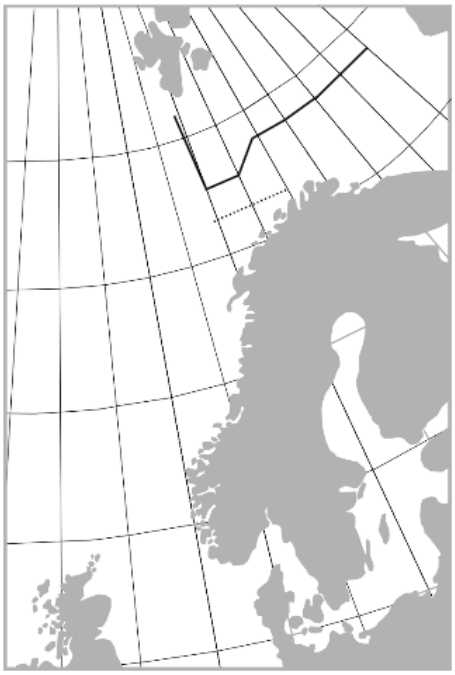

Figure 1.6: Lines showing the 1000 year (dotted line) and 100 year (solid) collision risk limits in the Barents Sea area. From Orsten (2013) and Standards Norway (2007).

Vessel-Ice Interactions

When a vessel runs into a piece of level ice, it will go through different stages of breaking the ice. At the initial contact phase the ice will smash against the ship hull. The edge of the ice will be crushed into pieces, before the ice floe starts deflecting due to being pressed down by the hull. The generated moment will then result in the floe breaking at some distance away from the crushing zone. The broken floe will then begin rotating down under the hull, then being pushed down, giving the remaining part of the ice room for moving into the hull. It then starts over with the same procedure. (Løset)

These different stages each generate different forces on the hull. At the first initial contact there will be a sudden force that starts acting on the vessel. Then the deflection bending force will start gradually, before it suddenly disappears at the moment the floe breaks. This is when the force needed to rotate and submerge the floe takes over, before the hull will hit the remaining ice floe and the process repeats. This means that when moving through ice, or while standing still in a moving ice field, there will be a variable load with a certain frequency. (Løset)

So there is a combination of different effects from viscous drag, material deformation, buoyancy and acceleration that causes the total impact from the ice

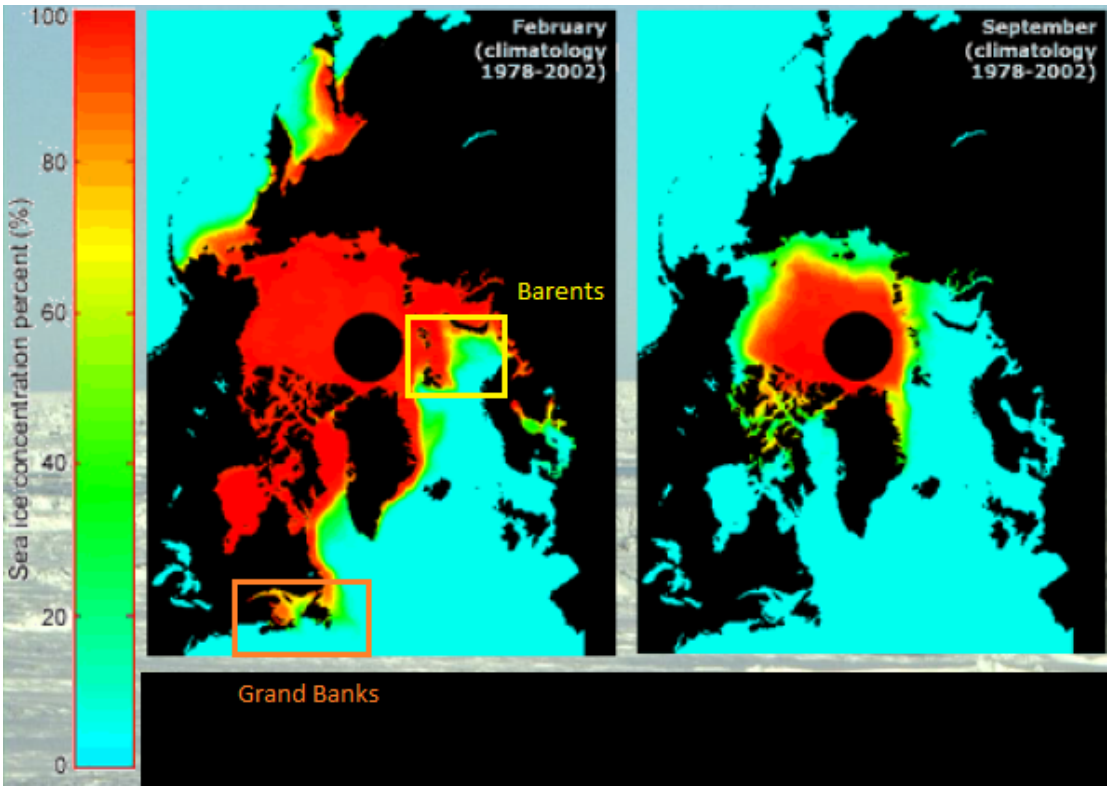

Figure 1.7: Sea ice concentration in Arctic areas. From Orsten (2013).

floe onto the vessel. The process is illustrated in Figure 1.8.

This is one of the reasons why ice loads are so rapidly varying and unpredictable. When it comes to managed ice, consisting of various pieces of randomly shaped and sized ice floes, there is another phenomena causing these sudden force fluctuations. When the vessel hits an ice floe and starts pushing it forward, it will eventually hit other ice floes, putting them into motion. As this continues, a chain reaction of ice floes pushing on each other is taking place. As new ice floes gets in contact, and other contact chains break apart, the load is changing unpredictably. This phenomenon of force interaction is referred to as *ice floe contact networks* (Kjerstad et al., 2014).

During ice tank tests in the DYPIC (DYnamic Positioning in ICe) project, which will be further described in Section 1.1.7, this phenomenon occurred. This is illustrated in Figure 1.9, which has a colored overlay showing ice floe contact networks identified by studying video material of the model test (Kjerstad et al., 2014).

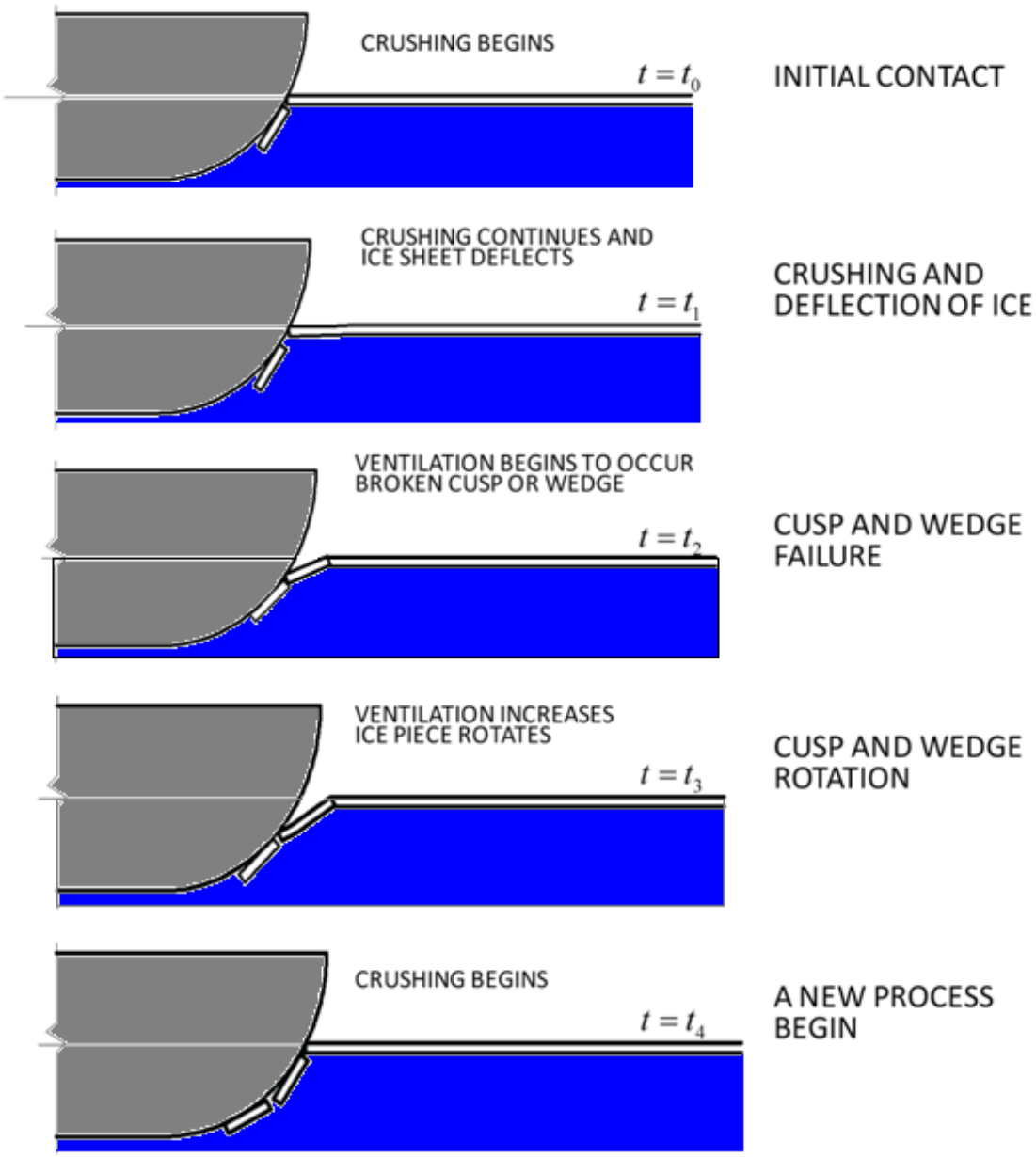

Figure 1.8: Interaction between a ship and level ice. Modified from Løset

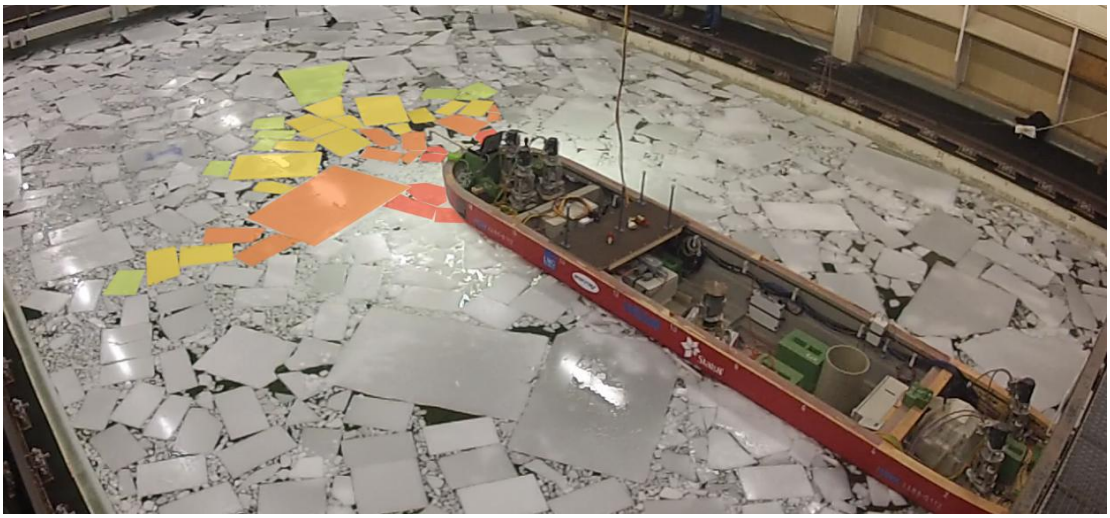

Figure 1.9: An ice floe contact network, identified by video material from the ice tank model test. Colored overlay is showing the movement of the ice floes. From Kjerstad et al. (2014)

1.1.6 DP and PM Operations in Ice Infested Areas

Ice Management

Ice management refers to the way of handling the incoming ice when operating in ice infested areas. The operating vessel or construction will usually not be able to persist the incoming ice by itself, making the operation impossible without finding a way to deal with the surrounding ice conditions. Ships in transit have the ability of navigating around icebergs. In this case ice detection is therefore the main challenge. For DP and PM operations on the other hand, ice drifting into the operation is proposing a threat. It is therefore important to being able to manage the ice in a way so that the operation can continue safely, in addition to detecting the severeness of the incoming ice and thus the importance of applying ice management. In short, ice management is transforming the natural ice conditions into something the operating vessel can handle within it positioning requirement and capabilities.

This is most commonly done by using ice breaking ships of different sizes to break the ice into pieces small enough to be handled by the operating vessel or floating construction of interest. This process is done stepwise. First an ice breaker drives through the ice breaking it into separate large ice fields. Then another ice breaker makes smaller fields out of the large ones. This is repeated until the final result is pieces of ice small enough for the operation to handle.

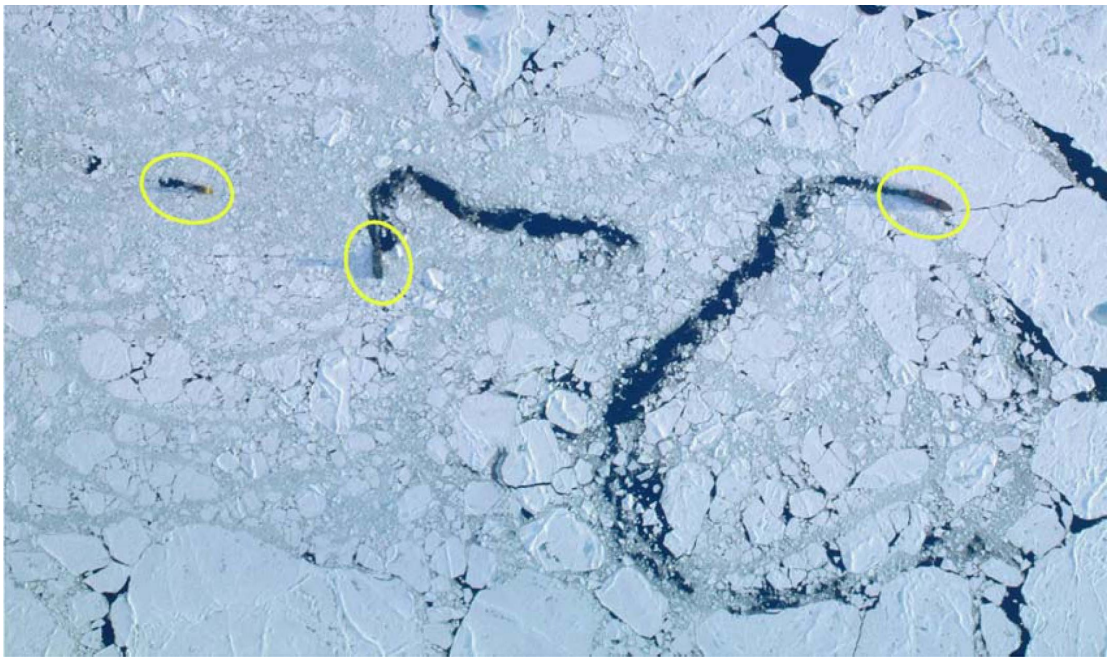

Figure 1.10: Ice management. It is seen how the ice breakers are breaking the ice into smaller pieces. The ships are marked with yellow circles. The DP vessel is to the left, and the two others are ice breakers. From Moran et al. (2006).

The first drilling operation in arctic ice using ice management was organized by the Swedish Polar Research Secretariat, as described in Keinonen et al. (2006). Two icebreakers were used to prevent too large ice features hitting the drilling ship. Figure 1.10 shows a photo of this operation.

Icebergs represent a greater challenge for Arctic operations. They can not be broken apart by ice breakers and must be handled differently based on their sizes and shapes. In the case of an incoming iceberg, the previously described procedure is therefore not an option. The most common way of handling icebergs is by towing them away to a safe distance.

See Keinonen et al. (2006) or Moran et al. (2006) for more on ice management.

The Unpredictability of Ice

One thing is how to manage the incoming ice by crushing it into smaller pieces, but more importantly; how do we know in which direction we need to take actions and how massive the ice is? Since most of the ice masses is located below the water surface it can be hard to see from above how thick the ice floes are, how the ice is varying in thickness, and which shapes and sizes the icebergs have. In addition

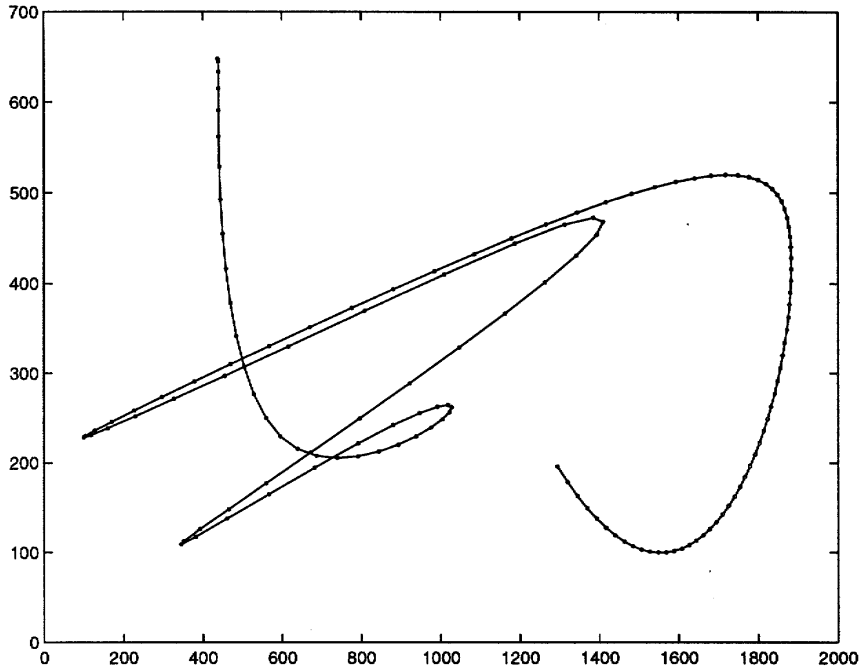

Figure 1.11: Example of ice drift pattern, from the Pechora Sea. From Løset and Onshuus (1999).

to this the currents and winds in the Arctic areas may change very rapidly, and ice areas can move due to not only the present conditions, but also due to forces from the surrounding ice fields.

Ice Detection

The traditional and probably most common method of detecting ice is by visual observation. This will work in many cases for getting a rough estimate on the conditions; it will probably reveal the most critical threats like icebergs. A major weakness of this approach is weather dependencies and risk of none detection of hazard. Fog and heavy snow will make it near impossible to see anything at all. Therefore there might be necessary to use other methods like radar detection from marine vessels or aircraft, satellite surveillance or detection from underwater vessels like AUVs (Orsten, 2013).

It can often be difficult recognizing an iceberg when it is located within sea ice, at least for small icebergs. This also makes it more difficult for radars to detect icebergs, as discussed in Lane et al. (2004). It is concluded in Lane et al. (2004) that it is possible to achieve satisfactory detection performance using a SAR (synthetic aperture radar) even in sea ice when tuning the radar image processing correctly. However, the practical possibilities of being able to use this

in the near future are limited.

There still are unsolved challenges in detecting and monitoring ice conditions in a sufficiently effective and reliable way. This is still a developing field, along with increasing numbers of safety critical operations in the Arctic.

Prediction

Since the ice field can be connected over a large area, exposed to forces from winds, current and other ice fields, its movements can be close to impossible to predict. The current can have a direction completely different from the wind, and the ice flakes can collide making them change behavior in an instant.

In Figure 1.11 it is shown an example of how unpredictably sea ice can behave. Considering this it is understandable that it is a challenging task knowing in which direction to apply ice management, and predicting if and when an iceberg will become a problem.

It also creates challenges when towing an iceberg away. Even though an iceberg might be easily towed away, there might not be obvious where it should be towed to. The ice drift direction might change, causing the iceberg to drift back to its original position, which can be difficult to predict.

1.1.7 Technology for Simulation of Ice Conditions

Overview of the Numerical Ice Tank

When developing technology for use in ice conditions it is necessary to perform various tests in an ice covered model basin. Since this is both time consuming and expensive, the possibility of performing the same tests in a numerical computer simulator would bring major advantages.

The Numerical Ice Tank (NIT) simulator was developed through the DYPIC (DYnamic Positioning in ICe) (Kerkeni et al., 2014) and Arctic DP (Skjetne, 2014a) projects, focusing on developing and testing dynamic positioning technology for arctic environments. The simulator model is presented and thoroughly described in Metrikin (2014). DYPIC is a three year (2010-2012) international research and development project funded by the national research agencies of Germany, France and Norway (Kerkeni et al., 2014).

The intention was not originally to develop the numerical simulator. As there became a need of further testing in addition to what was done in the physical model tank, the simulator was developed. This made it possible to save time and

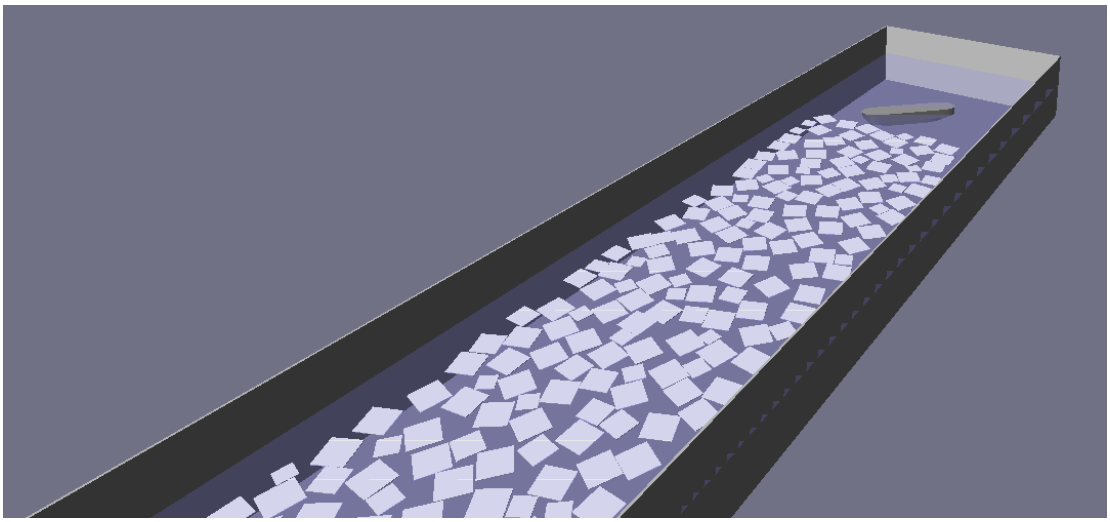

Figure 1.12: The ice tank simulator scene.

run several scenarios that would not be doable otherwise.

As discussed in Metrikin (2014) there has been developed other ice tank simulation models earlier. What differs this one from the other numerical ice tank models is the low relative velocities, leading to the hydrodynamic ice breaking effect being less important, while increasing the focus on mechanical ice properties. It also has a larger focus on broken ice modelling, related to contact force computation and collision detection (Metrikin, 2014).

The ice floes are modeled as discrete units, meaning they are each freely moving bodies in 6DOF, interacting with each other as well as the vessel hull. The ice fraction mechanics is also modeled, meaning it is also possible to simulate a vessel moving through a fully ice covered area.

The simulated environment is a model vessel located in a laboratory ice tank. The tank can contain an ice field with a predefined size and with ice floes of a predefined dimension and density. The floe sizes can be equal or a distribution of different sizes. The simulator is then able to perform a simulation of the movements, forces and behavior of the vessel and ice field interacting with each other.

Since the original purpose of the simulator model was being able to make ice tank testing scenarios simpler and faster, it is originally designed for running in model scale. Later it has been adapted in order to make it possible to also run simulations in full scale, but in this thesis it will be used for model scale simulations only.

It is possible to create simulations in a variety of conditions, since the ice floe

sizes can be adjusted, as well as the tank size, ice field size (making it possible to have an ice field smaller than the tank) and ice floe density. Material properties of the ice, like density and thickness can also be adjusted. All this can be accessed through an XML file, making changes possible without having to build the code project all over.

When using the simulator for testing DP and PM systems, instead of moving all the ice floes towards the ship, the reference system can be moved towards the ice, making a scenario similar to a constant positioned structure having ice drifting onto it. This means the ship will move towards and through the ice field.

The first version of the simulator was using the commercial physics engine Vortex to simulate the motions of the vessel and the ice floes, in addition to calculating the contact forces between the floes and from the floes to the vessel. It assumed the ice floes to be unbreakable, behaving like rigid bodies. This model worked promising and was used for simulating DP in open water and ice, as well as for a towing test. The results were compares to tests in the model tank.

In the second version there were developed models allowing the ice to break apart. This resulted in a more realistic model and made it possible to simulate a vessel in level ice.

In the third version the physics engine was changed form Vortex to NVIDIA PhysX, since that was a freely available solution. (Kerkeni et al., 2014)

Simulator Software Architecture

An overview of the simulator workflow structure is seen in Figure 1.13. The simulator setup includes writing all the parameters and settings in the previously mentioned input XML file, as well as creating the structural mesh of the vessel to be used for the simulations. During the work of this thesis, the already configured Arctic drillship (see Section 1.1.7) was used.

When the simulation starts, the first thing to happen is the initialization process. It is thoroughly described in Metrikin (2014), and includes initialization of the ice tank boundaries, the fluid, creation of the vessel and generation of the ice field, as well as initializing the physics engine with all the contacting surfaces and their properties. The simulation scene is shown in Figure 1.12.

The ice floes are generated, with a certain specified size distribution. They can be generated as rectangles or polygons. They are then distributed within the specified ice field area, and modeled as separate 6DOF 3D bodies.

After the simulation environment is initialized the program enters the simulation loop. The first phase of this loop is collision detection. The intersection

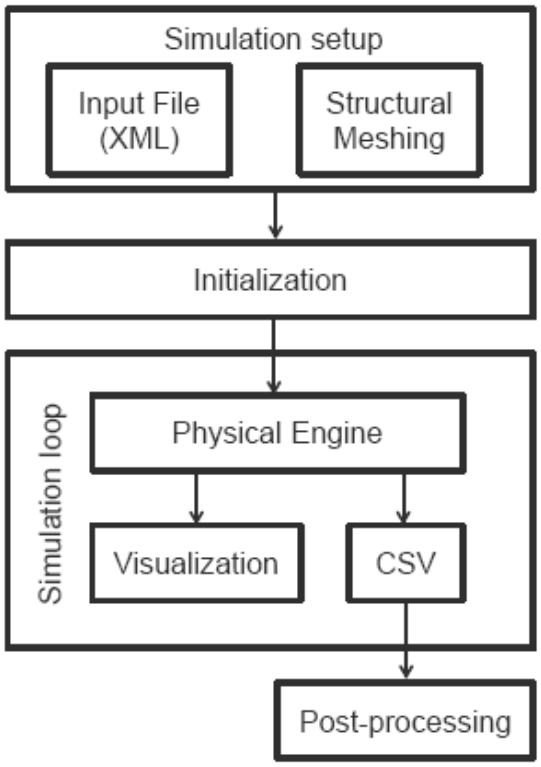

Figure 1.13: An overview of the workflow and architecture of the numerical ice tank simulator. From Metrikin (2014).

between all bodies are detected, determining which ones are colliding, and therefore going to influence each other. The next step is ice crushing constraint, where the mechanical properties of the ice is introduced in order to determine how the ice will get influenced by the collision in terms of the shape of the intersection area between the floes and the vessel, and how this intersection is affected by ice crushing. Next is the external force computation, finding the forces acting on each simulated object. This includes gravity forces, thruster forces and fluid forces.

Now all the forces are known, and the next step is for the multibody solver to apply this in order to calculate the movements of all the bodies in the simulation. After that is complete, the ice fracturing step calculates how the ice is affected by the acting forces in terms of bending and cracking. Finally, new ice floes are created from the ones that have split.

The last step is time integration, where the positions of all bodies are updated from their velocities and the duration of the time step.

While simulating the visualization graphics are updated. It is also generated .csv files containing data from the simulation at each time step, making it possible to analyze it later (Metrikin, 2014).

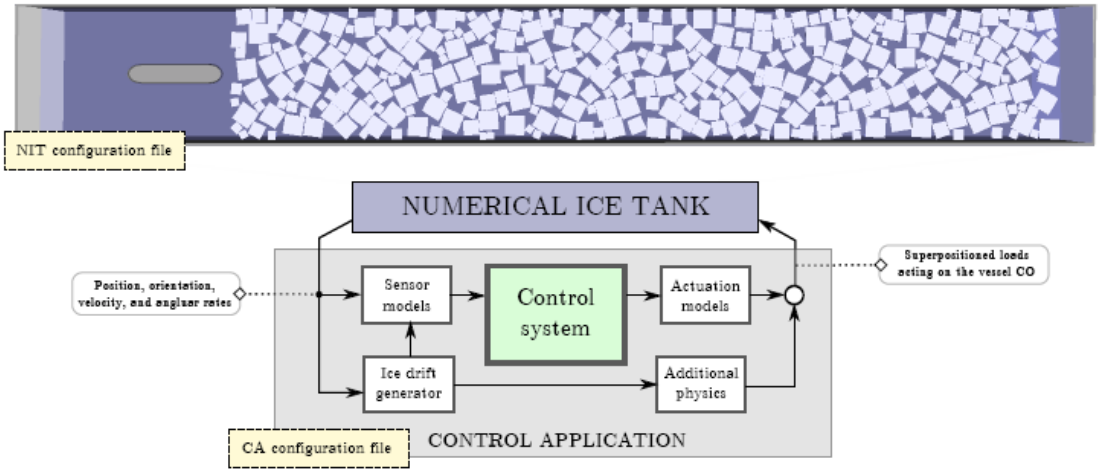

Figure 1.14: An overview of the interaction between the numerical ice tank and its related components. From Kjerstad and Skjetne (2014a).

Controller Interaction

This project uses a controller based on a Simulink model structure which is set up for taking a number of inputs from the simulator and outputting values back to it. It is then possible to create a controller inside this model, utilizing the inputs from the simulator. It can generate outputs that is fed back through the output ports, making them available to the simulator for processing.

The structure of the NIT in relation with the controller and other components is shown in Figure 1.14.

The inputs are values like positions, angular positions, velocities and angular velocities. There are also input ports for references and controller gains. Even though some of these are constants it can be useful to have them as inputs to the system since this makes it possible to change their values without having to regenerate the C++ code. Desired thrust forces are sent to the output ports.

After the controller model is made, Simulink Coder is used to generate C++ code from the model. This makes the controller model usable by the simulator, controlling the vessel in the ice tank.

Code generation and the setup procedure for connecting the Simulink modeled controller into the NIT, as well as how to initialize and run simulations, is covered in Gjessing (2014).

Parameter	Model scale	Full scale
Length in design waterline (m)	6.67	198.73
Length between perpendiculars (m)	6.13	184.00
Breath, moulded (m)	1.37	41.33
Draught at design waterline (m)	0.4	12.00
Stem angle at design waterline ($^\circ$)	45	“
Frame angle at midship ($^\circ$)	45	“
Displacement volume (m^3)	2535	68457
Center of gravity from aft perp. (m)	3.18	95.34
Block coefficient	0.75	“
Metacentric height (m)	0.357	10.7
Total thrust (N)	201	$7.2 \cdot 10^6$

Table 1.1: Parameters for the Arctic drillship used in the NIT and in the DYPIC project. From Kjerstad and Skjetne (2014a) and Kerkeni et al. (2013a).

No.	Comment	x [mm]	y [mm]	F [N]
1	Port-Bow	2272	316	22
2	Center-Bow	2644	0	22
3	Stb-Bow	2272	-316	22
4	Center-Stern	-3102	0	45
5	Port-Stern	-2664	190	45
6	Stb-Stern	-2664	-190	45

Table 1.2: Thruster parameters for the model scale Arctic drillship used in the NIT and in the DYPIC project. From Kjerstad and Skjetne (2014a).

The Arctic Drillship

The vessel used during this project is the Arctic drillship that was also used in the DYPIC project. It has six azimuth thrusters; three in the bow and three in the stern, with specifications as described in Table 1.2 (Kjerstad and Skjetne, 2014a). The model scale version of this ship is implemented in the NIT. It has a scaling factor of 30.

The other specification parameters of this ship are listed in Table 1.1.

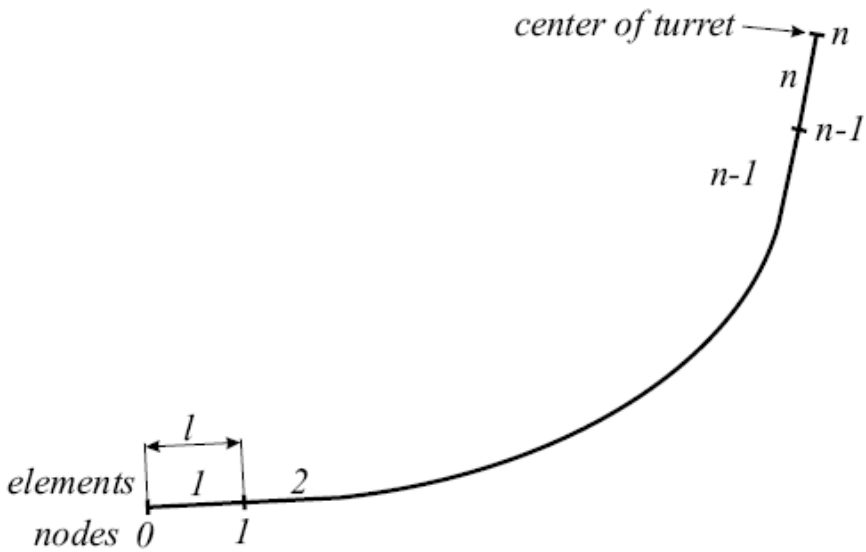

Figure 1.15: A mooring line showing the element discretization. The elements, of length l and numbered from the anchor towards the turret, are considered as separate rigid bodies connected through a joint. From Aamo and Fossen (2001).

1.1.8 Finite Element Modelling

Introduction

Finite Element Modelling (FEM) is a widely used technique in structural engineering for describing the behavior and performance of structural components. Since the majority of construction parts are a combination of several different forms and shapes, they are often too complex for being described with exact equations as a simple beam or column. It can therefore be useful to instead partition it into several smaller elements. Each element is then considered for itself, and the reaction of each element is calculated, as well as the interaction between the elements. With the help of the computation power of modern computers quite complex and large constructions can be modeled quite accurately with the use of a sufficient amount of elements.

For complex constructions this has to be done in three dimensions. For a long and slender construction like a mooring line it will, however, be sufficient for most cases to model it using a one dimensional FEM model. This means the cable will be parted along its length into smaller pieces of cable. These elements will then be considered as separate rigid bodies, able to transfer three dimensional forces between them, but no moment forces, assuming the cable has no bending or torsional stiffness. This approach is used in Aamo and Fossen (2001).

FEM of a Mooring Line

The forces of a free hanging mooring cable in water can be calculated by solving the catenary equations for a cable (see Aamo (1999)). This has been commonly used in computer simulations to estimate the forces from a mooring system. It can be sufficient when operating in shallow waters, since shorter mooring lines will cause the drag forces to be small compared to the static cable tensions. The mooring lines will also come to rest more quickly after moving, so that the static solution will be a good approximation.

When operating in deeper waters, the effects caused by the velocity of the cable will be responsible for a larger share of the total forces. The quasi-static approach of using only catenary equations will therefore be insufficient in this case (Aamo and Fossen, 2001).

This is when FEM is useful. A FEM taking into account the cable velocities, using Morrisons equation (Faltinsen, 1990) to model the hydrodynamic forces on each cable element, will be able to simulate cable forces quite realistically. This is demonstrated by Aamo and Fossen (2001).

1.2 Motivation

Conventional DP systems for open water have been available commercially for decades. The design methods for open water DP are well known (Fossen (2011), Sørensen (2012)) and have been proven to perform well through years of use for instance in the North Sea. The open water systems are well suited for handling large waves, strong currents, inpredictable wind gusts and other disturbance factors. It has become a common feature for a large variety of vessels and operation categories, ranging from oil rigs to cruise ships.

The nature of sea ice loads are however significantly different from the kind of loads you will experience in open water, in terms of strength, inpredictability and large fluctuations. The open water systems are known to be incapable of handling this kind of conditions without modifications (Kerkeni et al. (2013b), Gürtner et al. (2012)). It has however been shown through a few DP operations that it is possible to get a satisfactory DP performance by using ice management operations to transform the natural sea ice conditions into conditions feasible for the DP vessel to handle (Keinonen et al. (2000), Moran et al. (2006), Keinonen et al. (2006)). This is still in an early phase, meaning there is a need for more research within this topic.

There has been performed several model tests investigating the DP performance of vessels in ice (Deter et al. (2009), Hals and Efraimsson (2011), Hals and

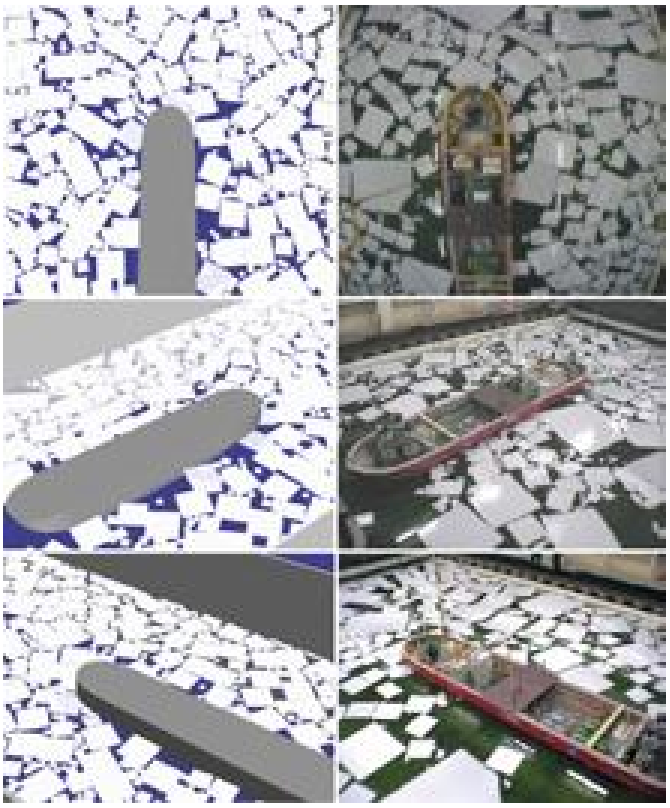

Figure 1.16: Ice simulator tests (left) compared with model basin tests (right). From Metrikin et al. (2013).

Jenssen (2012)). The results from model tests and full scale operations has shown that even when adapting the conventional control systems to handle ice loads there is still a need for other strategies to make the vessels handle the ice loads better (Metrikin et al., 2013). These may include better ice detection in order to find the path of least resistance through the ice, optimization of ice management strategies and other supporting features, and in general get a better understanding through test trials, simulations and other research methods in order to better adapt offshore systems into the Arctic environment. Some of these techniques are being discussed in this paper.

The nature of the ice makes physical experiments with ice operation a time consuming and expensive task. Performing model tank experiments require an artificial ice cover to be created, and this ice cover will change for each experiment performed, eventually resulting in the need to remake it. Full scale test trials are naturally even more expensive and time consuming. It is therefore of great advantage being able to do some of these tests in a computer simulated environment, where conditions can be changed instantly between simulations, the ice cover in one simulation is not affected by the previous one, and the setup pro-

cedure does not cost much in terms of either time or money. This, and the fact that there are very few off-the-shelf solutions for analyzing DP in ice (Metrikin et al., 2013), motivated the development of the Numerical Ice Tank in Metrikin (2014) and Kerkeni et al. (2014). This simulator will be further investigated in the work of this thesis.

It will always be necessary to perform both physical model tests and full scale tests in order to verify the simulation results. Still there is a lot to gain by doing as many scenarios as possible in a computer simulated environment.

1.3 Scope and Objectives

Previous works within the field of Arctic station keeping operations has mostly been restricted to DP. For some operations, it might be more desired to use PM due to the decreased fuel consumption when using a mooring system to handle mean loads. The Numerical Ice Tank (Metrikin, 2014) could be a suitable environment for investigating the performance of a mooring system in ice conditions. The main objective of this thesis is to implement a mooring system within the NIT and see how it performs. If the method is working, this can be used to simulate various scenarios in a realistic and accurate way, using any kind of turret mooring system combined with any control strategy.

A turret mooring model will be implemented as a FEM and integrated in the NIT. Its performance is then analyzed through simulations both in the NIT simulator and isolated in Simulink. It will then be used to create a linearized mooring model for use in control design.

A TAPM controller will be implemented to provide additional damping to the moored vessel in surge and sway. It will have PID action for heading control.

There will be performed an analysis of the setpoint chasing technique, and it will be incorporated in the simulator and tested through simulations. Other methods of improving the PM performance will be discussed.

Chapter 2

Mathematical Modelling

2.1 Vessel Modelling

2.1.1 Reference Frames

In order to keep track of what is referring to directions related to the vessel and what is in relation to the surrounding environment, there is necessary to clearly define these two reference frames and having a way of converting values between them. This is thoroughly covered in Fossen (2011).

The earth-fixed reference system is used when measuring positions and angles of the vessel, usually by using the *North-East-Down* (NED) frame (see Fossen (2011) for an explanation of geographic reference frames). The vessel state in the earth fixed frame can be described in six degrees of freedom as the following generalized position vector

$$\boldsymbol{\eta} = [x, y, z, \phi, \theta, \psi]^\top, \tag{2.1}$$

where x, y and z are the positions in respectively north, east and downwards directions and ϕ, θ and ψ are the angles about each axis in the earth-fixes reference frame.

In the *vessel fixed reference frame*, which is used when applying thruster forces and other forces that is naturally related to the vessel, the generalized velocity vector is

$$\boldsymbol{\nu} = [u, v, w, p, q, r]^\top, \tag{2.2}$$

where u, v and w are the velocities in surge, sway and heave, respectively, and p,

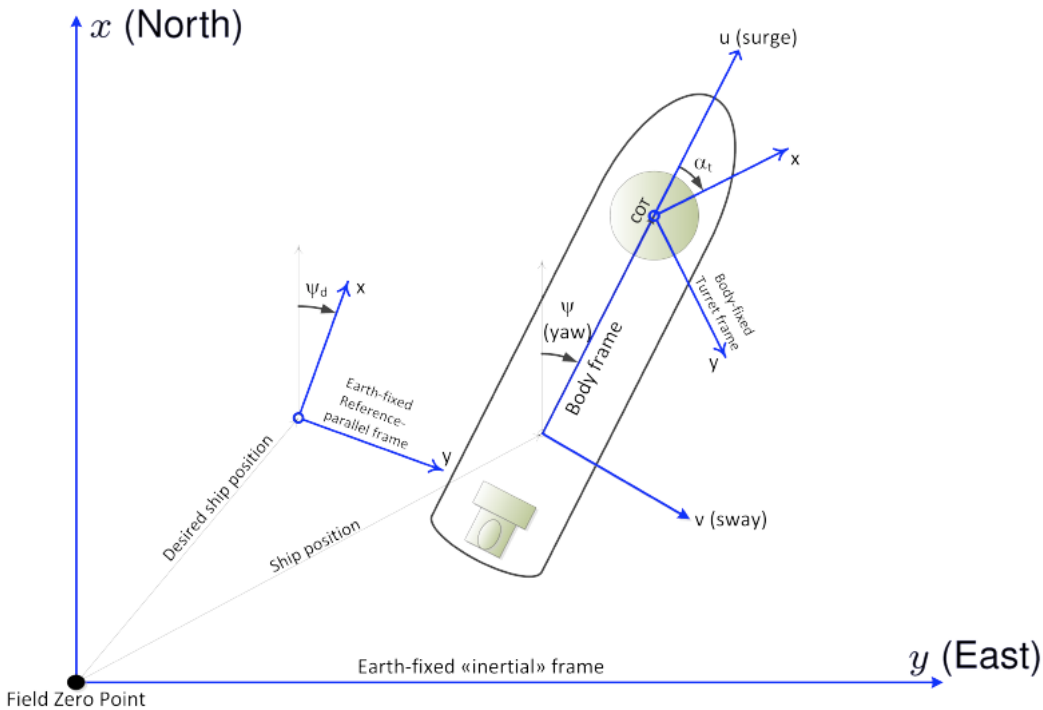

Figure 2.1: The relations between the NED frame, reference parallel frame, body frame and turret fixed frame. From Skjetne (2014b).

q and r are the angular velocities of the vessel in roll, pitch and yaw.

In order to relate these systems together there is used a rotation matrix, which values depend on the different angles on the vessel. The vessel related velocity vector and the earth related position vector can thereby be connected through the differential equation

$$\dot{\boldsymbol{\eta}} = \boldsymbol{R}(\boldsymbol{\eta})\boldsymbol{\nu}. \tag{2.3}$$

This is not only valid for a six degree of freedom (DOF) system. When we are handling surface vessels it is usually not needed to keep track of movements in heave, pitch and roll, at least not for DP or PM control purposes. (2.1) and (2.2) can therefore be reduced to a 3DOF system,

$$\boldsymbol{\eta} = [x, y, \psi]^T \tag{2.4}$$

$$\boldsymbol{\nu} = [u, v, r]^T. \tag{2.5}$$

This will reduce the rotation matrix to a three by three matrix being a function of the yaw angle, ψ, only:

$$\boldsymbol{R}(\psi) = \begin{bmatrix} cos(\psi) & -sin(\psi) & 0 \\ sin(\psi) & cos(\psi) & 0 \\ 0 & 0 & 1 \end{bmatrix} \tag{2.6}$$

The 3DOF rotation matrix also has the useful property

$$\boldsymbol{R}^{-1}(\psi) = \boldsymbol{R}^{T}(\psi) \tag{2.7}$$

(Sørensen, 2012).

In addition to these two reference frames it can also be useful to introduce a *reference parallel frame*, also referred to as the *hydrodynamic frame* (Nguyen and Sørensen, 2009a). This frame is aligned with the vessel position reference, and will be an earth fixed reference frame.

For turret mooring systems, where the turret is not assumed to always be aligned with the mooring lines, a turret parallel frame can be used. This is further discussed in Section 2.2.2.

See Figure 2.1 for a visualization of the relations between the three most common reference frames.

2.1.2 Vessel and Mooring Dynamics

In addition to the differential equation from (2.3) we consider the various forces acting on the vessel in order to make a second differential equation for the rigid body kinetics. Using the method covered in Fossen (2011), the most relevant forces can be summarized as:

Inertia forces:

$$\boldsymbol{M}_{RB}\dot{\boldsymbol{\nu}} + \boldsymbol{M}_{A}\dot{\boldsymbol{\nu}}_r + \boldsymbol{C}_{RB}(\boldsymbol{\nu})\boldsymbol{\nu} + \boldsymbol{C}_{A}(\boldsymbol{\nu}_r)\boldsymbol{\nu}_r \tag{2.8}$$

Damping forces:

$$\boldsymbol{D}(\boldsymbol{\nu}_r)\boldsymbol{\nu}_r \tag{2.9}$$

Restoring forces:

$$\boldsymbol{G}(\boldsymbol{\eta}) \tag{2.10}$$

Environmental forces:

$$\boldsymbol{\tau}_{wind} + \boldsymbol{\tau}_{waves} \tag{2.11}$$

Thruster forces:

$$\boldsymbol{\tau}_{thr} \tag{2.12}$$

$\boldsymbol{M}_{RB}$ is the mass matrix, $\boldsymbol{M}_A$ is added mass, $\boldsymbol{C}_{RB}$ and $\boldsymbol{C}_A$ are Coriolis and centripetal force matrices. $\boldsymbol{\nu}_r$ is the relative speed between the vessel and the water, meaning current is taken account for. $\boldsymbol{D}(\boldsymbol{\nu}_r)$ and $\boldsymbol{G}(\boldsymbol{\eta})$ are, respectively, damping and restoring force functions.

For moored vessels the mooring force will occur in addition to this. It can have both proportional components, meaning a linear function of the distance from equilibrium, and linear or nonlinear damping components due to viscous forces on the mooring lines under water, which would be a function of the velocity vector. By collecting the mooring forces in $\boldsymbol{\tau}_{moor}$, the overall nonlinear equation will be

$$\begin{aligned}\boldsymbol{M}_{RB}\dot{\boldsymbol{\nu}} + \boldsymbol{M}_A\dot{\boldsymbol{\nu}}_r + \boldsymbol{C}_{RB}(\boldsymbol{\nu})\boldsymbol{\nu} + \boldsymbol{C}_A(\boldsymbol{\nu}_r)\boldsymbol{\nu}_r + \boldsymbol{D}(\boldsymbol{\nu}_r)\boldsymbol{\nu}_r + \boldsymbol{G}(\boldsymbol{\eta}) \\ = \boldsymbol{\tau}_{wind} + \boldsymbol{\tau}_{waves} + \boldsymbol{\tau}_{thr} + \boldsymbol{\tau}_{moor}\end{aligned} \tag{2.13}$$

For the purpose of DP and PM there are some of these terms that can be simplified and linearized. When performing stationkeeping the speeds of the vessel are low, since it is first of all supposed to move as little as possible. This means that the Coriolis and centripetal terms will be very small and can be neglected. Also the nonlinear parts of the damping term will disappear, since these would be a higher order function of the velocities. The restoring forces can usually be considered linear around the working point.

The mooring forces can be modeled differently depending on the working conditions and the accuracy requirements, but for controlling purposes it can often be sufficient to use a linearized version of the mooring model. This means it can be expressed as

$$\boldsymbol{\tau}_{moor} = -\boldsymbol{R}^T(\boldsymbol{\psi})\boldsymbol{K}\boldsymbol{\eta}, \tag{2.14}$$

where $\boldsymbol{K}$ is a matrix of spring coefficients. This assumes the equilibrium of the mooring system to be at $\boldsymbol{\eta} = \boldsymbol{0}$, which might not be the case. A translation from NED coordinates to the mooring equilibrium might therefore be needed. The rotation matrix is needed here since the mooring forces are acting in relation to the sea floor and not to the vessel frame.

A more complete process plant model of a mooring system for simulation purposes will be covered later in this thesis.

Except from considering the mooring force as a restoring force, there will be no other restoring forces in any of the degrees of freedom we are considering in this 3DOF model.

Finally this yields a simplified version of (2.13),

$$\boldsymbol{M}\dot{\boldsymbol{\nu}} + \boldsymbol{D}\boldsymbol{\nu} + \boldsymbol{R}^T(\psi)\boldsymbol{K}\boldsymbol{\eta} = \boldsymbol{\tau}_{wind} + \boldsymbol{\tau}_{waves} + \boldsymbol{\tau}_{thr}, \tag{2.15}$$

where

$$\boldsymbol{M} = \boldsymbol{M}_{RB} + \boldsymbol{M}_A \tag{2.16}$$

is the mass matrix including added mass. The mooring restoring force $\boldsymbol{K}\boldsymbol{\eta}$ assumes the *field zero point*, which is the equilibrium point of the mooring system, to be at $\boldsymbol{\eta} = \boldsymbol{0}$. If that is not the case, this can easily be altered by using the vector difference between $\boldsymbol{\eta} = \boldsymbol{0}$ and the *field zero point* instead.

Even though this is a linearized model it is still a nonlinear equation due to the rotation matrix.

Combining (2.15) and (2.3) we get the system equations commonly used as a control plant model for stationkeeping,

$$\begin{aligned} \dot{\boldsymbol{\eta}} &= \boldsymbol{R}(\psi)\boldsymbol{\nu} \\ \boldsymbol{M}\dot{\boldsymbol{\nu}} &= -\boldsymbol{D}\boldsymbol{\nu} - \boldsymbol{R}^T(\psi)\boldsymbol{K}\boldsymbol{\eta} + \boldsymbol{\tau}_{wind} + \boldsymbol{\tau}_{waves} + \boldsymbol{\tau}_{thr}. \end{aligned} \tag{2.17}$$

When using this model in an open water DP or PM setting only the low frequency motions are of interest. This is because it is not desired to have the control system compensating for the first order wave loads, since it would require lots of energy and wear and tear, not being able to compensate for it anyway. Therefore the wave frequency components would need to be filtered out, and the only relevant wave forces would be the slowly varying higher order effect like drift forces.

For more on this, see Fossen (2011), Fossen (2002), or Sørensen (2012)

Damping forces can also be linearized around the working area, adding another velocity proportional term to the total equation. This is still a quite simple model, but it will be more accurate than just implementing the mooring with a proportional spring force term. The mooring force including damping would then be

$$\boldsymbol{\tau}_{moor} = -\boldsymbol{R}^T(\boldsymbol{\psi})\boldsymbol{K}\boldsymbol{\eta} - \boldsymbol{D}_{moor}\boldsymbol{\nu}. \tag{2.18}$$

(Simplified from the mooring model in Strand et al. (1998).)

This damping coefficient matrix could also be combined into the general vessel damping coefficient matrix.

Damping will also be discussed later in this paper.

2.1.3 Thruster Dynamics

In some cases when designing a control system it is sufficient to assume the thrusters can deliver the desired amount of force within a relatively short time period. In other words this means assuming you will always get the demanded thrust at once. In the opposite case it is necessary to include a thruster model in the system equations, taking account for thruster dynamics like phase lag and reduction of thrust amplitude at higher frequencies. A simple but often sufficient way of approximating the thruster dynamics, as described in Sørensen (2012), is by the following first-order model,

$$\dot{\boldsymbol{\tau}}_{thr} = -\boldsymbol{A}_{thr}(\boldsymbol{\tau}_{thr} + \boldsymbol{\tau}_c), \tag{2.19}$$

where $\boldsymbol{\tau}_c$ is the commanded thrust vector from the controller, and $\boldsymbol{A}_{thr}$ is a matrix containing the thruster time constants.

2.1.4 Bias Model

Since this is a simplified control plant model there might be some dynamics and uncertainties not accounted for, as well as some slowly varying changes due to sensor errors or other external conditions. These can be accounted for by collecting them in a bias model. A commonly used one is the first order Markov model (Sørensen, 2012)

$$\dot{\boldsymbol{b}} = -\boldsymbol{T}_b^{-1}\boldsymbol{b} + \boldsymbol{E}_b\boldsymbol{w}_b, \tag{2.20}$$

where $\boldsymbol{T}_b$ is a matrix of time constants, $\boldsymbol{w}_b$ is a Gaussian white noise vector, and $\boldsymbol{E}_b$ is a scaling matrix for the input noise.

Including the bias and thruster models in the total model from (2.17) we get

$$
\begin{aligned}
\dot{\boldsymbol{\eta}} &= \boldsymbol{R}(\psi)\boldsymbol{\nu} \\
\dot{\boldsymbol{b}} &= -\boldsymbol{T}_b^{-1}\boldsymbol{b} + \boldsymbol{E}_b\boldsymbol{w}_b \\
\boldsymbol{M}\dot{\boldsymbol{\nu}} &= -\boldsymbol{D}\boldsymbol{\nu} - \boldsymbol{R}^T(\psi)\boldsymbol{K}\boldsymbol{\eta} + \boldsymbol{R}^T(\psi)\boldsymbol{b} + \boldsymbol{\tau}_{wind} + \boldsymbol{\tau}_{waves} + \boldsymbol{\tau}_{thr} \\
\dot{\boldsymbol{\tau}}_{thr} &= -\boldsymbol{A}_{thr}(\boldsymbol{\tau}_{thr} + \boldsymbol{\tau}_c)
\end{aligned} \tag{2.21}
$$

See Sørensen (2012) or Fossen (2011) for more on system modelling.

2.2 Mooring System Modelling

2.2.1 Phenomena Acting on a Mooring System

In addition to the damping effect from the interaction between the vessel hull and the water, the mooring system will generate a significant amount of damping. Since the mooring system has a relatively complex geometry these effects are hard to model in an exact way. The damping of moored structures is described in Triantafyllou et al. (1994).

A mooring system consists of several mooring lines usually made of either steel wire, chains, synthetic rope or a combination of those. When the mooring lines are moving transversely through the water they will be subject to a drag force, resulting in an effective damping to the system. For simple cylindrical bodies moving through a current, the drag force can be calculated as a result of the Reynolds number, turbulence, current shear and cable surface. The resulting force can be estimated and incorporated into a drag coefficient.

For a mooring system it is not sufficient to simplify the mooring line as a rigid cylinder, even though a short piece of for instance steel wire can still be considered a cylinder. Due to flexible movements in the mooring structure there are some phenomena amplifying the damping effect, making the effective damping coefficient different from the nominal value.

Vortex Induced Vibrations

When a flow is passing a cylindrical body there are generated vortices in the flow behind the body, causing a periodic force acting on the body. When these vortices are acting in a frequency close to the resonance frequency of the mooring line, this is causing what is known as vortex induced vibrations (VIV). This increases the force required to move the cable through the water and therefore the damping coefficient will increase (Triantafyllou et al., 1994).

Wave-slow Motion Interaction

Due to that the drag force is a quadratic function of speed between water and the cable (Triantafyllou et al., 1994), the wave motions are making the effective drag larger due to the large speeds at certain points in the wave period. This increases the effective drag coefficient.

Cable Material Damping

This refers to the internal damping in the material of the mooring line. This damping is negligible in the case of steel wire or chain. There can however be some damping generated between chain links or in the connections between wires (Triantafyllou et al., 1994).

Soil Friction

When a cable is partially lying on the seabed it will be restricted from moving by the friction against the seabed. This will act as damping, and also increase the stiffness of the mooring system since the suspended part of the mooring line becomes shorter. Analysis has shown that for low frequency motions these effects are negligible, but for wave frequency motions they can be significant (Triantafyllou et al., 1994).

2.2.2 Finite Element Modelling of a Mooring System

Modelling a Single Mooring Line

See Section 1.1.8 for an introduction to FEM.

The mooring cable model used for this project was implemented by Ole Morten Aamo in 1999 for use with the *ABB Integrated Vessel Simulator* (Aamo, 1999).

Its main functionality lies in the C program *cable.c*. Its main function runs the cable simulation for one timestep of the surrounding simulation environment, stepping through several internal time steps, before it returns. It uses the current state of the cable together with top and bottom positions, to calculate its behavior. It can output top- and bottom forces, as well as the position of each node along the cable.

We have implemented it in a Matlab MEX interface, making it possible to run simulations from Matlab or Simulink.

The *cable.c* function is defined as following:

```
int cable(double x[], double sfp[], double Ftop[], double Fbot[],
    double *Lout, double tp[], double d[], double rok[], double E[],
    double A0[], double ef[], double L[], double dL, double Cdn[],
    double Cdt[], double Cmn[], double ksv[], double kshl[], double
    ksht[], double ne[], double vc[], double dT, double dt, double rov,
    double D, int ns, int nc, int tne, int negs);
```

The inputs are:

x[] :	Vector of node positions and velocities in three dimensions.
sfp[] :	Vector of seafloor touchdown points.
Ftop[] :	Three dimensional force vector for the top of the mooring line.
Fbot[] :	Three dimensional force vector for the bottom of the mooring line.
Lout :	Length of upper section at end of timestep. Used when winding the cable.
tp[] :	Position of top point.
d[] :	Cable diameter of each segment.
rok[] :	Mass density of each cable segment.
E[] :	Young's modulus of each segment.
A0[] :	Cross section area of each segment.
ef[] :	Factor for stiffness calculation for each segment.
L[] :	Length of each segment.
Cdn[] :	Normal drag coefficient of each segment.
Cdt[] :	Tangential drag coefficient of each segment.
Cmn[] :	Mass coefficient of each segment.
ksv[] :	Vertical seafloor interaction stiffness of each segment.
kshl[] :	Longitudinal horizontal seafloor interaction stiffness of each segment.
ksht[] :	Transversal horizontal seafloor interaction stiffness of each segment.
ne[] :	Number of finite elements for each segment.
vc[] :	Specification of currents. Array of rows on the form [depth,vx,vy,vz], where vx, vy and vz are current velocity in the x, y and z directions respectively.
dT :	Time step to run cable for, meaning the time step of the surrounding model.
dt :	Internal time step in the cable function.
rov :	Mass density of the surrounding water.
D :	Water depth.
ns :	Number of cable segments.
nc :	Number of currents.
tne :	Total number of elements in the cable.
negs :	Flag for how to handle negative strain. 0=continue, 1=exit.

Since the program is supporting having several cable segments with different properties, the segment specific inputs are vectors consisting of one element per segment.

The variables *x[]*, *sfp[]*, *Ftop[]*, *Fbot[]* and *Lout* are used as outputs. The integer return from the function itself is used as an error indicator where *0=OK, 1=out of memory, 2=negative strain.*

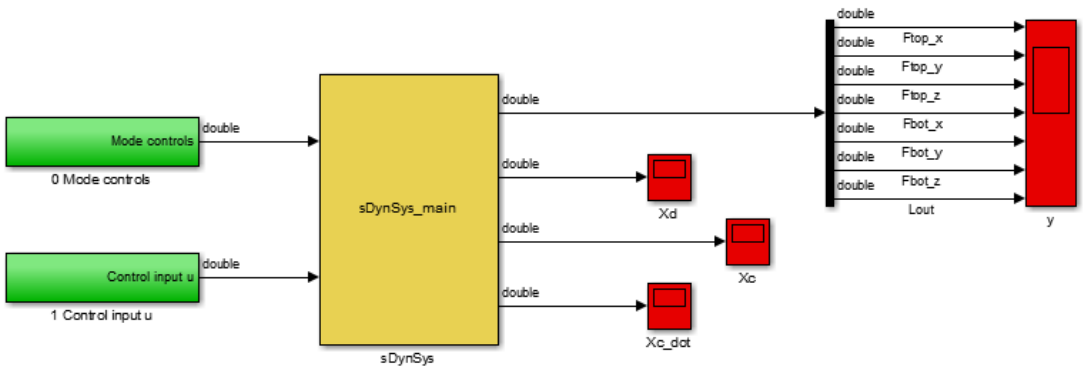

Figure 2.2: The S-function model. The inputs are provided as a vector on the left side, while outputs and state vector can be accessed on the right side.

Integrating the FEM Cable Model in Simulink

Simulink has an S-function block, which is useful when integrating C functions as part of a dynamic system. An S-function template developed in our group at the Marine Technology Centre, suitable for modelling with discrete or continuous dynamic states, was used to implement the FEM of the mooring lines. It makes it possible to have a system with the desired amount of internal states, using input signals to calculate changes in states and generate outputs.

The cable function is handled as a discrete update function. All the cable properties are provided as parameters, while the positions and velocities of each node, as well as the seafloor touchdown points, forces and upper segment length, are used as states for the dynamic system. The output is set to be the top force triplet, bottom force triplet and the current length of the upper segment.

The mooring line parameters, as well as simulation properties and initial values, are set in a separate Matlab file, which has to be run prior to running the Simulink model, so that the variables are accessible by the model. Another Matlab function, which is run from this parameter script, is generating an initial state for the mooring line, which is then used to generate initial values for the model.

Testing for a Single Cable

First Test In the first test the cable is suspended freely without any motions. The cable is 500 meters long, spans over 400 meters in x-direction, and the anchor is located at 200 meters depth.

Below is the cable configuration part of the initializing Matlab script, showing

all the mooring line parameters for the simulation. The numbers are retrieved and somewhat modified from the test cases in the cable FEM documentation.

```
%% Dynamical system configuration File
% Project description
System.Project        = 'Example: Dynamical System Simulation';
System.Model          = 'Test model';


%% Mooring line parameters

% Segment paramaters. Vectors containing one element per segment.
rok=[7700]';        % Cable segment density
L=[500]';           % Segment lengths
E=[2.1e8]';         % Young's modulus
d=[0.2]';           % Cable segment diameters
A0=(pi/4)*d.^2      % Cross section area
emfact=[1]';        % Factor for stiffness calculation. 1=normal, 2=chain
Cdn=[1]';           % Normal drag coefficient
Cdt=[0.3]';         % Tangential drag coefficient
Cmn=[1.5]';         % Added mass coefficient
ksv=[100]';         % Vertical seafloor interaction stiffness
kshl=[0]';          % Longitudinal horizontak seafloor interaction
    stiffness
ksht=[0]';          % Transversal horizontal seafloor interaction
    stiffness
ne=[20]';           % Number of elements in each segment

% Water properties
D=200;              % Water depth
ro=1035;            % Water density

% Currents. nc*4 dimensional array of rows on the form [depth,vx,vy,vz],
%     where vx, vy and vz are current velocity in the x, y and z
%     directions respectively. (nc>0).
c=[1 0 0 0;
    ];

errtol=1.0E-6;      % Error tolerance
negs = 0;           % Flag for handling negative strain (0=continue,
    1=exit)

dT = 0.2;           % Timestep to run cable for
dt = 0.02;          % Internal timestep in cable

X=400;
```

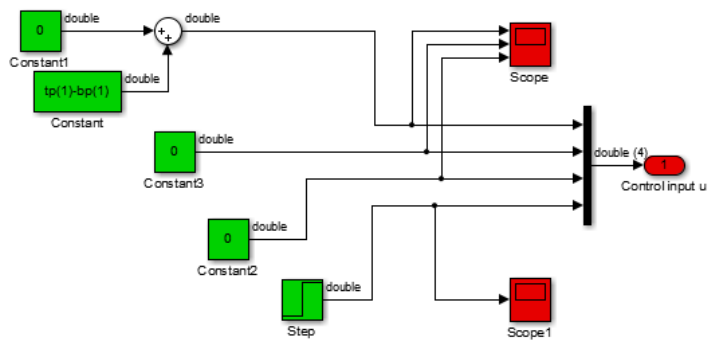

Figure 2.3: The inputs to the s-function in the first simulation, when no motions of the cable are introduced.

```
bp=[0;0;D];        % Initial bottom (anchor) position
tp=[X;0;0];        % Initial top position

ns = length(L);    % Number of segments
[nc,foo] = size(c); % Number of currents
```

After running the initialization script the Simulink model can be run. The inputs to the s-function is set as shown in Figure 2.3, setting the x-position of the top point equal to the difference between top and bottom point, using the variables defined from the initialization file. The y and z coordinates are set to constant zero, as well as the cable winding speed.

After running the simulation the cable is hanging as shown in Figure 2.4. It can be seen that the cable is touching the seabed around 100 meters from the anchor, meaning there should be no force in z-direction on the anchor. This is confirmed by considering Figure 2.5, where we see that, although there are some forces going in the vertical direction they are of a very small magnitude compared to the other forces, meaning they are practically zero.

There are some oscillations occurring on the z force, still with quite a low magnitude compared to the other dimensions of this system. They are probably caused by some numerical phenomena, since they turned out to be affected by changing the number of elements in the model.

The forces in y-direction are zero, which makes sense since there are no forces acting on the cable and it is entirely located in the xz-plane.

Figure 2.5 also shows that the top force in x-direction is close to the opposite of the bottom force in x-direction. This is as expected since there are no forces acting on the cable between these two points. The z-force on top is quite large,

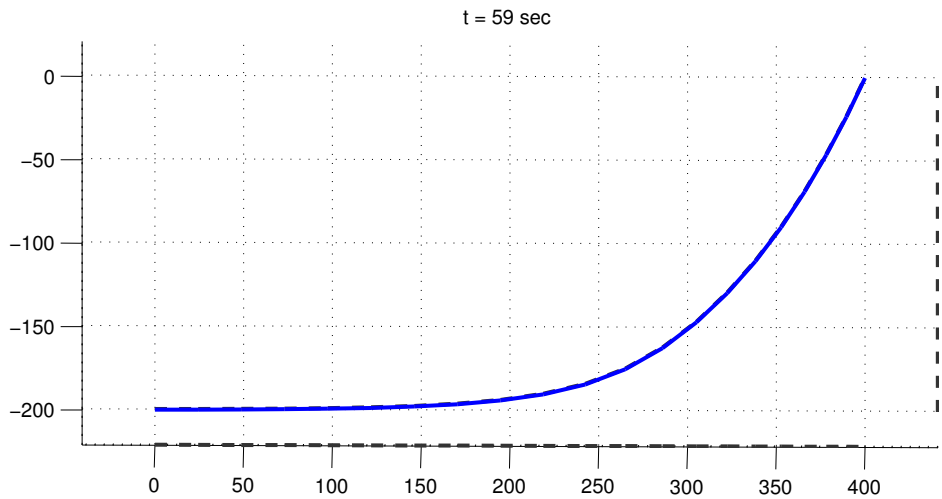

Figure 2.4: The shape of the mooring line in the first test scenario.

since it holds the weight of the cable.

Second Test For the next test the top point is moved along the x and y axis, both in positive direction. This is done by connecting a ramp function to the corresponding input ports. Both are moving at 0.5 m/s. The y-motion is not started before after 30 seconds, while the x-motion is running all the time. The simulation is run for 100 seconds.

From Figure 2.7 it can be seen how the forces in x-direction is gradually increasing throughout the whole simulation. It seems to be a little affected by the motion along the y axis, but not much. It is clearly seen on the y-plot when the cable starts to move in that direction. On the bottom it does not feel the y-force before a while after the y-motion has started, which is reasonable due to the cable lying on the seafloor, as well as being restricted by drag forces from the water.

The z-force on the top is somewhat increasing, but what happens on the bottom is more interesting. There are some oscillations at some point, before the force starts to steadily increase. This indicates that the cable is lifting from the ground, but as we can see on Figure 2.6 it is not by much.

The oscillations can be caused by a variety of phenomena, including numerical issues, hydrodynamic forces and seafloor interactions. This will not be discussed in detail here.

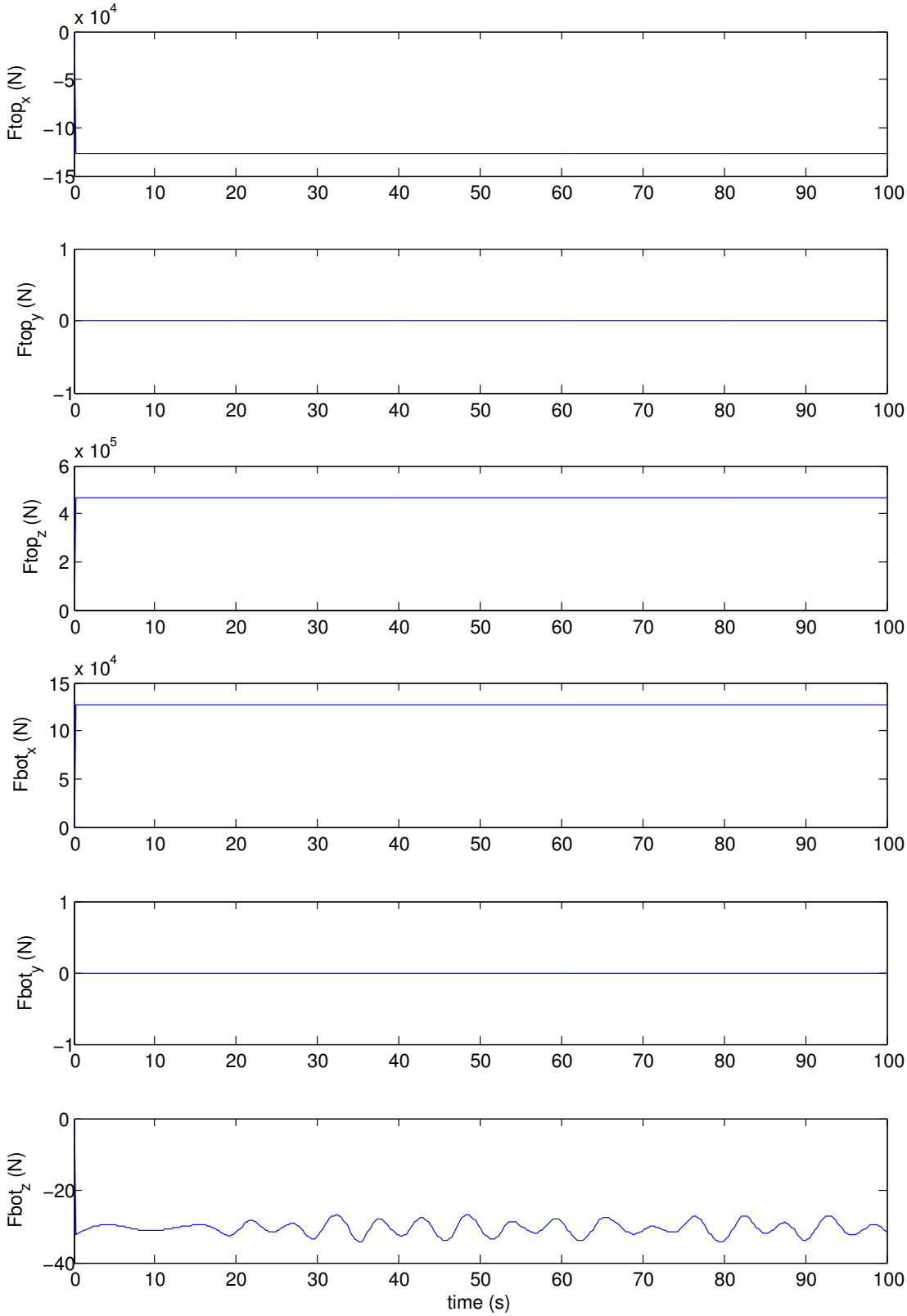

Figure 2.5: The force triplets on the top and bottom end of the cable. First test scenario.

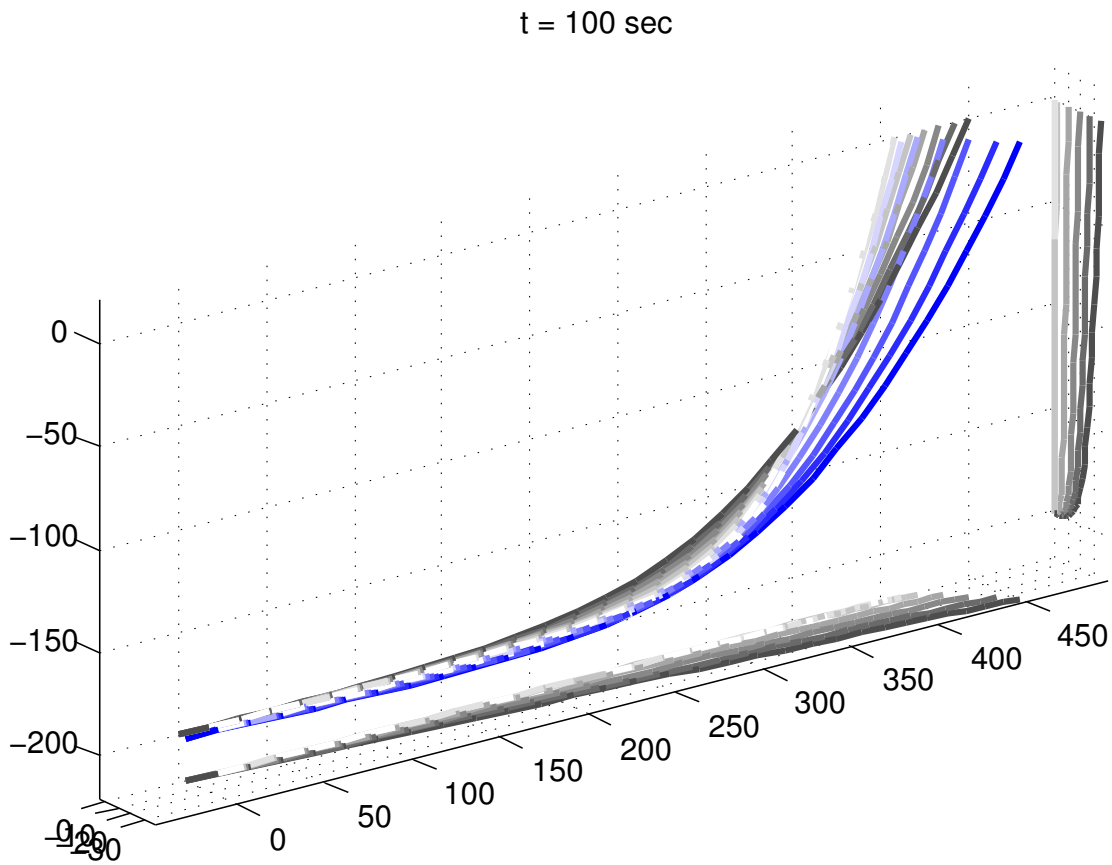

Figure 2.6: The shape of the mooring line, with trajectories, in the second test scenario. The shadows along each plane shows how the cable is moving in each dimension.

Third Test Next is to test the winding feature. The cable is now winded by 1.5 m/s, starting at t=20. In addition to that the cable is now divided into two segments; the lower 200 meters being the same as earlier, while the upper 300 meters have its mass density reduced to 1500 kg/m. Apart from that all other values are the same, for simplicity.

The segment part of the parameter file will then look like the following:

```
% Segment paramaters. Vectors containing one element per segment.
rok=[7700 1500]';     % Cable segment density
L=[200 300]';         % Section lengths
E=[2.1e8 2.1e8]';     % Young's modulus
d=[0.2 0.2]';         % Cable segment diameters
A0=(pi/4)*d.^2;       % Cross section area
emfact=[1 1]';        % Factor for stiffness calculation. 1=normal,
    2=chain
```

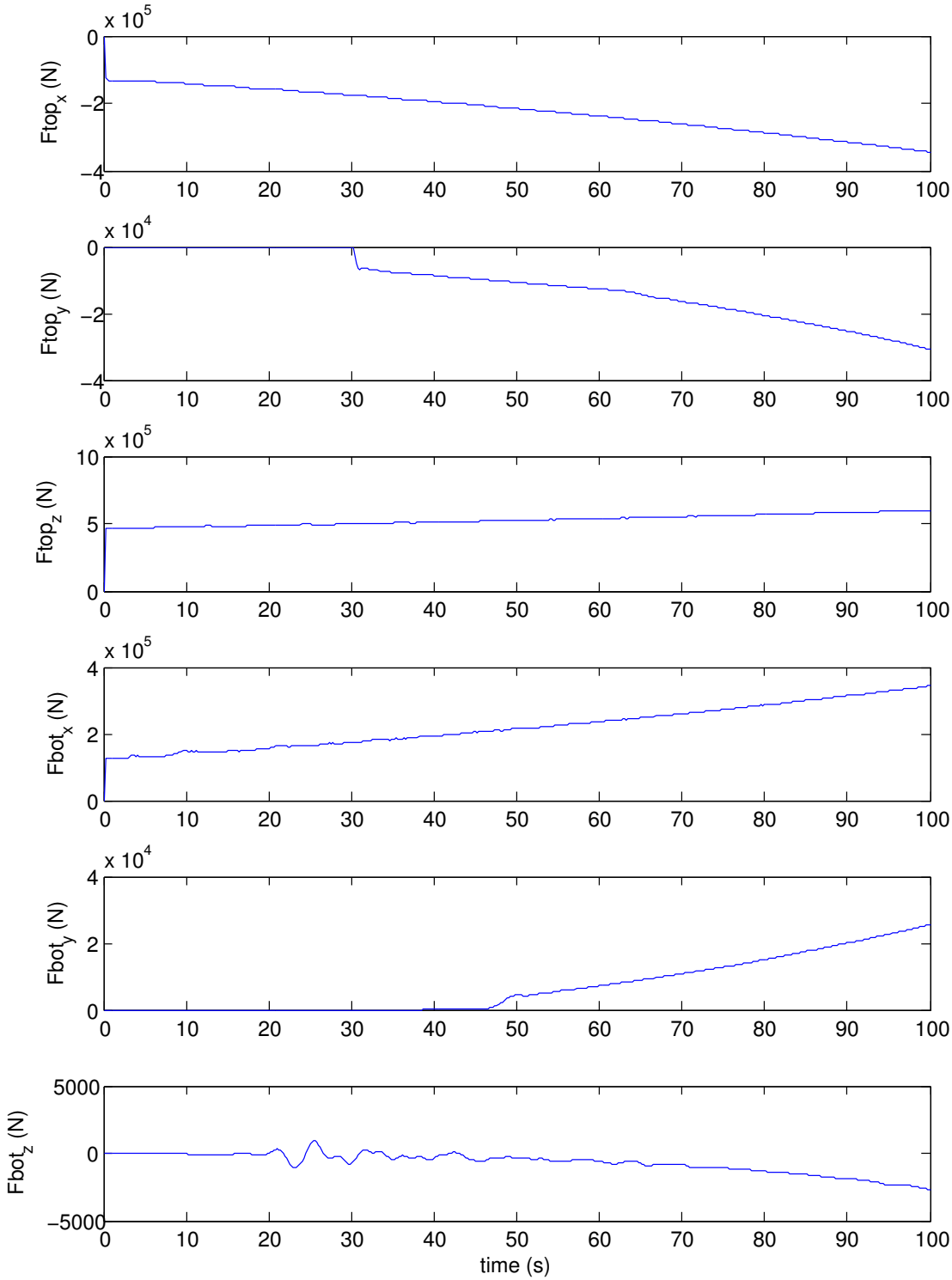

Figure 2.7: The force triplets on the top and bottom end of the cable. Second test scenario.

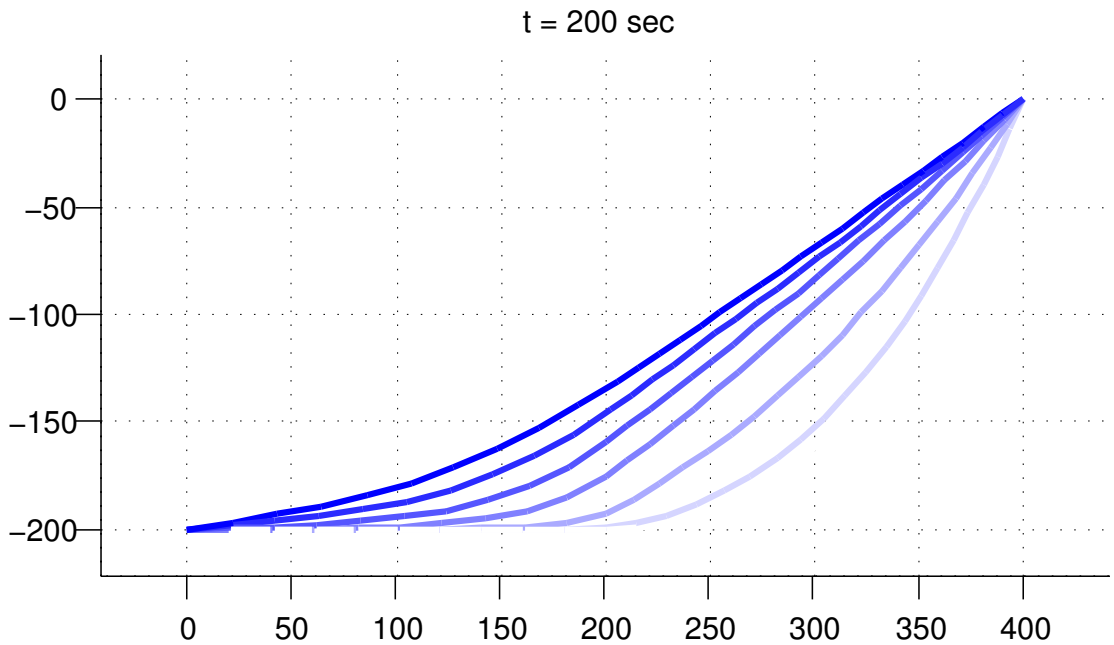

Figure 2.8: The shape of the mooring line in the third test scenario. The cable is winded in by 0.5 m/s starting after 20 seconds. The simulation is run for 200 seconds. It has two segments; a heavy one at the bottom and a lighter one at the top.

```
Cdn=[1 1]';            % Normal drag coefficient
Cdt=[0.3 0.3]';        % Tangential drag coefficient
Cmn=[1.5 1.5]';        % Added mass coefficient
ksv=[100 100]';        % Vertical seafloor interaction stiffness
kshl=[0 0]';           % Longitudinal horizontak seafloor interaction
    stiffness
ksht=[0 0]';           % Transversal horizontal seafloor interaction
    stiffness
ne=[10 20]';           % Number of elements in each segment
```

On Figure 2.8 it is possible to see how the lighter top segment affects the shape and movement of the cable. The cable is eventually lifting from the ground, which is clearly seen from the z-force plot in Figure 2.9. The x-force plot shows how the force is heavily increasing as the cable is winded.

Fourth Test Last test is moving the top point for a short time, then stopping, then moving it again and stopping. This is interesting in order to see how the drag affects the cable, how a sudden motion influences the mooring line and how it reacts when coming to rest.

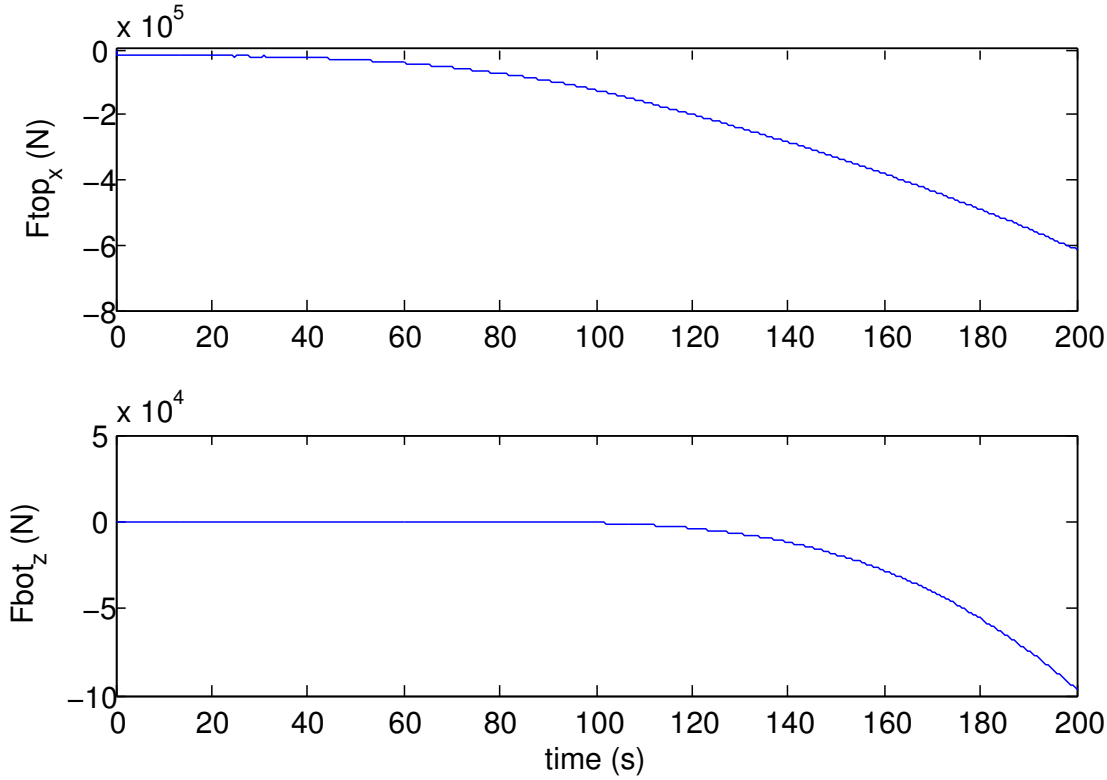

Figure 2.9: The forces in x-direction at the top and in z-direction at the anchor. Third test scenario. It is clearly seen when the cable lifts from the ground.

The input given to the system is shown in Figure 2.10. The top point is first moved diagonally along the x and y axes, then moved further diagonally 90 degrees to the first trajectory.

When looking at the force plots in Figure 2.11 it is quite interesting to see how the forces are having a quite large value when the cable is moving, while they are reduced when it comes to rest. This indicates that the drag forces are quite significant.

It is also seen that the forces settle at a higher value when the cable is stopped further away from the initial point, which is expected.

Another interesting observation is that the anchor is feeling the y-force from the top point translation several seconds after the motion has stopped. The top point starts moving after 10 seconds and stops at 15 seconds, but the force at the anchor is not rising before around 25 seconds. The same phenomena occurs when the top point is moved a second time.

It shows that the motion is using some time to travel down the mooring line.

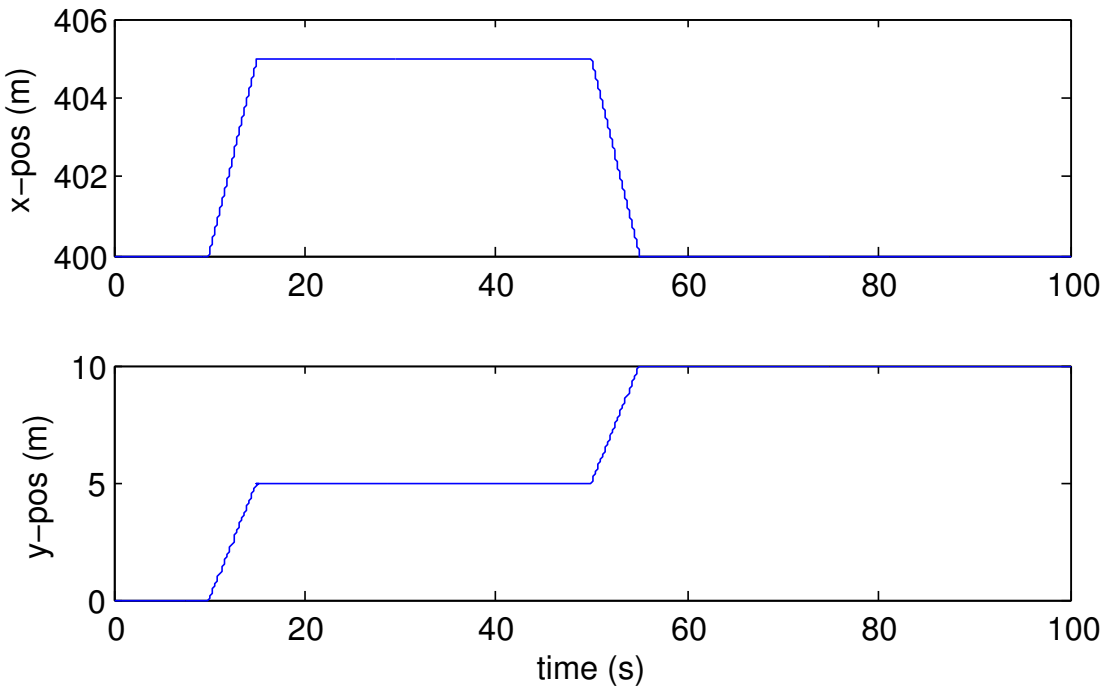

Figure 2.10: The input to test number four. The top point is first moved diagonally along the x and y axes, then moved further diagonally 90 degrees to the first trajectory.

When animating the response (which unfortunately is difficult to include in this paper), it is possible to see how the motions are generating waves along the cable.

The plot also shows how the force is hitting the anchor like a wave, since it has a quite large peak before it settles.

There was no point including the mooring line plot here since the motions are too small to make it interesting.

Combining Single Cables Into a Turret

After concluding that the single mooring line model is working properly, this model can be duplicated and assembled into a turret mooring system with an arbitrary number of mooring lines.

This will now be demonstrated by rotating the coordinate system of each line. This means each line is still working in its own coordinate system, being aligned with its x axis and having its origin at the anchor position. One of the reasons to do it this way is that it makes the initialization of the mooring lines easier, since the initial node coordinates in the line frame will then be the same for each line,

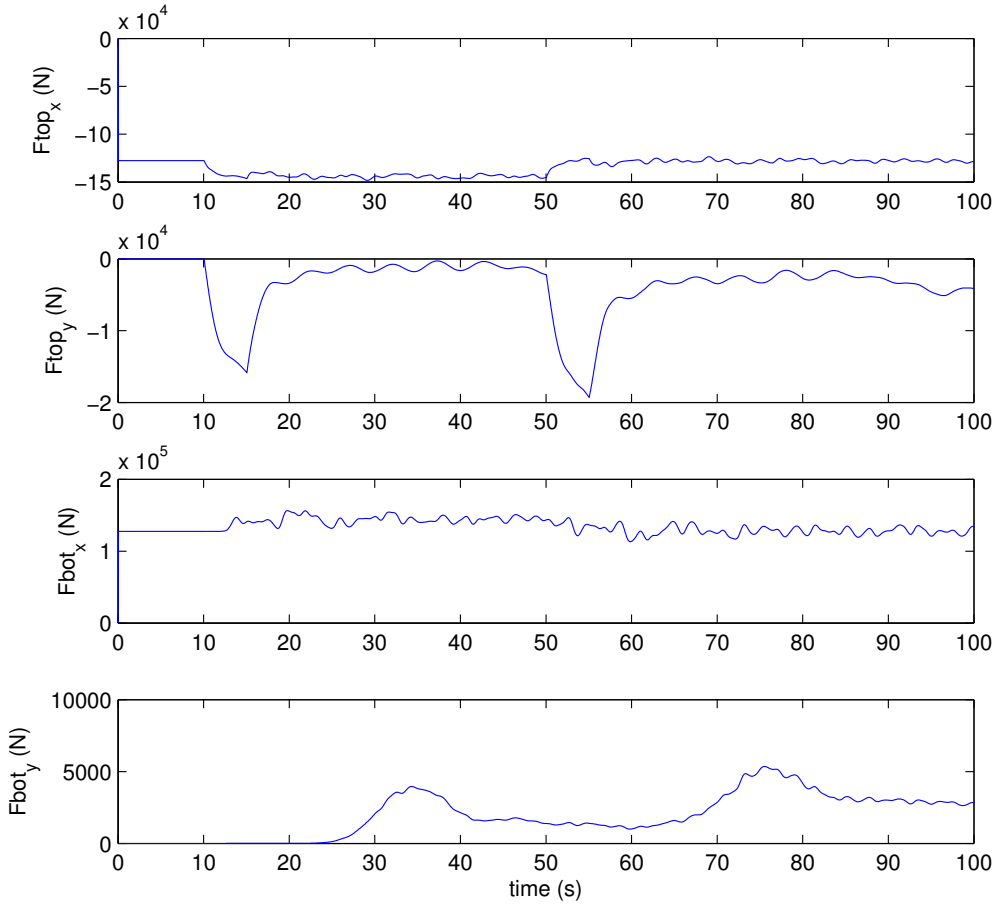

Figure 2.11: The forces in x- and y-direction in both ends of the cable for the fourth test. It is interesting to see how the velocities of the top point is generating significant drag forces.

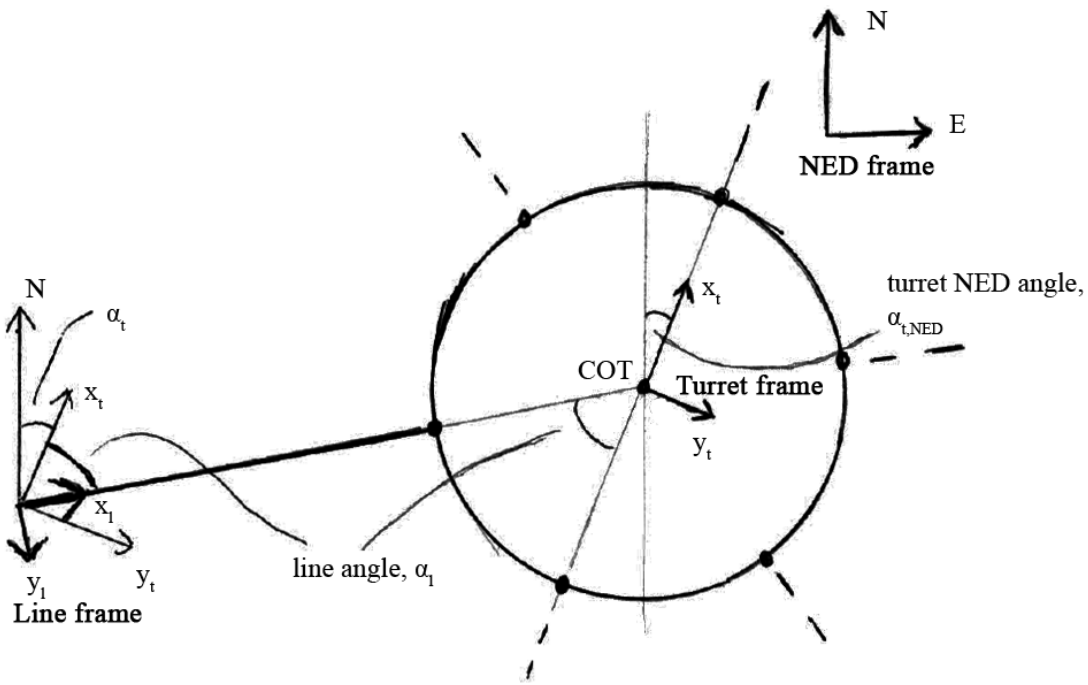

Figure 2.12: Illustration of the turret- and line reference frames, in relation to the NED frame. Each line has its own reference frame aligned with the initial position of the line, meaning the x-axis is going through the anchor point and the cable top point at zero turret NED angle.

no matter where it is located around the turret. This makes it possible to use the same line initialization as initial values for all the lines in the turret.

The forces generated by each line in its coordinate system will then be transferred back to the NED frame. (See Section 2.1.1.)

The different reference frames are illustrated in Figure 2.12.

In addition to the line forces in yaw, sway and heave there can be generated a moment force in yaw, given that the mooring lines are mounted at a certain distance from the center of turret (COT). When the turret is forced to rotate away from its equilibrium, the lines will try to pull it back, generating a moment. Se Figure 2.13

The mooring line model from Figures 2.2 and 2.3 is now expanded as shown in Figure 2.14. It is contained in a block taking four inputs:

- Turret position offset, being how far the turret is located from its equilibrium

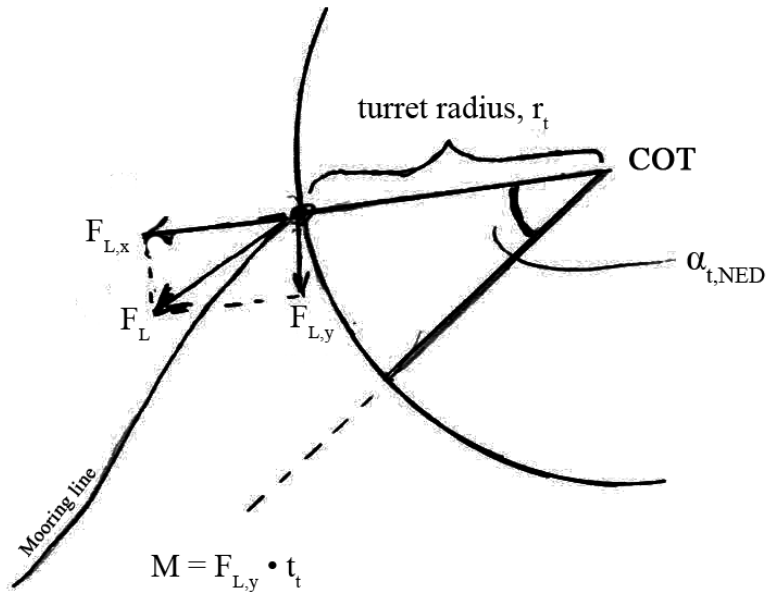

Figure 2.13: The lines will generate a moment on the turret when the turret is forced to rotate.

position.

- Turret NED angle offset, being the angle from its equilibrium.
- Turret diameter: the distance from COT to where the cables are mounted.
- Line angle: The angle of the point where this single line is mounted, in turret frame.

The position- and angle offsets will now need to be converted into a cable top point position, which is what the s-function takes as input. This must also include the offsets caused by the angle offset, meaning the turret radius must be taken account for.

The position offset is initially converted from the NED frame to the turret frame. This is done by the use of a 3 DOF rotation matrix (2.6), as described in Section 2.1.1, where the coordinate system is rotated by the line angle plus the turret angle.

Now, while in the turret reference frame, the turret radius is subtracted from the x coordinate, meaning the input offset is now describing the offset to where the cable top point is actually located. Now, by rotating from the turret frame to the cable frame, the offset will be described in the right coordinates for the FEM. Since the initial state of the cable is not taking account for the turret radius, this

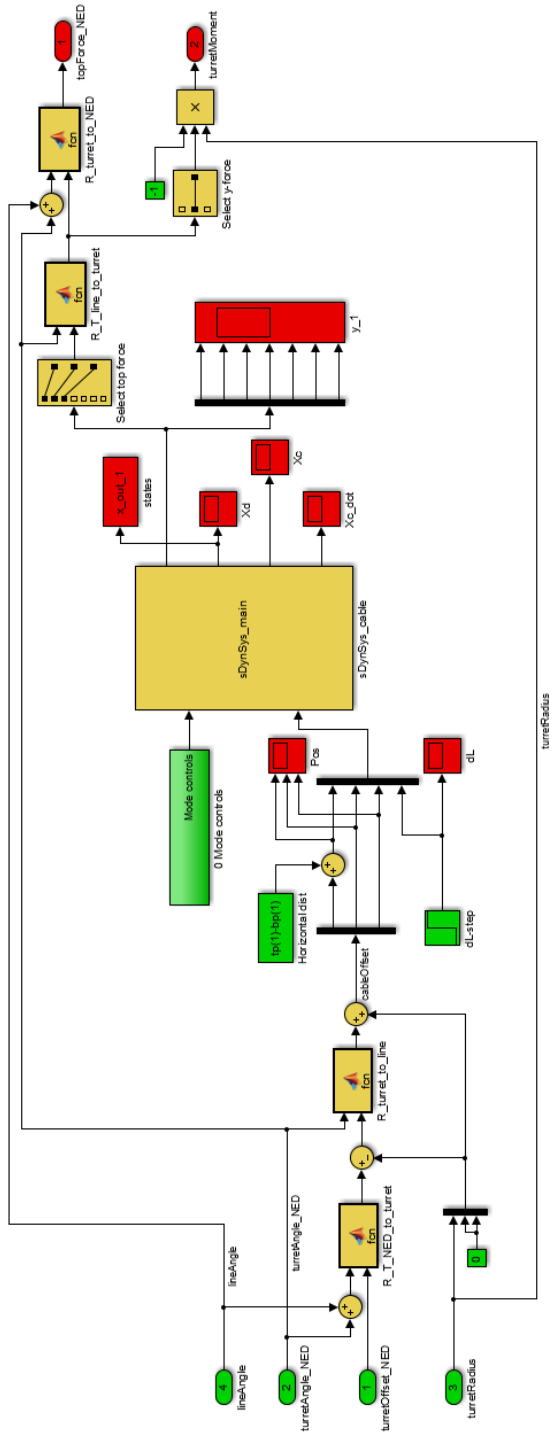

Figure 2.14: The Simulink model for a single cable in a turret. It is contained in a subsystem block, having the inputs turret position offset, turret NED angle, turret radius and the angle this cable is having on the turret. The outputs are the resulting forces from the cable in north, east and down directions, as well as the moment contribution from this cable on the turret. For an enlarged version of this figure, see appendix.

has to be added back to the x value after rotating to line frame. This means that the offset will still be including the turret angle, but the mooring equilibrium will be at zero, not adding the radius.

Before entering as input signals to the s-function the initial distance from the anchor to the top point is added (like in Figure 2.3), since the FEM is using the top point position (in cable frame), and not the offset as input.

The output values are then used to find the turret moment contribution. By rotating back from line frame to turret frame the y-component would be the component normal to the turret radius. By multiplying with the turret radius we will get the moment force.

Finally, rotating back with the turret angle plus the line angle will render the NED force from this cable, which returns as an output together with the moment.

This single cable model can now be duplicated in order to create a turret with an arbitrary number of arbitrarily placed cables.

Figure 2.15 is showing an example of a turret mooring with six lines. This model is then encapsulated in a subsystem taking only a 4DOF turret offset as input and returns forces and moments as output.

Testing the Turret Mooring

The response of the turret mooring is now demonstrated by providing it with a combination of ramp inputs and observing the responses.

The mooring line configuration from Figure 2.15 is used, meaning we have a turret of six evenly distributed lines. The lines are the same as the one described in the beginning of Section 2.2.2.

Since the lines are evenly distributed there should be no forces generated from the mooring system when the turret offset is at zero. It can be seen from Figure 2.18 that this is the case when the input to the system initially remains at zero.

Then the turret is moved along the x-axis (north) before being put to rest for some seconds before being moved back, past its equilibrium and then stopped. At the end the turret is rotated 90 degrees while staying at the same position. The upper plot in Figure 2.17 shows the input.

The force plot in Figure 2.18 is showing how the mooring reacts to its input. It can be seen that the force is taking a step immediately after the turret starts moving. This makes sense due to the drag forces caused by the cables moving through the water. When the turret stops we can see that the force jumps down with around the same amount, which makes sense. It then settles at a negative

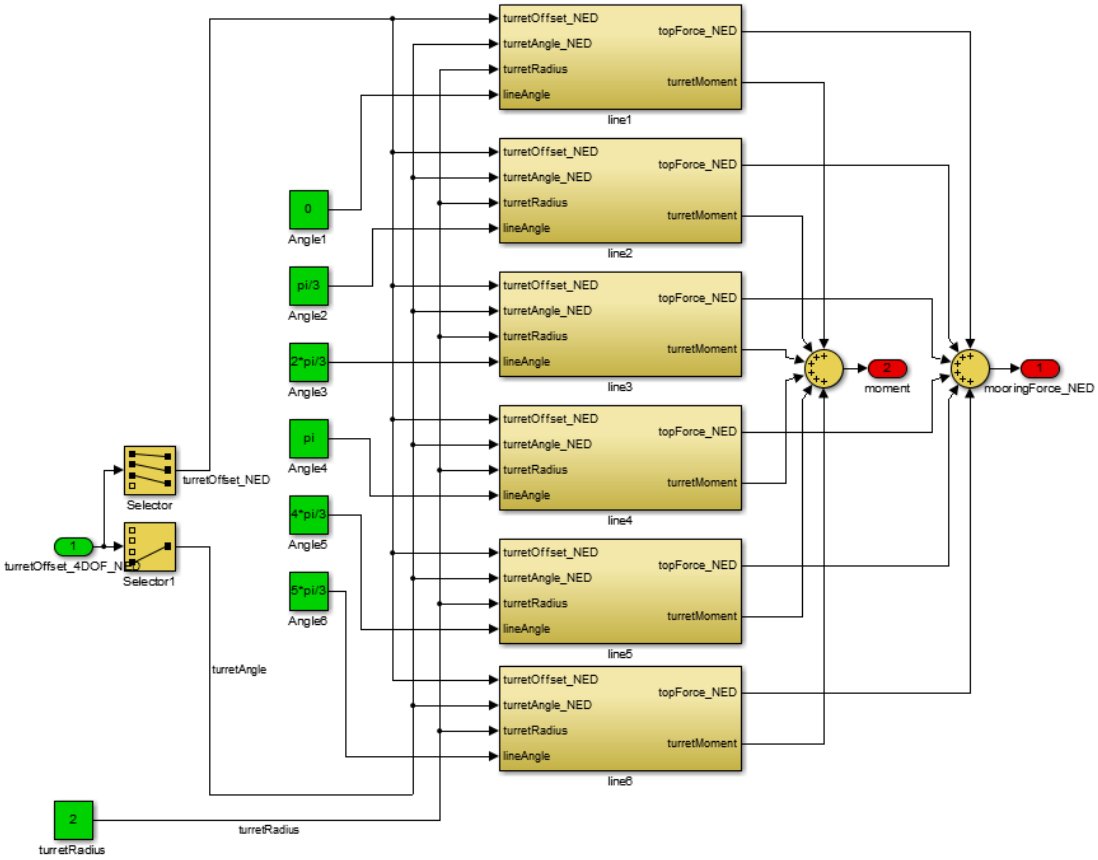

Figure 2.15: The Simulink model for the complete turret mooring. The turret offset and angle is supplied to each cable subsystem, together with the turret radius and the angle of each cable.

value, which is correct since the turret is moved in positive direction. The y-force remains at zero, since the turret is not moved along the y-axis. The z-force is near constant and positive, since the cables are hanging down, pulling in positive z-direction.

When the turret moves back the force jumps the opposite way of the previous time, since the speed is in the opposite direction. The force is reduced, and settles at a positive value, since the turret is put to rest at a negative position along the x-axis.

The moment plot in Figure 2.17 is showing the moment from each line plotted together with the total moment. When the turret rotates towards the end of the simulation it can be seen that the moments from each line is close to similar, which should be the case since the rotation is causing the same effect on each of the cables.

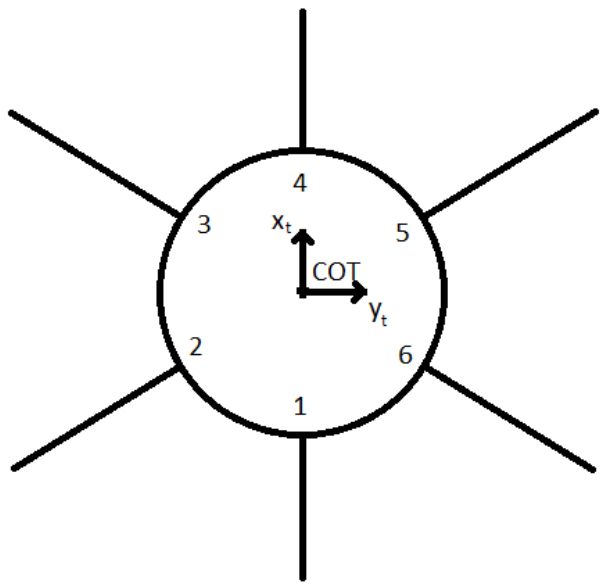

Figure 2.16: The numbering of the lines used in the test setup, as referred to in the text and in Figures 2.15 and 2.19.

It can also be seen that there are generated a moment from some of the cables when the turret is moved along the x-axis. This makes sense since the cables going away from the x-axis will start pulling sideways on the turret. Still, when studying the total moment plot, it is observed that the total moment remains at zero, since the cables on each side of the turret cancel each other out.

Another observation from Figure 2.18 is that the forces are not influenced by the rotation. This is as expected since the increased tension in each line when rotating will cancel each other out. There are still some jumps in the y-force when the turret is rotated, which might be caused by for instance numerical errors. However, these forces are very small compared to the magnitude of the other forces acting on the system, so they can be considered non-existent.

The vertical force should in theory increase slightly when the turret rotates, since all the cables are pulled a bit further from the anchor position. This effect is slightly visible on the plot in Figure 2.18, but the increase is, as expected, very small.

The forces from each of the cables are shown in Figure 2.19, together with the input on the first plot. The first line is the one at 0 degrees, meaning it is entering the turret at negative x-value, going along the x-axis. It is seen that it does not contribute to the force in y-direction, and generates a negative x-force. See Figure 2.16 for how the lines are arranged.

Line 2 and 3 have opposite signs on the x-force, while it can be observed that

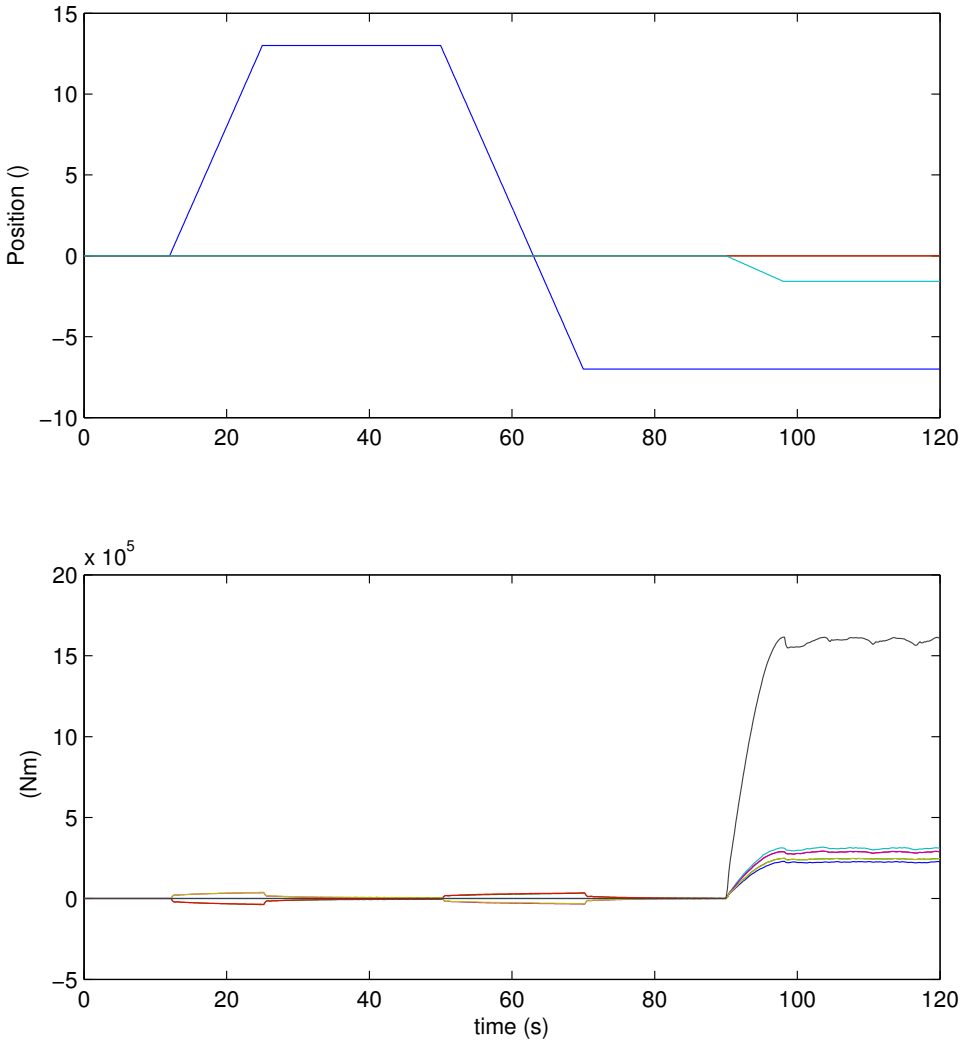

Figure 2.17: The input (upper plot) and resulting moments (lower plot) of the turret mooring system. The moment plot shows the moment from each cable as well as the total moment force. It shows that the moments from each cable are close to equal, although there are some differences caused by the tension differences in the cables due to the offset of the turret.

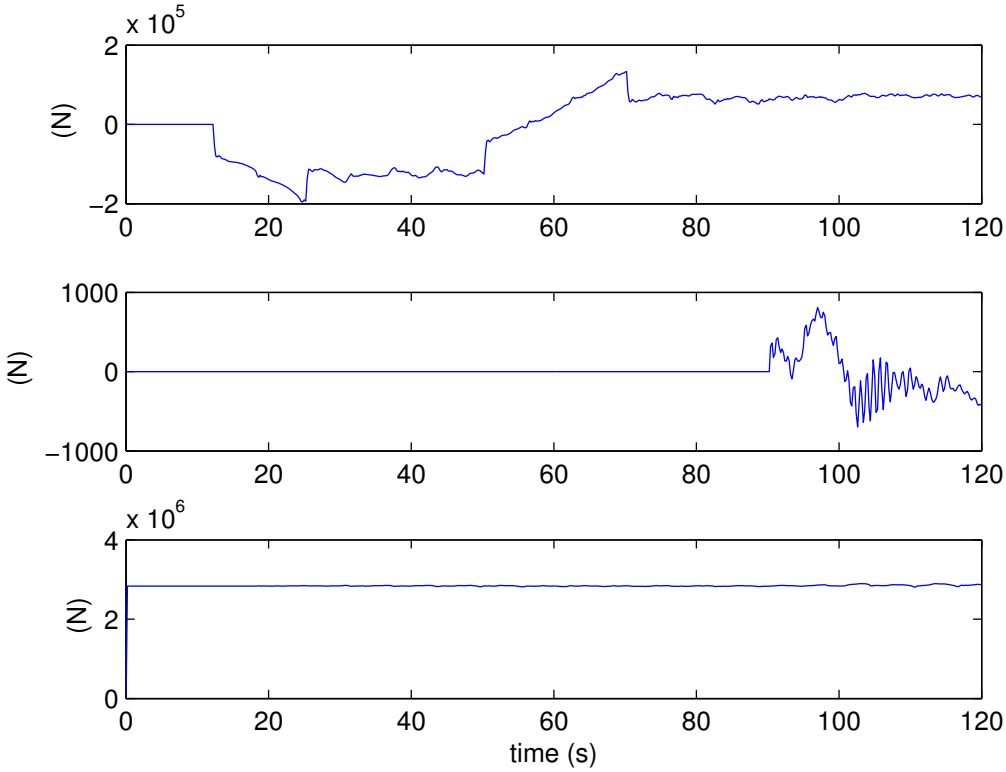

Figure 2.18: The resulting total forces from the turret in x (north), y (east) and z (down) from providing the input from the upper plot in Figure 2.17. There are some oscillations in the force after the turret has stopped moving, which might be caused by the cable wave motions observed and discussed in Section 2.2.2.

what seems to be the drag force is acting in the same direction. The y-forces from these lines are initially the same, but they are influenced in opposite directions from the motion along the x-axis, since they are going in opposite x-directions.

Line 5 and 6 have the opposite reactions from line 3 and 2 (in that order), except from the drag term which is still acting the same way; opposite of the speed. Line 3, which is going straight north, has, line line 1, zero y-force.

Overall, the mooring system model seems to be acting as it should.

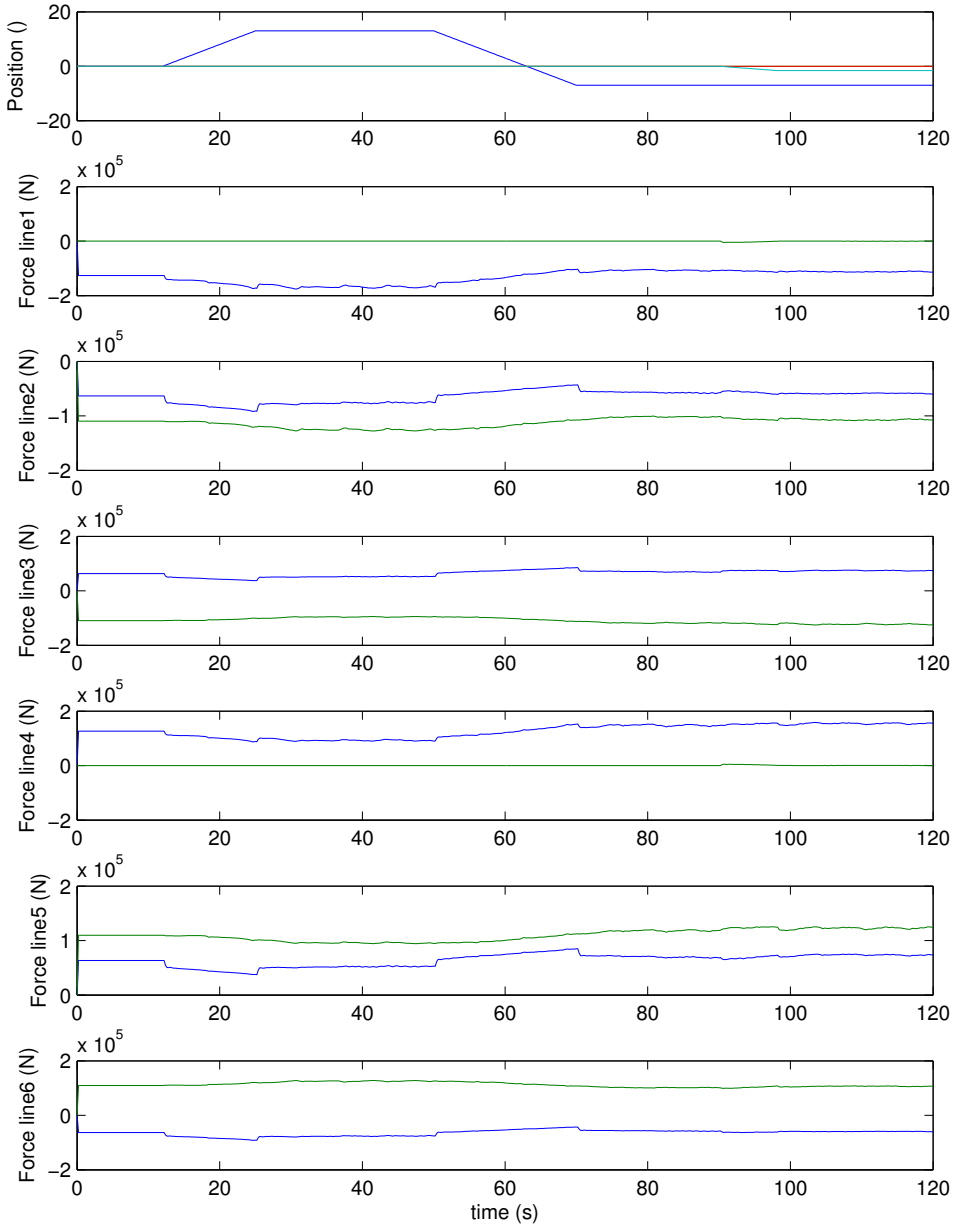

Figure 2.19: The forces from each line on the turret in x (blue) and y (green) directions (NED). The z-forces are left out since they are close to constant and therefore not interesting. See Figure 2.16 for how the lines are arranged. The upper plot shows the input (x-pos, y-pos and angle).

Chapter 3

Control Strategies

3.1 Linearized Model

3.1.1 Linearization Method

For the purpose of stability analysis and controller design, it is desired to have a low-fidelity, linearized control plant model of the mooring system, as discussed in Section 1.1.3. Since the FEM mooring model from Section 2.2.2 is based on numerical simulations, linear coefficients can not be derived directly from the model. A way of estimating these is by running the FEM model with different inputs, recording its behavior and deriving the coefficients from the results.

The linear mooring model is to be used with the linearized (although not entirely linear, due to the rotation matrix) vessel model (2.17). This means that the mooring stiffness coefficient matrix $\boldsymbol{K}$ and the linear mooring damping matrix $\boldsymbol{D}_{moor}$ has to be determined.

The model used in this linearization will be further described in Section 4.1.1.

3.1.2 Determining the Mooring Stiffness Matrix

The stiffness matrix was determined by running the model while giving the turret a stepwise increasing offset, giving it time to settle at each position. The values are then collected and used to estimate a linear coefficient.

The upper plot of Figure 3.1 shows the stepwise input consisting of a sum of ramp functions, meaning the turret will move with a constant velocity between the steps. The position is changed along the x-axis, and the resulting forces are

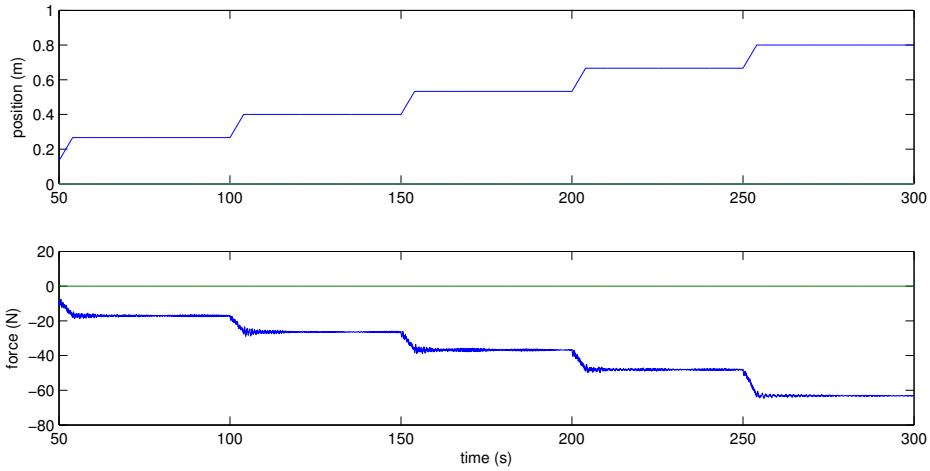

Figure 3.1: Testing the mooring stiffness by moving the turret as shown in the upper plot, resulting in the forces shown in the lower plot. Here the turret is moved along the x-axis.

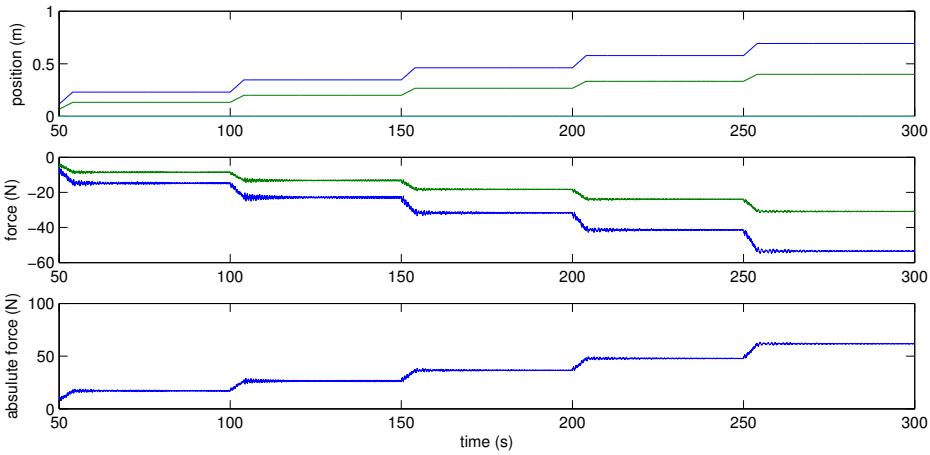

Figure 3.2: Testing the mooring stiffness by moving the turret as shown in the upper plot. Here the turret is moved at a 30 degree angle from the x-axis. The second plot shows the forces along the x- (blue) and y-axes (green) separately, while the lower plot shows the vector norm of these forces, meaning the absolute force.

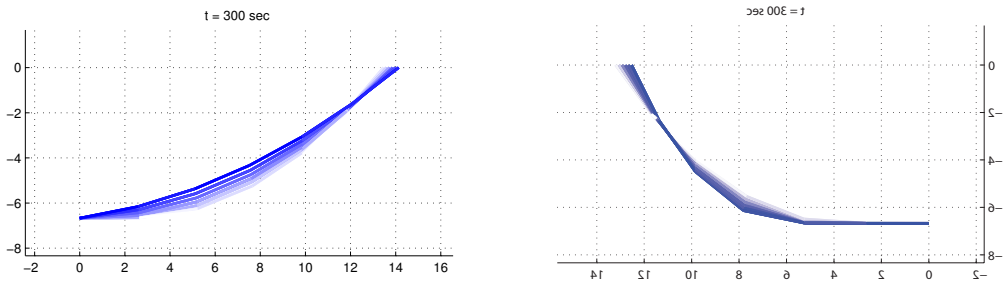

Figure 3.3: A plot of the shape of mooring line 1 (left) and 4 (right) (see Figure 2.16) during the stepwise simulation for stiffness determination while the turret is moving along the positive x-axis. The right plot is mirrored since that shows better how the lines are placed against each other.

Distance from equilibrium (m)	0	0.27	0.40	0.53	0.67	0.80
Force at 0 degrees (N)	0	17.0	26.5	37.0	48.0	63
Force at 30 degrees (N)	0	17.0	26.5	36.5	48.0	61.5

Table 3.1: Table showing the result of the stiffness test.

shown in the lower plot of the same figure.

In order to check the symmetry properties of the mooring system another test is done where the turret is moved at a 30 degree angle from the x-axis. This means the mooring will generate forces in both y- and x-directions. The turret is now moved along an axis lying between two mooring lines, since this is a six line mooring system as shown in Figure 2.16.

The turret is chosen to move from zero to 0.8 meters from its equilibrium, since at 0.8 meters the highest tensioned line is close to being stretched out. This is shown in Figure 3.3 which shows the shape of the two mooring lines facing each other in the xz-plane while the turret is moved along the positive x-axis. It corresponds to moving it 24 meters in full scale.

The values in Table 3.1 is obtained by reading the plots in Figures 3.1 and 3.2. It is seen that the result is nearly the same for the two directions of movement. Plotting these values gives the result seen in Figure 3.4.

It shows that the values are close to linear, but as the position offset gets higher both lines are getting steeper, indicating that linearization is less accurate further away from zero. Taking this into account the first four points were used

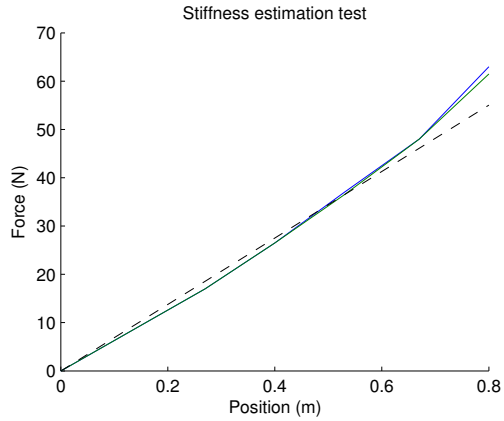

Figure 3.4: The results from the stiffness test. It shows that the values are close to linear, but the curve tends to become steeper for higher values. The chosen linearization is showed as a dashed line.

for making a linear regression. This resulted in the linear coefficients of 69,2 and 68,5 for the two cases respectively. From this result the stiffness coefficient value is chosen as

$$k_{moor} = 68,8N/m \tag{3.1}$$

which is plotted as a dashed line in Figure 3.4.

Due to the symmetry of the turret mooring it is safe to assume the same properties for all directions. Therefore the linearly approximated mooring stiffness matrix in 3DOF results in

$$\boldsymbol{K} = \begin{bmatrix} 68,8 & 0 & 0 \\ 0 & 68,8 & 0 \\ 0 & 0 & 0 \end{bmatrix}. \tag{3.2}$$

The turret is usually freely rotating with respect to the vessel. Assuming this, the restoring force in yaw from the mooring system is assumed to be zero.

3.1.3 Determining the Mooring Damping Matrix

The damping matrix was determined by moving the turret at constant rate while recording the force output, and then moving it through the same trajectory with different velocities. The forces are then compared for the different velocities, and then linearized with respect to velocity.

While the turret is moved with constant velocity, the restoring forces will still

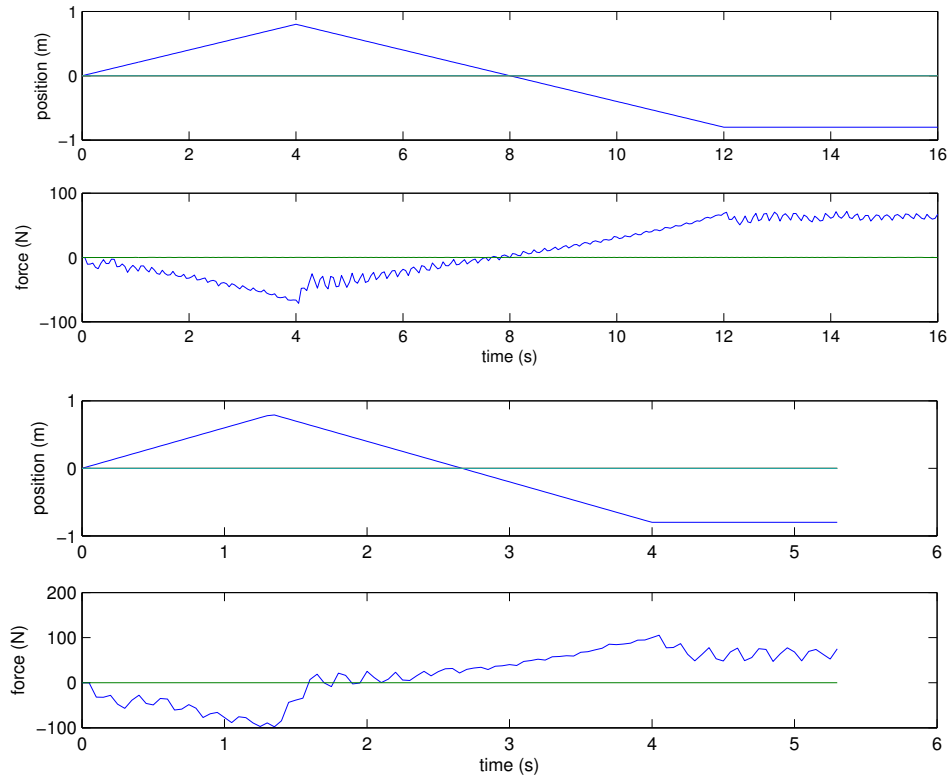

Figure 3.5: Plots of position and forces for two different speeds during estimation of the damping coefficient. Upper plots show the result at 0.2 m/s while the lower plots show result at 0.6 m/s. It is seen that the steps in force when the velocity changes is larger for higher speeds.

make the forces change significantly. Comparing the forces at the same position for different speeds will however give an estimate of how large the damping effect is.

In order to keep a constant velocity as long as possible, the turret is first moved towards the outer limit on the negative x-axis, before moving the opposite direction until it reaches its limit in the opposite direction. This also makes us able to measure the force at the equilibrium point at constant velocity. The turret is moved to 0.8 and then to -0.8, for the same reason as in Section 3.1.2. The speed is ranging up to 1 m/s, corresponding to 5,5 m/s full scale.

To get a more reliable result the forces are compared at two positions; at $x = 0$ and at $x = -0,5$. Measuring at the later occurring point of -0,5 gives the system more time to settle at constant speed and get rid of transient motions. This is seen in Figure 3.5. Since the interesting part here is how the force changes between different speeds, it does not matter that the different positions are having

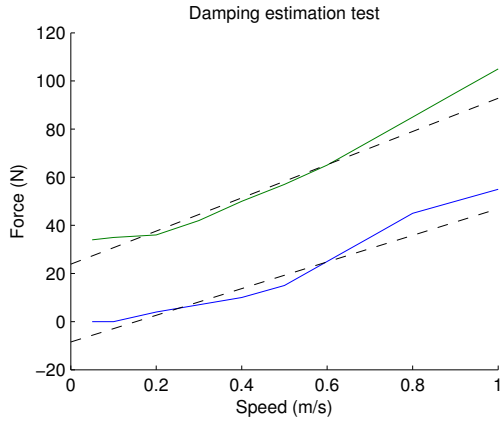

Figure 3.6: Results of plotting the force readings at different speeds. The blue line is the force at x = 0 and the green line is at x = -0.5. The dashed lines are linear regression lines from point 2 to 8 (see Table 3.2).

Speed (m/s)	0.05	0.1	0.2	0.3	0.4	0.5	0.6	0.7	0.8	0.9	1
Force at x=0 (N)	0	0	4	7	10	15	25	35	45	50	55
Force at x=-0.5 (N)	34	35	36	42	50	57	65	75	85	95	105

Table 3.2: Table showing the result of the damping test. Due to oscillatory behavior the readings might be inaccurate.

different restoring force values. It might however be nonlinear effects due to varying tensions in the cables and other factors, which is another reason to do the test at two positions; to see if this gives a significantly different damping result.

The recorded force values are seen in Table 3.2. They are plotted in Figure 3.6. As with the stiffness measurement results the force curve tends to get steeper further away from zero. It might therefore be a good choice to linearize closer to zero, meaning excluding some of the points from the linearization. The curve is also less steep for low velocities, which makes sense. It might therefore be reasonable to exclude also some of the lower points.

Out of eleven points, doing a linear regression on the points 2 to 8 for each series resulted in the two dashed lines in Figure 3.6. The linearization for $x = 0$ resulted in a linear coefficient of 55,4 while at $x = -0,5$ is was 68,9.

The latter value could be given slightly higher voting due to the more stable force value (see Figure 3.5). However, since it is more safe to underestimate the damping when considering for instance stability analysis, the linear damping coefficient is chosen to be

$$d_{moor} = 60\frac{N}{m/s}. \tag{3.3}$$

This value might however not be very accurate, due to the many uncertainties concerning nonlinear effects, and the possibility of inaccurate plot readings.

The resulting linear mooring damping matrix will then become

$$\boldsymbol{D}_{moor} = \begin{bmatrix} 60 & 0 & 0 \\ 0 & 60 & 0 \\ 0 & 0 & 0 \end{bmatrix}. \tag{3.4}$$

The same assumption about a rotating turret can be made when considering the damping, meaning the turret is rotating freely without friction. This results in zero damping contribution from the mooring system in yaw.

The damping matrix can then be added to the linear vessel damping matrix in (2.17). However, if the mooring system would have different damping properties in the north- and east (x and y) directions, the damping matrix would have to be multiplied with a rotation matrix in order to transfer it to vessel frame, meaning it could no longer be combined with the vessel damping matrix.

3.1.4 Including the Mooring with the Arctic Drillship Vessel Model

In order to make a linearized control plant model for the Arctic Drillship described in Section 1.1.7 we need its damping- and mass matrices.

The damping coefficients for this ship were approximated by Kjerstad and Skjetne (2014a) through experimental tests in the simulator. The values were obtained by running the simulated vessel in open water using a constant force input. The result was

$$\boldsymbol{D} = diag(75, 100, 3205). \tag{3.5}$$

The mass matrix $\boldsymbol{M}$ is the sum of the rigid body mass and added mass of the ship. However, the NIT is not incorporating added mass effects (Kjerstad and Skjetne, 2014a), and the mass matrix, following from the rigid body masses of the ship, will therefore be,

$$\boldsymbol{M} = diag(2535, 2535, 8485). \tag{3.6}$$

Now these matrices is used in (2.17) to create a control plant model for the Arctic Drillship,

$$\begin{aligned}\dot{\boldsymbol{\eta}} &= \boldsymbol{R}(\psi)\boldsymbol{\nu} \\ \boldsymbol{M}\dot{\boldsymbol{\nu}} &= -\boldsymbol{D}_{tot}\boldsymbol{\nu} - \boldsymbol{R}^T(\psi)\boldsymbol{K}\boldsymbol{\eta} + \boldsymbol{\tau}_{wind} + \boldsymbol{\tau}_{waves} + \boldsymbol{\tau}_{thr}.\end{aligned} \tag{3.7}$$

where $\boldsymbol{D}_{tot}$ is the sum of the damping matrices,

$$\boldsymbol{D}_{tot} = diag(60, 60, 0) + diag(75, 100, 3205) = diag(135, 160, 3205). \tag{3.8}$$

3.2 Problem Statement

Even though the position moored vessel is a nonlinear system, the results from Section 3.1 are showing that, given a constant heading angle, this is quite close to being a linear system. Using linear design methods and stability analysis is therefore likely to give good results.

Since the linear system from (3.7) has no coupled effects between the 3DOFs, hence all matrices are diagonal, the system can be decoupled into surge, sway and yaw separately. That means we can find the natural period in each DOF according to

$$T_n = \frac{2\pi}{\omega_n} = 2\pi\sqrt{\frac{m}{k}} \tag{3.9}$$

since the natural frequency

$$\omega_n = \sqrt{\frac{k}{m}}. \tag{3.10}$$

where k is the spring stiffness and m is the mass (Tipler and Mosca, 2008). The same applies for rotational motion where the linear stiffness is replaced with the rotational stiffness, while the mass is replaced with the moment of inertia. Bu using the numbers from (3.6) and (3.2) we get

$$T_{n,1} = T_{n,2} = 2\pi\sqrt{\frac{2535}{68,8}} = 38,1s. \tag{3.11}$$

where the indices 1 and 2 denotes surge and sway respectively.

The natural period will be the same for surge and sway since the restoring- and mass values are the same. The damping will on the other hand be different, according to (3.8), so its behavior would not be entirely the same for surge and sway. It should also be noted that this is for the simulated model ship which is not taking account for added mass, as mentioned in Section 3.1.4, which in reality might be different for surge and sway. It would change the total effective mass of the system, so the natural period will be different when including added mass. (For more on added mass, see Faltinsen (1990).)

Since the moored vessel does not have any restoring in yaw without a controller, it will not have any natural period in this DOF either.

The natural period of 38 seconds in surge and sway should be safely outside the range of first order wave loads. Using Froude scaling (Steen, 2011), the time in full scale will be

$$T_{n,S} = T_{n,M} \cdot \sqrt{\lambda} = 38,1 \cdot \sqrt{30} = 209s, \tag{3.12}$$

where λ is the scaling factor and M and S denotes model- and full scale respectively. This natural period is quite large, since the natural period of moored structures is often lying between 80 an 200 seconds (Sørensen, 2012). This might be an indication that the mooring system should have had more stiffness, especially when considering ice loads.

In the north sea waves do rarely have a period above 22 seconds, while the wave spectrum peak lies around 12-15 seconds (Faltinsen, 1990). However these long natural periods can be excited by slowly varying second order wave loads, wind or current.

The control objective for the general station keeping problem is to stay as close as possible to the reference position, or to a slowly varying reference trajectory. In the case of position mooring, as will be discussed in the next section, this reference trajectory can be generated such that the mooring system is utilized as effectively as possible.

This is done while having to compensate for disturbance forces from the environment, being for instance wind, waves, current and ice forces.

In ice infested areas the ice provide damping, reducing the wave height. Wave loads are therefore not so much of a concern in these areas. Wind, current and ice loads are usually the primary concern in these areas, the latter being the most challenging due to its strength and its rapidly, randomly varying behavior.

For this case the control objective for normal conditions might be to alter the natural frequency in surge and sway by adding some restoring force from the controller, in order to make the system respond more quickly and reduce

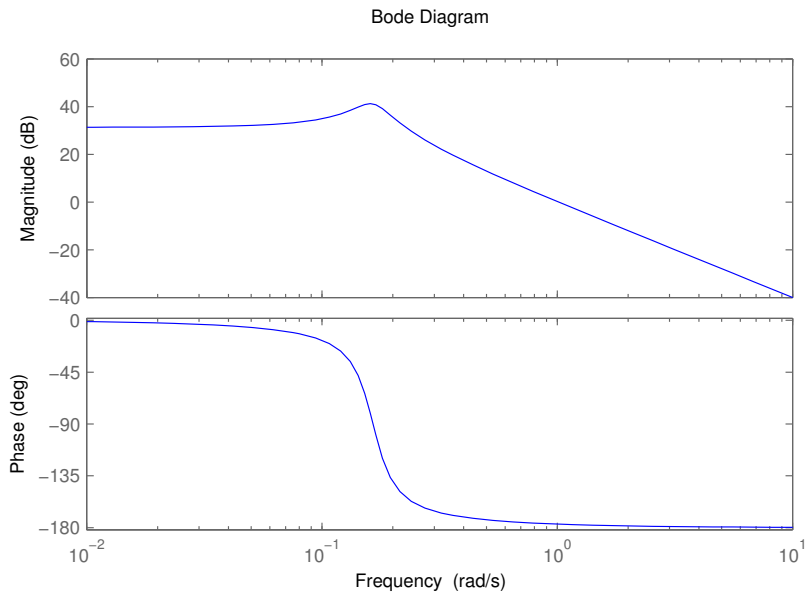

Figure 3.7: Bode diagram of the moored vessel in surge, from force input to position.

oscillations from low frequency disturbances. It is also desired to increase the damping, also to reduce oscillatory behavior. The yaw position is to be controlled entirely by the control system to stay at the desired reference. This should be possible to achieve by using a PID controller (see Fossen (2011)).

3.3 Controller Gains

Since the system can be decoupled it is possible to make a simple analysis of its dynamic properties by looking at one of its DOFs making a single input, single output system. Let us assume a constant heading angle at zero, and consider only the surge motion. We will then have the system equation from (3.7) reduced to

$$\begin{bmatrix} \dot{\boldsymbol{\eta}}_1 \\ \dot{\boldsymbol{\nu}}_1 \end{bmatrix} = \begin{bmatrix} 0 & 1 \\ -\frac{\boldsymbol{K}_{11}}{\boldsymbol{M}_{11}} & -\frac{\boldsymbol{D}_{tot,11}}{\boldsymbol{M}_{11}} \end{bmatrix} \begin{bmatrix} \boldsymbol{\eta}_1 \\ \boldsymbol{\nu}_1 \end{bmatrix} + \begin{bmatrix} 0 \\ 1 \end{bmatrix} \boldsymbol{\tau}_1 \tag{3.13}$$

where the index 1 denotes the first element in the vectors. $\boldsymbol{\tau}_1$ is the total disturbance force in surge. Entering the numbers from (3.8), (3.6) and (3.2) the system matrix will be

$$\begin{bmatrix} 0 & 1 \\ -\frac{\boldsymbol{K}_{11}}{\boldsymbol{M}_{11}} & -\frac{\boldsymbol{D}_{tot,11}}{\boldsymbol{M}_{11}} \end{bmatrix} = \begin{bmatrix} 0 & 1 \\ -\frac{68,8}{2535} & -\frac{135}{2535} \end{bmatrix} = \begin{bmatrix} 0 & 1 \\ -0,027 & -0,053 \end{bmatrix} \tag{3.14}$$

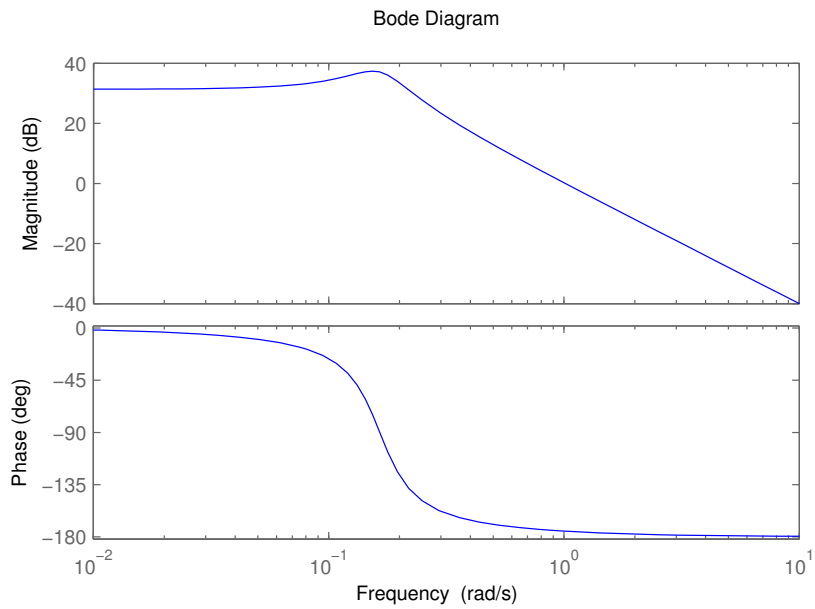

Figure 3.8: Bode diagram of the moored vessel in surge, from force input to position, after adding an active damping of 80 N/$\frac{m}{s}$.

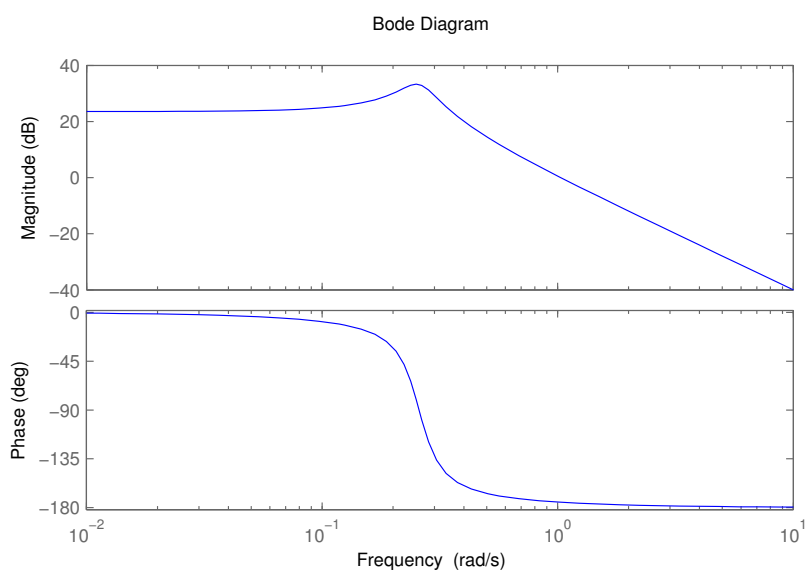

Figure 3.9: Bode diagram of the moored vessel in surge, from force input to position, after adding an active damping of 80 N/$\frac{m}{s}$ and an extra restoring force of 100 N/m.

This is a system on the form $\dot{\boldsymbol{x}} = \boldsymbol{A}\boldsymbol{x} + \boldsymbol{B}\boldsymbol{u}$, which can be used for frequency analysis applying the position η_1 as output by including the output equation on the form $y = \boldsymbol{C}\boldsymbol{x}$,

$$y = \begin{bmatrix} 1 & 0 \end{bmatrix} \begin{bmatrix} \boldsymbol{\eta}_1 \\ \boldsymbol{\nu}_1 \end{bmatrix}. \tag{3.15}$$

By making a bode diagram of this system it is possible to investigate the frequency response of the vessel in surge.

Figure 3.7 shows the bode diagram made with the *bode* function in Matlab, showing that the resonance peak is located around $\omega = 0.17\frac{rad}{s}$, which is consistent with the period of 38.1 s from (3.11). It might be desired to lower the resonance peak by adding some extra damping.

Let us try to add an active damping of 80 N/$\frac{m}{s}$, meaning the thrusters will be commanded to create 80 N of force to counteract a velocity of 1 m/s. Considering the max thrust of 201 N for the Arctic Drillship (see Section 1.1.7), this seems feasible, without doing any further analysis. The result after adding 80 to the damping coefficient is seen in Figure 3.8. The resonance peak is lower, but it is still present.

By using the setpoint chasing technique it can be possible to add stiffness to the system while still utilizing the mooring system. This will affect the resonance peak, which is demonstrated in Figure 3.9 by adding 100 to the stiffness coefficient. This number is just used as an example to show the effect, which is that the resonance peak is shifted to a higher frequency.

The PID controller for yaw angle was showing a satisfactory performance in simulations with a proportional gain of 100. This was used in the decoupled yaw model in Matlab to analyze performance, tuning the damping coefficient by trial and error to a satisfactory value. This turned out to be 180.

Adding integral gain was also done by simulation tests. This resulted in an integral gain of 10.

The controller gain matrices is then turning out to be

$$\boldsymbol{K}_p = diag(0, 0, 100), \boldsymbol{K}_d = diag(80, 80, 180), \boldsymbol{K}_i = diag(0, 0, 10). \tag{3.16}$$

The proportional gains in surge and sway will be determined when applying setpoint chasing.

For more on controller design, bode diagrams or linear systems analysis, see for instance Balchen et al. (2003) or Chen (1999).

3.4 Setpoint Chasing

3.4.1 Introduction

TAPM systems have traditionally been used for adding an additional damping force on moored structures in sway and surge, as well as keeping a steady heading by applying restoring and damping forces in yaw. This means all the restoring forces in surge and sway are relying only on the mooring system. (Nguyen and Sørensen, 2007)

In some cases this can cause problems due to the natural period of the moored structure in sway and surge being close to low frequency, non-linear wave forces and wind. By applying more restoring forces from the thrusters the natural period can be changed, and the amplitude of oscillation can be reduced. However it is not desired to create a proportional controller around the *field zero point* (defined as the equilibrium point of the mooring system, with no external forces), since the thruster action would then start to take parts of the mean load, which for most conditions is the purpose of the mooring system. We would therefore want to introduce proportional control, but without compensating for the mean loads, leaving that part to the mooring system.

This leads to the introduction of setpoint chasing. It is the concept of using a system to create a setpoint close to where the mean loads on the structure and the mooring forces balance each other out, sending this as a reference to the controller. The mooring system will then still take the mean load, while proportional control is applied around this setpoint, tuning the controller gain for obtaining the desired natural frequency and behavior of the system.

By setting outer boundaries for the setpoint it is also possible to use the reference model to prevent overloading the mooring system by applying thruster restoring action when approaching critical mooring line loads.

With setpoint generation the TAPM system can be divided into three levels, as shown in Figure 3.10: Actuator control, plant control and local optimization (Nguyen and Sørensen, 2009a).

The actuator control receives the desired forces to be applied on the vessel, generating a force command for each thruster by using thrust allocation systems.

The plant control is using the vessel measurement data and a position reference to generate the commanded force for the actuator control.

The local optimization layer is where the setpoint is generated by using measurement data and a setpoint generation system. This is fed through a reference model in order to for instance generate smooth transitions when the setpoint is

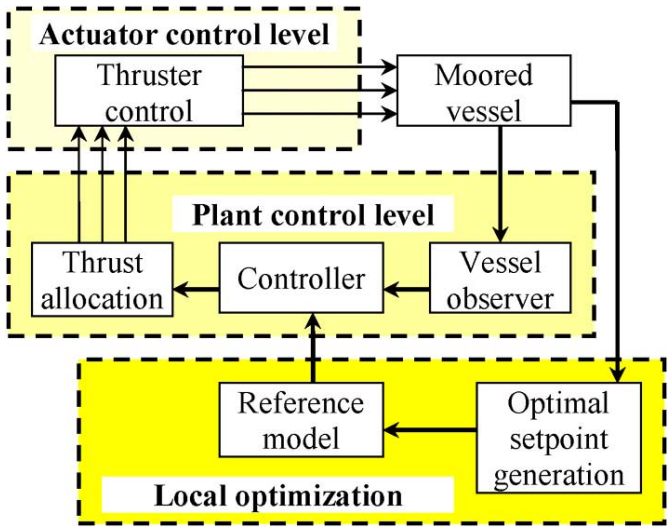

Figure 3.10: The three-leveled structure of a TAPM system using setpoint generation. From Nguyen and Sørensen (2009a).

rapidly changed, so that the vessel is able to follow the reference. It is then provided as a reference signal to the controller (Nguyen and Sørensen, 2009a).

3.4.2 Setpoint Generation: Normal Conditions

The goal of setpoint generation during normal conditions is to find the position where the mean loads are exactly canceled out by the mooring system forces (Nguyen and Sørensen, 2009a). By low-pass filtering the position of the vessel we will achieve a mean position. When the vessel tends to stay at a certain distance from the *field zero point* over a period of time, this will be a result of mean forces acting on the vessel. This assumes we have no integral action from the controller, which would not be necessary for a normal conditions TAPM system anyway, since it is supposed to have a steady state error in order to utilize the mooring system. By using the low-passed position as a setpoint we will therefore get a setpoint moving after the vessel when its position is altered by a mean force.

Now let us define the setpoint as

$$\boldsymbol{\eta}_r = [x_r, y_r]^\top \tag{3.17}$$

the setpoint generation equation can be a low pass filter,

$$\dot{\boldsymbol{\eta}}_r = -\boldsymbol{\Lambda}\boldsymbol{\eta}_r + \boldsymbol{\Lambda}\boldsymbol{\eta}_{xy}, \tag{3.18}$$

where $\mathbf{\Lambda}$ is a diagonal, non-negative matrix of filter cutoff frequencies

$$\mathbf{\Lambda} = diag(1/T_{s1}, 1/T_{s2}), \tag{3.19}$$

and $\boldsymbol{\eta}_{xy}$ is the low frequency (LF) position vector in surge and sway, $\boldsymbol{\eta}_{xy} = [x_{LF}, y_{LF}]^\top$.

This should ensure that the mooring system is utilized with its full potential, while the controller can contribute with both proportional and derivative action to increase the station keeping performance.

3.4.3 Setpoint Generation: Extreme Conditions

During extreme conditions there is a risk of the mean environmental forces being larger than the mooring system can handle. This means that the approach from Section 3.4.2 of generating a setpoint to ensure that the mooring system handles all of the mean load would lead to a potential disaster.

By preventing the setpoint from following the mean position of the vessel, the controller would start to command a restoring force from the thrusters. It would still be desired for the mooring system to handle some of the mean loads. The setpoint should therefore still not be located at the *field zero point*, but somewhere close to where the mooring line loads are at a maximum, still remaining within a certain safety limit.

The critical line load is determined off-line from a structural analysis of the mooring line. Assuming that the line tension is only depending on the distance from the anchor to the ship, the maximum distance to avoid critical line tensions can be predetermined. Since this does not consider for instance current and wave loads on the cables a significant safety margin has to be incorporated (Nguyen and Sørensen, 2009a). Defining the safety factor γ and critical tension T_{crit} it can be stated that the horizontal distance from the anchor to the turret has to satisfy for each line i

$$f(X_i^{hor}) < \gamma T_{crit} \tag{3.20}$$

where the line force $f(X_i^{hor})$ is a function of the horizontal distance only, assuming constant vertical distance from the anchor to the ship. This means the critical horizontal distance can be written (Nguyen and Sørensen, 2009a)

$$X_{i_{crit}}^{hor} = f^{-1}(\gamma T_{crit}). \tag{3.21}$$

For a turret moored vessel this would imply that there is a maximal radius of which the turret has to stay inside to avoid critical line tensions. By incorporating

this into the setpoint generating algorithm, it can be ensured that the setpoint will always be set to avoid too large line tensions while still ensuring maximal utilization of the mooring system.

3.4.4 Controller Choice for Different Conditions

For TAPM systems without setpoint chasing the controller will normally not be used for either proportional or integral control action in surge or sway, as mentioned in Section 3.4.1. This is because these modes are supposed to be handled by the mooring system. The controller will only be used for damping action in surge and sway, as well as PID control in yaw, to keep the heading angle as desired.

When introducing setpoint chasing proportional control will also be introduced in surge and sway. A general PID control law can be defined, as in Nguyen and Sørensen (2007),

$$\begin{aligned} \dot{\boldsymbol{\xi}} &= \tilde{\boldsymbol{\eta}} \\ \boldsymbol{\tau}_c &= -\boldsymbol{H}_i \boldsymbol{K}_i \boldsymbol{R}^\top(\psi)\boldsymbol{\xi} - \boldsymbol{H}_p \boldsymbol{K}_p \boldsymbol{R}^\top(\psi)\tilde{\boldsymbol{\eta}} - \boldsymbol{H}_d \boldsymbol{K}_d \hat{\boldsymbol{\nu}}, \end{aligned} \tag{3.22}$$

with $\tilde{\boldsymbol{\eta}} = \hat{\boldsymbol{\eta}} - \boldsymbol{\eta}_d$, $\boldsymbol{\eta}_d$ being desired position and heading, $\hat{\boldsymbol{\nu}}$ is the velocity vector, $\boldsymbol{K}_p$, $\boldsymbol{K}_i$ and $\boldsymbol{K}_d$ are proportional, integral and derivative control gain matrices and $\boldsymbol{H}_p$, $\boldsymbol{H}_i$ and $\boldsymbol{H}_d$ are projection matrices used to enable and disable the controller modes. $\boldsymbol{\tau}_c$ is the commanded force from the controller, $\boldsymbol{\xi}$ is the integrator state.

For instance setting $\boldsymbol{H}_i = \boldsymbol{H}_p = \boldsymbol{H}_d = diag(0, 0, 1)$ will make this a PID controller for heading only, while setting $\boldsymbol{H}_p = diag(1, 1, 0)$ will activate proportional control in surge and sway (Nguyen and Sørensen, 2007).

Controller for calm sea conditions

As suggested in Nguyen and Sørensen (2007), calm conditions will only require heading control. The mooring system will be sufficient for keeping the ship in its position, but since it provides negligible stiffness in yaw it is still necessary to have heading control from the thrusters.

Controller for Normal Sea Conditions

During normal sea conditions it is useful to enable damping from the controller to reduce the motions on the vessel. Also, when using setpoint chasing, the

Heading PID	Damping	Proportional	Integral	Sea state
✓				Calm sea
✓	✓	✓		Normal sea
✓	✓	✓	✓	Extreme sea

Table 3.3: TAPM controller modes for different sea states when using setpoint chasing. Modified from Nguyen and Sørensen (2007).

proportional controller can be activated, using a reference input from the setpoint generation algorithm.

Since the setpoint is following the vessel position in order to optimize use of the mooring system, the thrusters are not supposed to provide any mean load compensation. Integral control should therefore not be activated here.

Heading PID control will still be activated.

Controller for Extreme Sea Conditions

During extreme conditions thruster assistance might be needed to reduce tensions on the mooring lines, as discussed in Section 3.4.3. Since the setpoint is now prevented from following the vessel position, integral action can be activated to remove stationary offsets away from the setpoint. Now the thrusters will provide mean force compensation, and since the setpoint should be located at an offset from the mooring system equilibrium, the mooring lines should be providing mean force compensation together with the thrusters.

When going back from extreme conditions to normal conditions the integral action should again be deactivated and the integrator state should be reset.

See Table 3.3 for an overview of the control modes in different sea states.

3.4.5 Creating a Setpoint Generation Model

A way of making a setpoint generation model in Simulink is now demonstrated.

Lowpass Filter for Normal Conditions Setpoint

As discussed in Section 3.4.2 the setpoint for normal conditions can be a low pass version of the low frequency position of the vessel. A low pass filter in Simulink is created here by using a transfer function block with the time constant matrix

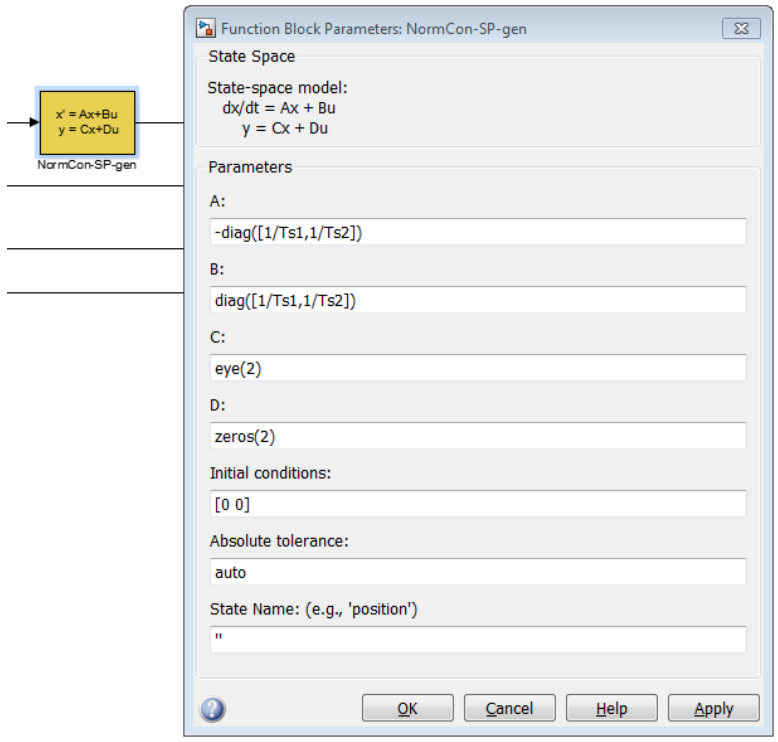

Figure 3.11: Transfer function block in Simulink for a normal condition setpoint. Low-pass filter with time constants Ts1 and Ts2.

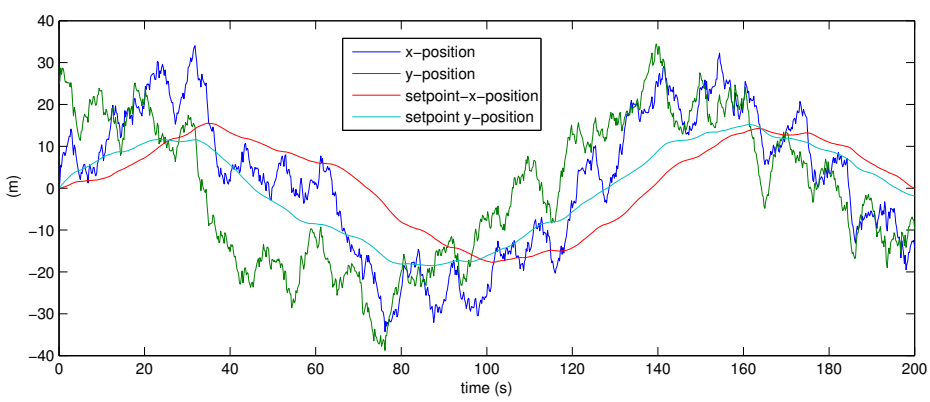

Figure 3.12: Plot of position input and setpoint position output from the normal conditions setpoint generation. The filter is here using time constants $T_{s1} = T_{s2} = 20$.

from (3.18) as both the system matrix A and the input matrix B as shown in Figure 3.11.

By generating a position signal with a random noise signal added, feeding it

into the lowpass filter setpoint generation we can see from Figure 3.12 that the output is a much smoother version of the position. This can then be used as a setpoint for normal conditions.

Switching Between Setpoint Conditions

A challenge when using different models for different conditions is how to switch between the different methods. The criteria for switching, as in when to switch back and forth between the modes, is one challenge. When operating close to the intersection area between the modes, there is another challenge to avoid switching back and forth all the time, causing chattering (as described in for instance Nguyen and Sørensen (2009b)).

One way of avoiding chattering is by using hysteresis, which is that the system remembers its last value, and holds it until a certain distance past the switching limit. Then it uses the new value until it has passed the limit by a certain distance in the other direction.

Another solution is to create some mechanism of fading between the modes, creating a smooth transition by using both modes at once during the transition period.

In this case with setpoint generation, since it is just a matter of preventing the setpoint of moving outside a certain limit, it should be possible to create a solution similar to the fading method by slowing down the movement of the setpoint when it approaches the limit, then stopping it completely when it is about to pass it. Below it is demonstrated a way of doing this in Simulink by making a limiter on the output from the low pass filter used for setpoint generation.

A Setpoint Radius Limiter for Extreme Conditions

The goal is to make a function that takes the lowpass-filtered setpoint from the normal condition setpoint generator and limit it from passing outside the maximum radius of the mooring system. This is done by using a Matlab script block connected to the output from the lowpass filter, as in Figure 3.13.

The following code is used inside the Matlab function block:

```
function sp_o = spLimiter(sp,fzp,rLimit)
%# Takes a 2DOF setpoint (NED) and limits it by the specified radius.
%
% Inputs:
%   sp - setpoint
%   fzp - field zero point
```

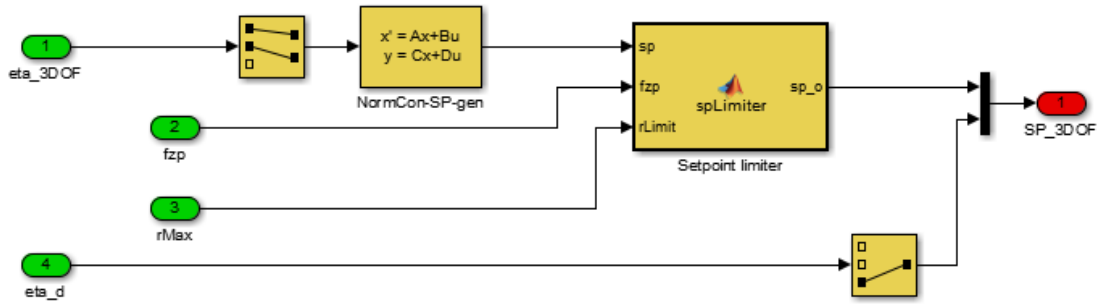

Figure 3.13: Simulink modeled setpoint generator including radius limiting. The yaw reference is used to feed straight through to the controller.

```
%    rLimit - radius limit
%
% Outputs:
%    sp_o - new setpoint

edgyness = 5;          % Sharpness of edge when limiting starts.
slowdownFactor = 0.9;  % Limits the steepness to prevent overshoot.

sp_fz = slowdownFactor*(sp-fzp); % Vector from fzp to sp
offst = norm(sp_fz);             % Length from fzp to sp
dir = sp_fz/offst;               % Unit vector
diff = -rLimit*dir+sp_fz;        % Vector from max radius to sp

limiting = (offst/rLimit)^edgyness; % Ratio of limiting
if (limiting > 1)                % When ratio is 1 the setpoint will be
    limiting = 1;                % at the edge. If zero the setopint
end                              % will not be limited.

sp_o = fzp+sp_fz-limiting*diff;

end
```

It will take the ratio corresponding to how far the setpoint is from field zero compared to how far away the limit is, and take this number to the power of some number (5 in the above code) in order to make the limiting low when far from the limit and rapidly increasing (until it hits 1) when closer to the limit.

This number will then correspond to how much of the distance from the setpoint to the limit that is to be subtracted from the setpoint, as handled by the last line: `sp_o = fzp+sp_fz-limiting*diff`. In other words, if the limiting is zero then the setpoint will not be changed, but if it is 1 the setpoint will be changed

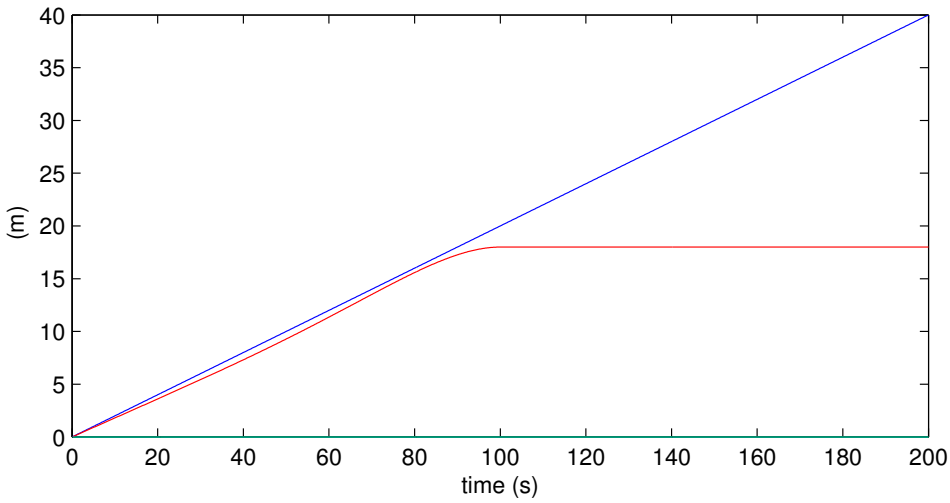

Figure 3.14: Applying a ramp input (blue) to the x-position of the setpoint limiter. The output (red) is limited when the radius approaches 18.

all the way towards the limit.

To prevent the output from overshooting, meaning the setpoint will be further out than the lowpass-setpoint, the input vector is scaled down by a factor (slowdownFactor).

The result is that the new setpoint is slowed down when it approaches the limit, creating a smooth transition between following the lowpass filtered setpoint and staying at the outer limit. This is demonstrated by applying a ramp input to the limiter having a radius limit of 18. The plot in Figure 3.14 shows how it works.

Now, by trying with the same input as when testing the lowpass filter in Figure 3.12 we get the setpoint trajectory as shown in Figure 3.15. It is seen how the setpoint is restricted at the limit. The plot also shows that the setpoint tends to stay a bit closer to field zero when fed through the limiter, as is also seen in Figure 3.12. This means the mooring system starts to get a little help from the thrusters before it really needs it, although it is not much before it reaches the limit. It is also better than the opposite case of the new setpoint overshooting, meaning the mooring and thrusters will work against each other. This is why the limiting (`slowdownFactor`) is added in the Matlab function.

In what degree this smooth transition, causing the setpoint to lag a little behind, is really needed is a matter of how sensitive the system is to sudden changes in the setpoint. It could also be solved by leaving it to the reference model to create smooth transitions, while allowing sudden jumps in the generated

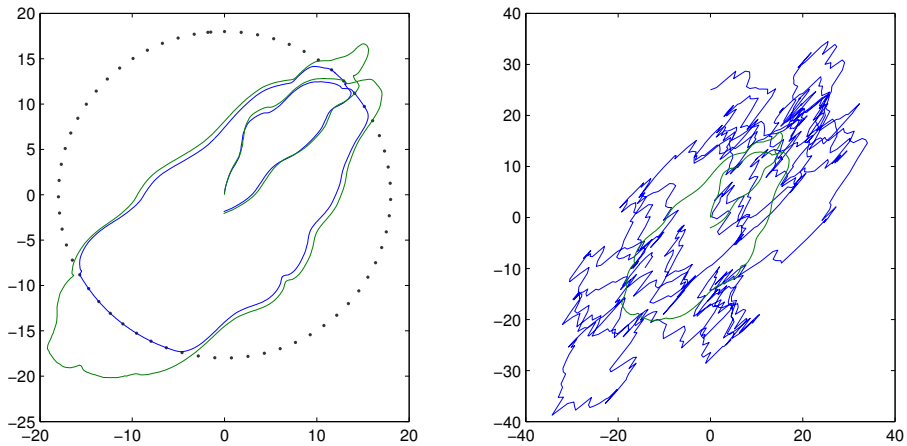

Figure 3.15: Trajectory plot of the setpoint (green) together with the input position (blue) on the right, and the setpoint (green) together with the setpoint restricted by the radius limiter (blue) to the left. The radius limit is set to 18 meters (dotted line) and the input and lowpass filter settings are the same as int Figure 3.12.

setpoint.

3.4.6 Stability Analysis of a TAPM Vessel Using Setpoint Chasing

Linearization

A linearization of the dynamic system around a working point is a useful way of simplifying the process of analyzing the stability properties of the system. Depending on how the nonlinearities behave it can in some cases be sufficient to analyze the linearized system. For a TAPM vessel the most significant nonlinearities are nonlinear damping, other nonlinear mooring forces and the rotation matrix (2.6) converting between NED and vessel coordinates.

A linear approximation of the mooring forces can be achieved by looking at the catenary equations for a mooring line or by analyzing the behavior of the FEM mooring model from Section 2.2.2. The damping can also be assumed linear for most purposes. A station keeping vessel will have small velocities, meaning nonlinear damping phenomena will also be small compared to linear effects.

By assuming the angle of the vessel is staying close to zero degrees, the rotation

matrix from (2.6) can be assumed to be $\boldsymbol{R}(\psi) \approx \boldsymbol{I}$. For analyzing the setpoint chasing behavior this should be a good approach, since the setpoint generation is only considering motions in the xy-plane, independently on the yaw angle ψ. The behavior should also be similar for all yaw angles.

Without including the external disturbance forces, we will then have turned (2.17) into

$$\begin{aligned} \dot{\boldsymbol{\eta}} &= \boldsymbol{R}(\psi)\boldsymbol{\nu} \approx \boldsymbol{I}\boldsymbol{\nu} = \boldsymbol{\nu} \\ \boldsymbol{M}\dot{\boldsymbol{\nu}} &= -\boldsymbol{D}\boldsymbol{\nu} - \boldsymbol{R}^T(\psi)\boldsymbol{K}\boldsymbol{\eta} + \boldsymbol{\tau}_{thr} \approx -\boldsymbol{D}\boldsymbol{\nu} - \boldsymbol{K}\boldsymbol{\eta} + \boldsymbol{\tau}_c \end{aligned} \tag{3.23}$$

where $\boldsymbol{M} = \boldsymbol{M}_{RB} + \boldsymbol{M}_A$ (mass and added mass), $\boldsymbol{D}$ is linear damping and $\boldsymbol{K}$ is linear mooring force. This will be a 3DOF model for the LF motions of the vessel. It is also assuming $\boldsymbol{\tau}_{thr} \approx \boldsymbol{\tau}_c$, meaning the thrusters will deliver the commanded force within a short amount of time.

The commanded thruster force $\boldsymbol{\tau}_c$ is determined by the controller. Using the controller from (3.22) for normal conditions; with proportional and damping action (see Table 3.3), we get

$$\boldsymbol{\tau}_c = -\boldsymbol{K}_p\tilde{\boldsymbol{\eta}} - \boldsymbol{K}_d\boldsymbol{\nu}, \tag{3.24}$$

assuming, like in (3.23), that $\boldsymbol{R}^\top(\psi) \approx \boldsymbol{R}(\psi) \approx \boldsymbol{I}$. $\tilde{\boldsymbol{\eta}} = \boldsymbol{\eta} - \boldsymbol{\eta}_d$, where $\boldsymbol{\eta}_d$ is the desired position, which is the xy-reference from the setpoint generator and the desired yaw angle, see (3.26). $\boldsymbol{K}_p$ is the proportional controller gain and $\boldsymbol{K}_d$ is the derivative controller gain.

The setpoint generator adds the differential equation from (3.18) to the system,

$$\dot{\boldsymbol{\eta}}_r = -\boldsymbol{\Lambda}\boldsymbol{\eta}_r + \boldsymbol{\Lambda}\boldsymbol{\eta}_{xy}, \tag{3.25}$$

where $\boldsymbol{\Lambda}$ is the matrix of filter cutoff frequencies from (3.36).

Since $\boldsymbol{\eta}_r$ is the setpoint position in the xy-plane, $\boldsymbol{\eta}_d$ would also have to include the desired yaw angle,

$$\boldsymbol{\eta}_d = \begin{bmatrix} \boldsymbol{\eta}_r \\ \psi_r \end{bmatrix}. \tag{3.26}$$

Also, the vessel position in the xy-plane, $\boldsymbol{\eta}_{xy}$, can be rewritten, in order to be a function of $\boldsymbol{\eta}$,

$$\boldsymbol{\eta}_{xy} = \begin{bmatrix} 1 & 0 & 0 \\ 0 & 1 & 0 \end{bmatrix} \boldsymbol{\eta}. \tag{3.27}$$

Our system of equations is then becoming

$$
\begin{aligned}
\dot{\boldsymbol{\eta}} &= \boldsymbol{\nu} \\
\boldsymbol{M}\dot{\boldsymbol{\nu}} &= -\boldsymbol{D}\boldsymbol{\nu} - \boldsymbol{K}\boldsymbol{\eta} - \boldsymbol{K}_p\boldsymbol{\eta} + \boldsymbol{K}_p \begin{bmatrix} \boldsymbol{\eta}_r \\ \psi_r \end{bmatrix} - \boldsymbol{K}_d\boldsymbol{\nu} \\
\dot{\boldsymbol{\eta}}_r &= -\boldsymbol{\Lambda}\boldsymbol{\eta}_r + \begin{bmatrix} \boldsymbol{\Lambda} & \boldsymbol{0} \end{bmatrix} \boldsymbol{\eta}
\end{aligned} \tag{3.28}
$$

Rewritten to matrix form we get a system on the form

$$
\begin{bmatrix} \dot{\boldsymbol{\eta}} \\ \dot{\boldsymbol{\nu}} \\ \dot{\boldsymbol{\eta}}_r \end{bmatrix} = \boldsymbol{A} \begin{bmatrix} \boldsymbol{\eta} \\ \boldsymbol{\nu} \\ \boldsymbol{\eta}_r \end{bmatrix} + \boldsymbol{B}\psi_r, \tag{3.29}
$$

where

$$
\boldsymbol{A} = \begin{bmatrix} \boldsymbol{0} & \boldsymbol{I}_3 & \boldsymbol{0} \\ -\boldsymbol{M}^{-1}(\boldsymbol{K}+\boldsymbol{K}_p) & -\boldsymbol{M}^{-1}(\boldsymbol{D}+\boldsymbol{K}_d) & \boldsymbol{M}^{-1}\boldsymbol{K}_{p,xy} \\ \boldsymbol{\Lambda}_{3DOF} & \boldsymbol{0} & -\boldsymbol{\Lambda} \end{bmatrix}, \tag{3.30}
$$

$$
\boldsymbol{B} = \boldsymbol{K}_p \begin{bmatrix} 0 \\ 0 \\ 1 \end{bmatrix}, \tag{3.31}
$$

defining

$$
\boldsymbol{K}_{p,xy} = \boldsymbol{K}_p \begin{bmatrix} \boldsymbol{I}_2 \\ 0 \end{bmatrix} \tag{3.32}
$$

$$
\boldsymbol{\Lambda}_{3DOF} = \begin{bmatrix} \boldsymbol{\Lambda} & \boldsymbol{0} \end{bmatrix} \tag{3.33}
$$

For this linear system to be stable, it has to have all its poles in the left half plane, meaning the real parts of all the eigenvalues of the system matrix $\boldsymbol{A}$ has to be negative (Balchen et al., 2003).

It is also worth to notice that the only input to this system is the desired yaw angle, since the x and y-positions are determined by the mooring system and the automatically generated setpoint.

Filling in the Numbers

In order to find the actual placement of the poles for this system, we will need to fill out the values for the matrix A. That means we must obtain numerical values

for the mass matrix $\boldsymbol{M}$, the damping matrix $\boldsymbol{D}$, the mooring stiffness matrix $\boldsymbol{K}$, the setpoint time constants $\boldsymbol{\Lambda}$ and the controller gains $\boldsymbol{K}_p$ and $\boldsymbol{K}_d$.

For this analysis, data for the model scale Arctic drillship (see Section 1.1.7) used in the NIT (see Section 1.1.7) is used, since the system is going to be utilized in this simulator later.

Using the mass matrix (3.6) and the damping matrix (3.5), what is left is to determine the controller proportional- and damping gains an the setpoint generator cutoff frequencies.

The proportional controller gains will determine how much more stiffness to add to the system besides the mooring stiffness. It will also be important to ensure satisfactory performance when approaching the outer limit, since it will be responsible for holding the ship back in order to prevent mooring overload. It may be desired to have some sort of switching mechanism to turn on integral action when approaching the setpoint limit. If necessary the proportional gains can also be changed, depending on the control objectives.

In this case the proportional gain will remain the same for all conditions. The choice depends of what natural period is desired for the system. Let us pick 20 seconds as the desired natural period. This gives

$$k = \frac{4\pi^2 \cdot 2535}{20^2} = 250N/m. \tag{3.34}$$

according to (3.11). Subtracting the mooring stiffness of 68.8 gives a needed extra stiffness of 181 N/m. That can be applied as the proportional controller gain.

The cutoff frequency of the SP generator should be significantly lower than the natural frequencies of the system (meaning the time constants should be higher than the natural periods). Setting the time constants to 200 s gives

$$\boldsymbol{\Lambda} = diag(0.005, 0.005), \tag{3.35}$$

The damping can be set to the values used in Section 3.3, meaning

$$\boldsymbol{K}_d = diag(80, 80, 180), \tag{3.36}$$

The damping- and proportional yaw control gains will also be set as in Section 3.3, but since the yaw motion is assumed decoupled from the sway- and surge motions it will not have any interaction with the setpoint chasing dynamics.

By inserting all these numbers the system matrix becomes

$$\begin{bmatrix} 0 & 0 & 0 & 1 & 0 & 0 & 0 & 0 \\ 0 & 0 & 0 & 0 & 1 & 0 & 0 & 0 \\ 0 & 0 & 0 & 0 & 0 & 1 & 0 & 0 \\ -0.099 & 0 & 0 & -0.061 & 0 & 0 & 0.071 & 0 \\ 0 & -0.099 & 0 & 0 & -0.071 & 0 & 0 & 0.071 \\ 0 & 0 & -0.011 & 0 & 0 & -0.399 & 0 & 0 \end{bmatrix} \tag{3.37}$$

which has the eigenvalues

$$\begin{aligned} \lambda_1 &= -0.032 \pm 0.31i, \\ \lambda_2 &= -0.0014, \\ \lambda_3 &= -0.037 \pm 0.31i, \\ \lambda_4 &= -0.367 \\ \lambda_5 &= -0.0014 \\ \lambda_6 &= -0.032. \end{aligned} \tag{3.38}$$

These do all have negative real values, implying that the system is stable.

3.5 Other Control Strategies When Operating in Ice

In order to achieve better performance in ice conditions, there are several other principles and techniques that can be useful.

Using reactive control objectives As discussed in Kjerstad et al. (2014), it is strategic to use reactive control in order to ensure effective transitions by minimizing sway motions of the vessel, since hitting the ice at at straight angle will reduce in significantly higher loads. This is similar to open water techniques for minimizing power consumption.

Proactive control objectives When the conditions are satisfactory, it is possible to gain extra performance by predicting the incoming ice features, to find the weakest spots, and then seek to pass through that area. This can be incorporated into a setpoint generator.

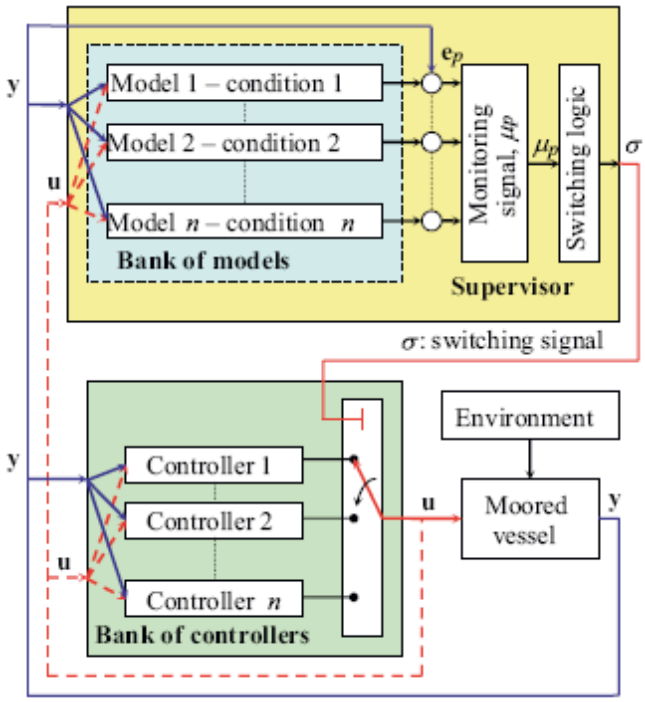

Figure 3.16: The structure of a hybrid control system. From Nguyen and Sørensen (2009b).

Also, when realizing a heavy ice feature has to be conquered, one can prepare by gaining momentum before hitting it, and therefore pass easier through it.

There is however a lack of reliable automatic systems for observing ice, so these approaches will need the operator to observe and take the decisions manually (Kjerstad et al., 2014).

Hybrid observers One problem with the highly unpredictable and strong ice loads shows up when using observers, needing a certain time to adapt its integral states. The integrator needs time to charge and unwind, and when sudden changes happen in the vessel position, the risk of unwanted effects due to integrator windup is large. Kjerstad and Skjetne (2014b) presents a solution for a hybrid observer design where the integrator is allowed to jump when the estimation errors get large. This turned out to have good performance.

Acceleration feed-forward Another way of predicting future position offsets is by investigating acceleration measurements. Since acceleration is directly a cause of forces acting on the structure, having those measurements will give an instant notice when a force suddenly hits. When an ice floe runs into the vessel the

controller can command thrust right away. This is however vulnerable to sensor noise.

A more common use of feed-forward terms is wind measurements. This is utilized in many commercial DP systems today.

Hybrid controller The problem of winding integrators is not only present for observers, but can also happen when using integral control. For normal conditions TAPM systems this is not so relevant since it is usually not utilizing integral action. It is however relevant for the switching setpoint chasing controller described in Section 3.4 when it comes to switching between normal- and extreme conditions controllers. It is also relevant for resetting the integral in the extreme conditions controller in case of sudden load changes.

For more on hybrid control, see for instance Nguyen et al. (2007) or Nguyen and Sørensen (2009b).

Chapter 4

Simulation Case Study

4.1 Integrating the Mooring Simulation Model With the NIT Simulator

4.1.1 Scaling the Mooring System to Arctic Drillship Model Scale

The testing parameters used in Section 2.2.2 were in full scale, so in order to use the mooring system in the model scale simulator the parameters has to be scaled down. Although these parameters are not designed specifically for the Arctic Drillship, they can be used as an initial approach, possibly to be further tuned later. By scaling down the scalable dimensions used in Section 2.2.2, which is primarily length dimensions, by the scaling factor of 30, the parameter file will become:

```
%% Mooring line parameters

% Segment paramaters. Vectors containing one element per segment.
rok=[7700]';        % Cable segment density
L=[16.7]';          % Section lengths
E=[2.1e8]';         % Young's modulus
d=[0.0067]';        % Cable segment diameters
A0=(pi/4)*d.^2;     % Cross section area
emfact=[1]';        % Factor for stiffness calculation. 1=normal, 2=chain
Cdn=[1]';           % Normal drag coefficient
Cdt=[0.3]';         % Tangential drag coefficient
Cmn=[1.5]';         % Added mass coefficient
ksv=[100]';         % Vertical seafloor interaction stiffness
```

```
kshl=[0]';          % Longitudinal horizontak seafloor interaction
    stiffness
ksht=[0]';          % Transversal horizontal seafloor interaction
    stiffness
ne=[6]';            % Number of elements in each segment

% Water properties
D=6.67;             % Water depth
ro=1035;            % Water density

% Currents. nc*4 dimensional array of rows on the form [depth,vx,vy,vz],
%    where vx, vy and vz are current velocity in the x, y and z
%    directions respectively. (nc>0).
c=[1 0 0 0;
    ];

errtol=1.0E-6;     % Error tolerance
negs = 0;          % Flag for handling negative strain (0=continue,
    1=exit)

dT = 0.05;         % Timestep to run cable for
dt = 0.01;         % Internal timestep in cable

X=13.33;
bp=[0;0;D];        % Initial bottom (anchor) position
tp=[X;0;0];        % Initial top position

ns = length(L);    % Number of segments
[nc,foo] = size(c); % Number of currents
```

The reason for the reduced amount of cable elements is that the program had problems handling a larger amount when scaled to this size. A larger number of elements would result in null-values in the node position coordinates, for some reason. This issue was not further debugged at this point, since reduction of elements made the system working. It might work to experiment with changing the external or internal time step values to be able to increase the element number, since some values of timesteps have caused numerical errors earlier.

In order to test the behavior of the scaled mooring, the same input as in Section 2.2.2 was used (see Figure 2.18). To convert it to model scale the ramp slope (the speed) was scaled according to Froude scaling (Steen, 2011), which means

$$V_M = \frac{V_S}{\sqrt{\lambda}}, \tag{4.1}$$

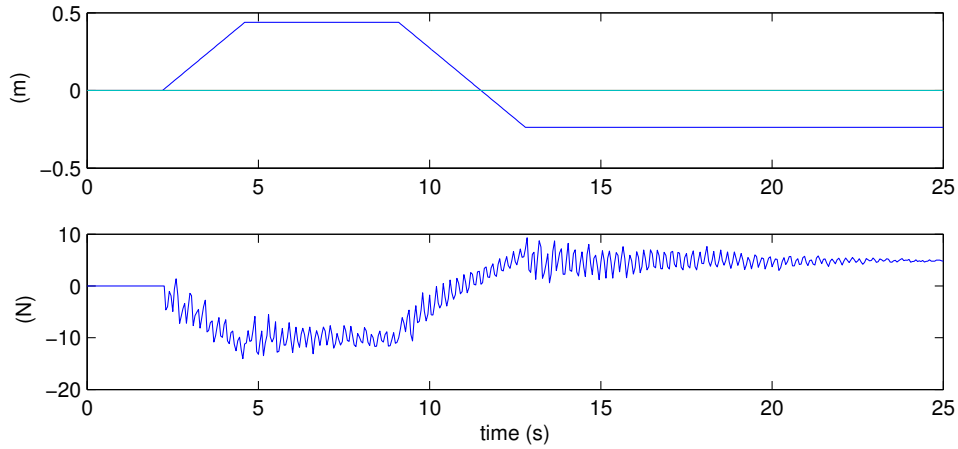

Figure 4.1: Turret position offset (upper) and mooring force in x-direction (lower) for model scale mooring.

where V_M is the model scale speed, V_S is the full scale speed and λ is the scaling factor of 30.

By also scaling the time accordingly, meaning

$$t_M = \frac{t_S}{\sqrt{\lambda}} \tag{4.2}$$

the length distances will be preserved as the linearly scaled distance, meaning $\frac{1}{30}$ of the full scale distance. t_M is the model scale time, t_S the full scale time.

This would therefore correspond to moving the turret 13 meters north, then back past the equilibrium to seven meters south of equilibrium, as in Section 2.2.2. In model scale it will become 0,43 and 0,23 meters, respectively.

From Figure 4.1 we can see that the force seems to settle at around 10 N when moved 0,43 meters away, then at around 5 N when 0.23 meters from equilibrium.

There are some oscillations on the mooring force output, which might be caused by numerical effects. It changed behavior when the time steps were changed, which is why these are different here than previously, as seen in the parameters file. Some oscillation might be actual resonance motion from the mooring lines as well.

Since a full mooring system design will not be covered here, the system will be adjusted by trial and error until the values seem reasonable. To get an idea of what kind of force amplitudes are reasonable for this vessel, the thruster data can be considered. From Table 1.1 it is seen that the model scale thrusters have

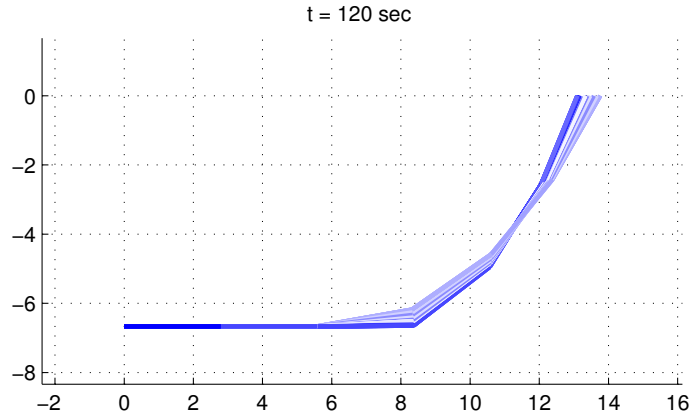

Figure 4.2: The mooring line shape on the first test run of the downscaled mooring.

a maximum total thrust capacity of 201 N. Comparing this with the force from Figure 4.1 shows that the mooring system is only providing around 5 % of the total thruster capacity when the ship is moved at an equivalent of 13 meters away in full scale. This seems to be a too low value, meaning the mooring system should probably be adjusted.

To make the same comparison in full scale, Figure 2.18 shows a mooring force around 10^5 at the same offset (13 meters). This is only 1,3 % of the total thruster force of $7.2 \cdot 10^6$ for the full scale ship.

Looking at Figure 4.2 gives an idea of how to improve the stiffness of the mooring system. The figure shows one of the mooring lines (line 1, as numbered in Figure 2.16) during the test run, and we see that a large part of the line is lying on the seafloor. Shortening the length of the line will result in a longer suspended section and a higher mooring stiffness.

Figure 4.3 shows the result of shortening the line from 16,7 to 15,7 meters. We see that the force is around three times of what it was before shortening the lines.

Other ways of increasing the stiffness could be to move the anchors further away without changing the line length, making the lines heavier or a combination of those mentioned.

Another aspect to check is the cross section dimension of the mooring lines. By converting the new line length of 15,7 meters back to full scale it becomes 471 meters. This was put back into the full scale FEM model to see what kind of tensions the full scale lines would get by moving the turret the same way as before. Assuming line 1, which is the one going south from the turret, will get the largest tension, its top force is plotted in Figure 4.4.

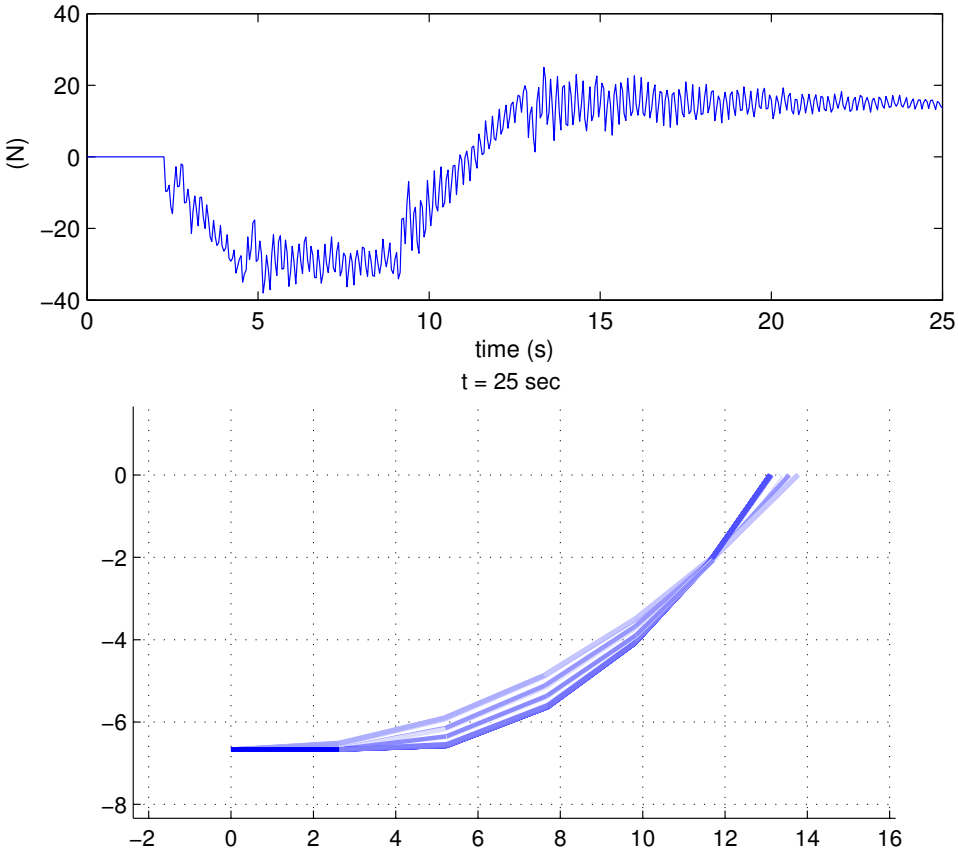

Figure 4.3: Upper plot: The mooring force in x-direction when making the same movement as in Figure 4.1, after shortening the lines. Lower plot: The mooring line shape during a test run after shortening.

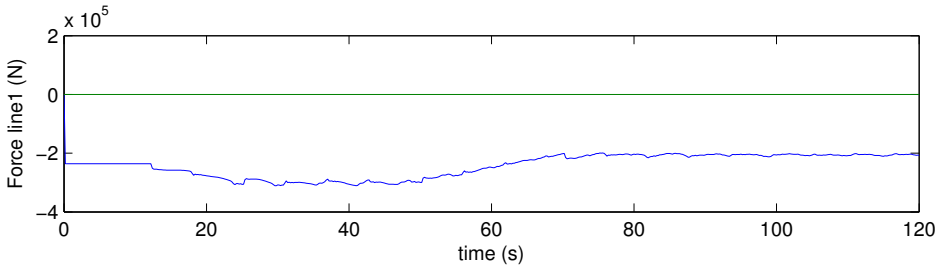

Figure 4.4: The top force of line 1 (as numbered in Figure 2.16) in full scale after shortening it to 471 meters.

The force is staying within $4 \cdot 10^5$. The cable diameter is 0.2 m, meaning a cross section area (of a round wire) of 0.031 m^2. The cable stress is therefore

$$\sigma_c = \frac{4 \cdot 10^5 N}{0.031m} = 12,7MPa. \tag{4.3}$$

The yield strength of steel is typically around 250 MPa (Wikipedia, 2015), meaning this is far within acceptable range. It is however important to have a large safety margin, since these forces can increase drastically when subject to large, unpredictable ice forces, and the material can be weakened over time due to fatigue and corrosion.

It is worth to notice that, as result of the scaling the damping effects seen in Figures 2.18 and 2.19 seems to be smaller on the downscaled simulation in Figure 4.3. Although it is more difficult to notice due to the oscillation disturbance it seems to be a damping effect present, however smaller in comparison with the full scale tests.

4.1.2 Testing the Scaled Turret Mooring in a Simulation Loop

For having a simpler way of testing the mooring system in a simulation loop without having to generate code and compile after every adjustment, the turret model is plugged into the Simulink test loop also used in Gjessing (2014). It is using a model of the vessel CyberShipII from the Marine Systems Simulator (MSS) Toolbox.

The model, shown in Figure 4.5, is connecting the CyberShipII to a block containing the mooring system and a DP controller. It is also generated a disturbance input force to simulate for instance wind. The mooring- and controller block is shown in Figure 4.6. The position error is inverted compared to a negative feedback error since the mooring uses the position offset distance from the *field zero point*. The output from the mooring is converted from NED frame to vessel frame by a rotation matrix. The mooring- and controller forces are fed separately into the vessel model since it is modified to apply the mooring force without feeding it through the built in thruster saturation in CyberShipII (see Gjessing (2014) for details).

Running the simulation showed that the mooring system is keeping the vessel stable and in position, as shown on the position plot in Figure 4.8. During the simulation the heading reference is changed from zero to $\frac{2\pi}{3}$, and it is seen that the DP controller manages to turn the ship, while the position stays in place. Here the DP controller is only providing damping in surge and sway, while the mooring

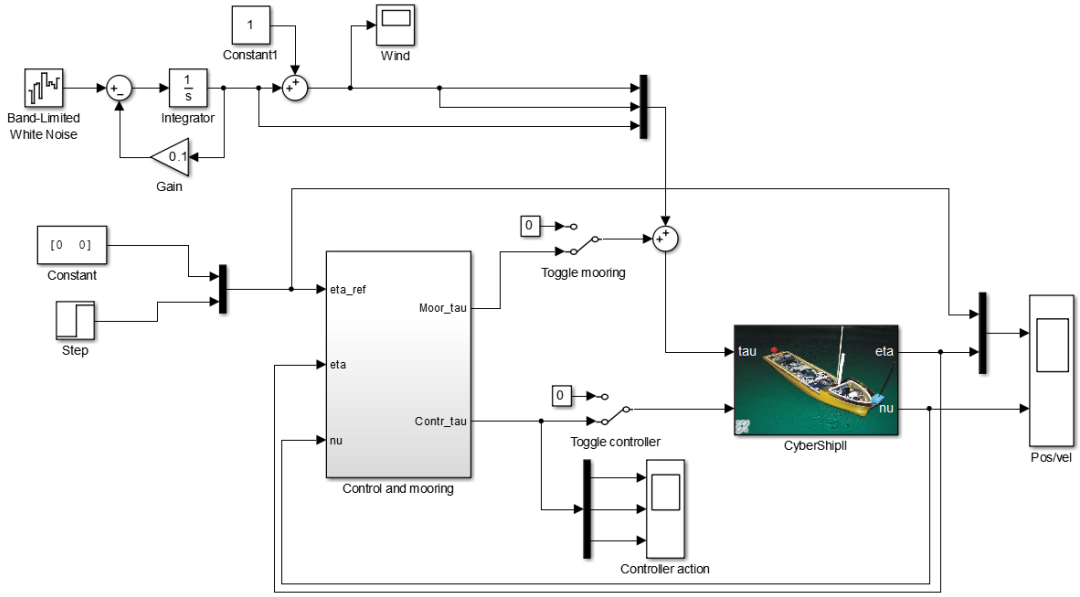

Figure 4.5: The Simulink model used for testing the mooring system on CyberShipII.

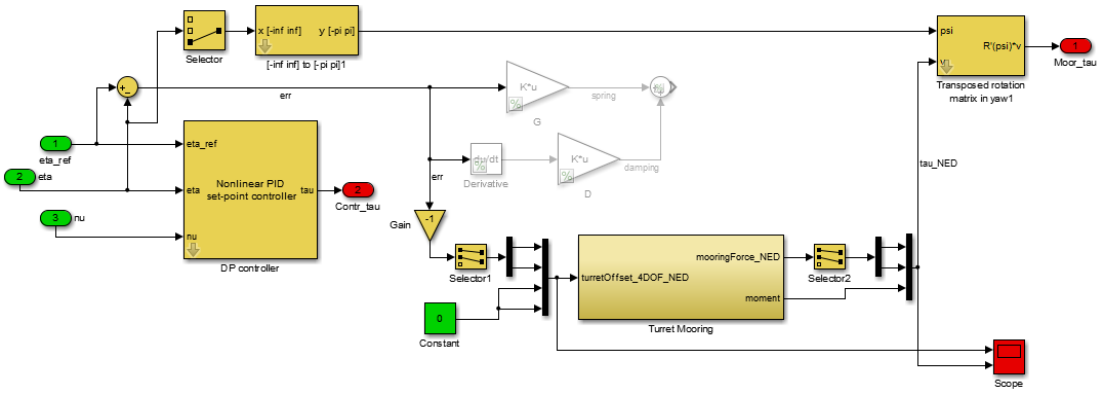

Figure 4.6: The control and mooring block in the Simulink model used for testing the mooring system on CyberShipII.

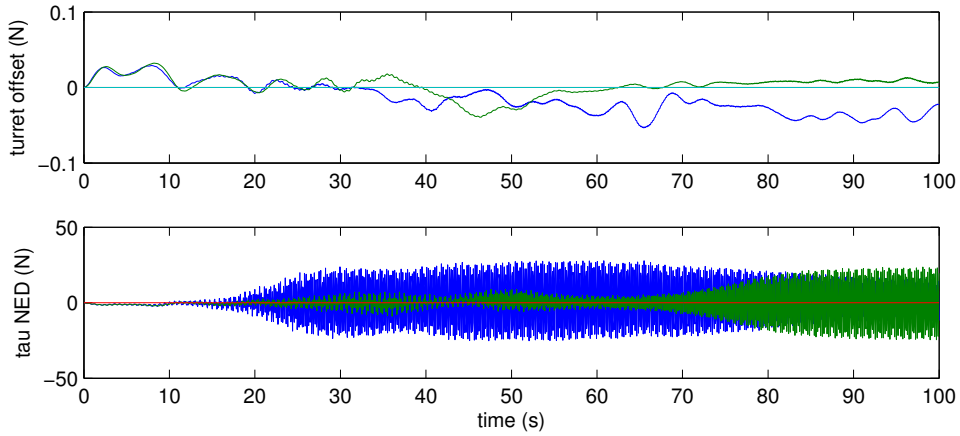

Figure 4.7: The turret offset and the resulting mooring force for the simulation loop test run.

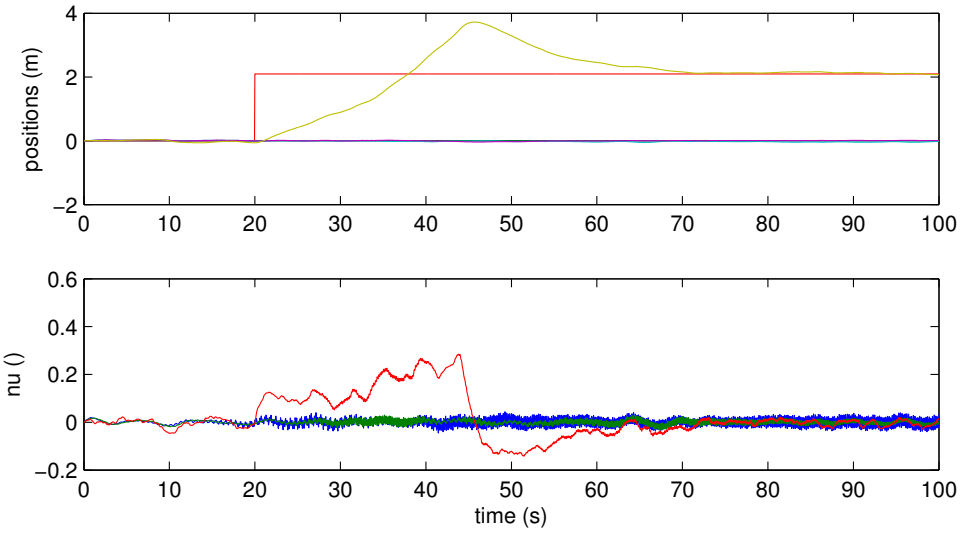

Figure 4.8: Positions and velocities for the CyberShipII in the simulation loop test run. The heading reference is showed in red while the heading is in yellow.

system handles the restoring. It has PID control in yaw, although it is not very well tuned, as seen in Figure 4.8, since this is not relevant for the mooring system testing.

It is seen in Figure 4.7 that the mooring force is having some high frequency oscillations. This might be due to numerical chattering, but as seen in Figure 4.8 it is not having any major influence on the position. It is however noticeable in the velocity plot. It might be possible to tune this to work better by experimenting with different timestep values, or by adding a lowpass filter in the loop.

It should also be mentioned that the CyberShipII is smaller than the Arctic Drillship. Therefore the mooring system is overdimensioned for this ship, however it is still helpful to do this simulation in order to get an idea of the stability and performance of the mooring model.

4.1.3 Connecting the Mooring Block Into the Simulator Controller Model

After verifying the functionality of the turret mooring model within Simulink, it should in theory be possible to simply copy and paste the turret mooring block directly into the simulator controller to get it to work with the NIT. In practice it required quite a lot of debugging work to get it to work properly.

When running code generation, Simulink has to include the code files used by the s-function (see Section 2.2.2), being the s-function main file, *sDynSys_main.c*, in addition to other files used from within that file. In this case that means the files *sDynSys_model.c*, which contains the model specific code, *cable.c*, containing the mooring cable FEM program, and *libGenericFunctions.c*, containing a library of other functions used by the s-function. These must be referenced in the *S-function modules* field in the s-function block parameters dialog, as done in Figure 4.9. By doing this, Simulink Coder will include the files in the generated code project, given that all these files are located within the current Matlab working directory.

As described in Section 2.2.2 the parameter initialization file has to be run before starting a simulation within Simulink. Some parameters, like the initial conditions, will be included as constants when generating the code. This means the file has to be run before starting the code generation.

The initialization file is generating an .ini file containing the rest of the parameters needed by the s-function at runtime. For simulation within Simulink this file has to be saved in the working directory, however, to work with the NIT it has to be saved in the Visual Studio project directory, normally being the directory containing the code project files. In this case it is the *examples* directory.

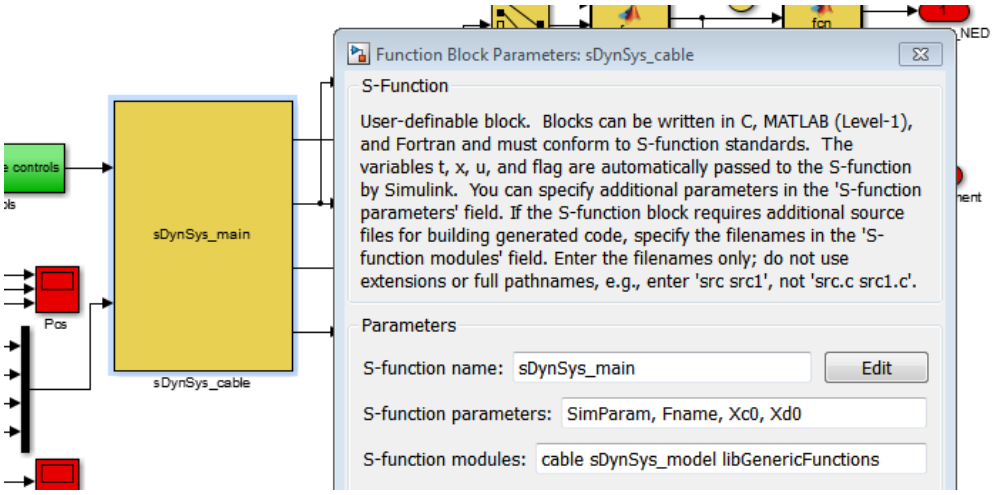

Figure 4.9: The s-function block parameters configuration, showing which files have to be included for code generation.

After generating the code the controller has to be set up in Visual Studio as covered in Gjessing (2014).

The model includes a standard PID controller for DP from the MSS library, which can be tuned from outside the controller since the controller gains are provided as inputs. This means the controller parameters can be changed without the need to regenerate the code. The mooring model can however not be changed without going through that process all over.

One of the main reasons it is difficult to change the mooring parameters without code regeneration is that the mooring lines must be initialized as a valid static solution. Since the initial values are implemented in the code during code generation, the code has to be changed.

Placing the Turret in the Front Part of the Ship

When applying the turret mooring forces directly on the vessel, it corresponds to having it placed at the vessel mass center. Since a turret is normally placed in the front part of the ship, it will generate a yaw moment when it applies sway forces on the ship, according to

$$\boldsymbol{\tau}_{moor,3} = r_t + l_t \cdot Y_t, \tag{4.4}$$

where $\boldsymbol{\tau}_{moor,3}$ is the total yaw moment contribution from the mooring, r_t is the moment generated from the mooring lines about the turret, while l_t is the length from the COT to the vessel mass center. It is assumed that the vessel reference

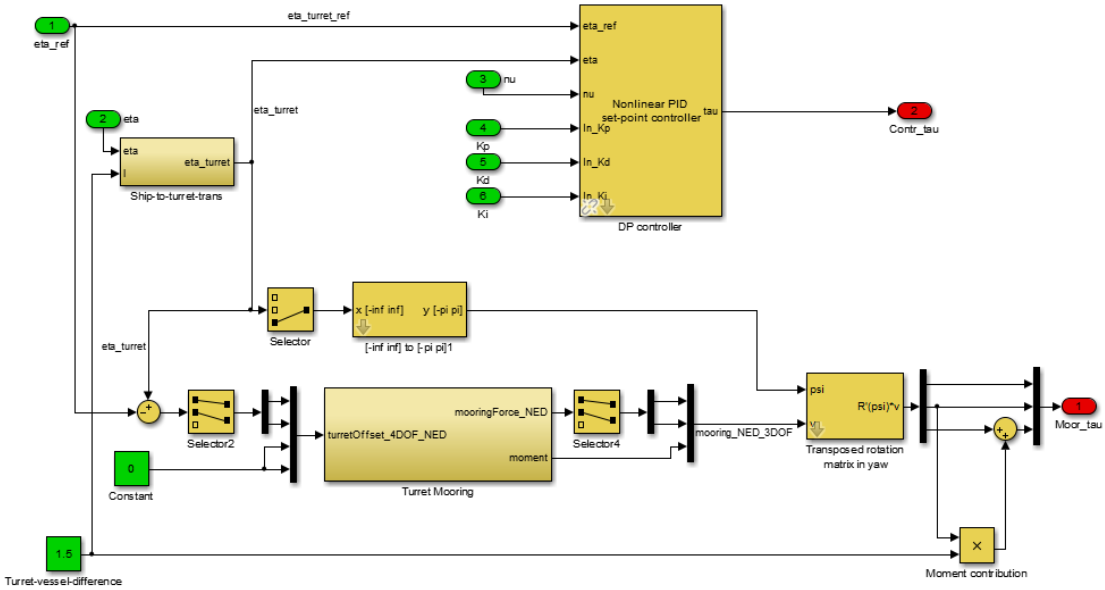

Figure 4.10: The controller and mooring Simulink model used with the simulator. The turret offset (being defines as the positive distance from the reference to the turret, hence the subtraction of the reference) is fed into the mooring model, while the forces are fed back to the simulator. It is using a standard PID DP controller.

frame has origin at the mass center. Y_t is the sway force generated by the turret in the vessel frame. This means it is necessary to apply a rotation matrix after the output from the mooring model and before calculating the moment generated by the mooring sway forces.

This setup is shown in Figure 4.10. The turret offset (being defines as the positive distance from the reference to the turret, hence the subtraction of the reference) is fed into the mooring model, while the forces are fed back to the simulator. The distance from mass center to the turret is used to generate a moment which is added to the moment output from the mooring model. Since the vessel is free to rotate about the turret it is assumed that the turret angle in NED frame will be constant at zero. This means the moment from the turret model will always remain close to zero, although it is not impossible for the model to generate a moment due to asymmetrical movements of the cables. The vertical position of the turret is also set to zero since the controller is operating in 3DOF.

In addition to the moment generation, the vessel NED position, which is what comes through the input port, has to be translated into the turret NED position. This is done by a subsystem block in the model (Figure 4.10) according to

$$\boldsymbol{\eta}_t = \boldsymbol{\eta} + \begin{bmatrix} l_t \cdot cos(\boldsymbol{\eta}_3) \\ l_t \cdot sin(\boldsymbol{\eta}_3) \\ 0 \end{bmatrix} \tag{4.5}$$

where $\boldsymbol{\eta}_t$ is the turret position in NED frame. The yaw angle is kept as the vessel angle here, but if using a freely rotatable turret the turret yaw angle fed into the turret mooring model will be set to zero. If having a manually rotatable turret it can be set to another value depending on its setting.

When using the turret coordinates as the reference point, the ship position must be initialized to another value than zero in order to keep the turret placed at zero. This is because the simulator handles the vessel position and not the turret position. The turret must initially be positioned at zero since the mooring lines are initialized for that configuration. However, if the turret is freely rotating and therefore always stays at zero, the vessel heading can be any value as long as the north- and east position of the turret is zero. Also, the reference position should still be set to zero, since it is now corresponding to the desired turret position. (This can be observed by examining the Simulink model in Figure 4.10 where the reference is used with the turret position and not the position feeded from the simulator.)

The vessel position making the turret stay at zero given a certain heading angle ψ will be the opposite of (4.5) with $\boldsymbol{\eta}_{t,1} = \boldsymbol{\eta}_{t,2} = 0$, meaning

$$\boldsymbol{\eta}_0 = - \begin{bmatrix} l_t \cdot cos(\psi) \\ l_t \cdot sin(\psi) \\ \psi \end{bmatrix} \tag{4.6}$$

4.2 Using the Mooring Model

A summary of things to know and remember about the procedure of using the turret mooring model, within the NIT simulator and in general:

- The turret radius is set in the Simulink turret model, meaning it is important to remember to set it correctly when scaling and configuring the rest of the parameters.
- It is important to set the Simulink solver to fixed step, and adjusting the step size to the same as the outer timestep value in the parameters file (the timestep to run the cable function for, dT).
- When running the model in the NIT the simulator time step must also be set to the same as the mooring model timestep, dT.

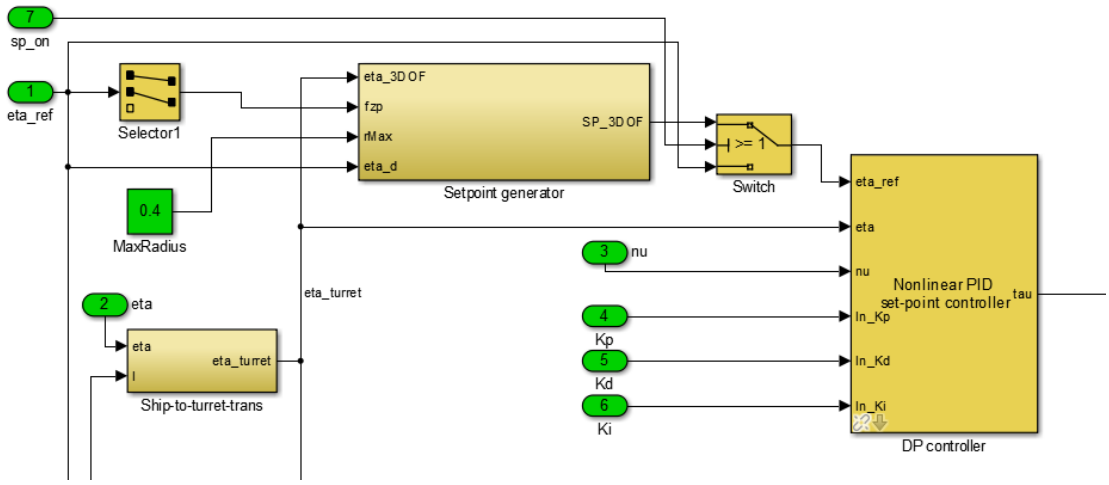

Figure 4.11: The NIT controller with the position vector feeded through the setpoint generator. The setpoint limit is set to 0,5 m. The field zero point is provided by the reference input (will stay at zero in this case).

- Before running a Simulink model containing the mooring model, or before generating code from Simulink, the S-function parameters file, defining all the mooring system parameters, has to be run.

- The .ini file generated from running the parameters file must be saved in the project directory of the simulator Visual Studio project when using the model with the NIT simulator. Usually the same folder as where the project solution file is saved. When running the model within Simulink it should be saved in the Matlab/Simulink working directory.

- The system should be initialized according to (4.6) so that the turret is in position $\boldsymbol{\eta}_{t,1} = \boldsymbol{\eta}_{t,2} = 0$, since the mooring lines are initialized for zero offset. The reference position should still be set to zero (north and east) since it now refers to the turret position.

4.3 Integrating the Setpoint Model With the Simulator

The setpoint chasing model from Section 3.4 is now to be implemented in the controller for the NIT. By adding the setpoint generator block to the controller model from Figure 4.10 it will now look like in Figure 4.11.

The setpoint limit is set in the model and provided to the setpoint generator

Parameter	Value	Full scale equivalent
Ice thickness (m)	0.03	0.9
Minimum floe size (side length) (m)	0.7	21
Maximum floe size (side length) (m)	1.3	39
Ice concentration	0.7	
Ice field length (m)	41.5	1245
Floe shape	Rectangular boxes	

Table 4.1: Ice tank configuration parameters.

block. It takes in the position vector and provides the lowpassed and possibly limited version of it to the controller. The field zero point is provided by the reference input, but it will stay at zero in this case. The time constants are now (unfortunately) being set inside the setpoint generator model.

There is a switch to enable or disable the setpoint generator, so that the code does not need to be regenerated to change that setting. It is connected to the port 'AFF_on' since it was not in use for anything else.

Unfortunately, when running the simulator with this setup, something went wrong and the force outputs turned into non-numeric-values. However, both the lowpass-setpoint generation block and the setpoint limiter block (see Figure 3.13) were found to be working separately. After debugging as much as the available time would allow, it was therefore decided to test these components separately in the simulations.

4.4 Simulations

4.4.1 Simulation Setup and Parameters

The simulator is set up according to Section 1.1.7. The ice field data is entered through the XML file together with the initial position of the ship and other relevant data. Some of the most relevant parameters are shown in Table 4.1. The width of the ice tank and ice field was varied between some of the simulations to prevent the tank walls from interacting with the ice.

The mooring system used is a six line turret mooring as described in Section 2.2.2 with parameters as described in Section 4.1.1. The vessel is the Arctic Drillship as described in Section 1.1.7.

For the damping PM controller the damping coefficient of 80 discussed in Section 3.3 is used in both surge and sway. A PID controller for yaw was chosen

through simulation tests as described in Section 3.3.

The setpoint generator time constants are set to 200.

In all the simulations the movement of the ship towards the ice is not started before after 12 seconds. This is to have any initial motion settle before starting the simulation. The sudden velocity change when the movement starts is creating some oscillation in the simulations, but it stops as soon as the ship hits the ice.

The position measurements are at the mass center of the ship, and not at the COT. Since the turret is initialized at zero, the x- or y-values therefore will change depending on the heading. This is further explained in Section 4.2.

4.4.2 Simulation Results

Scenario 1: 0 degrees, only mooring

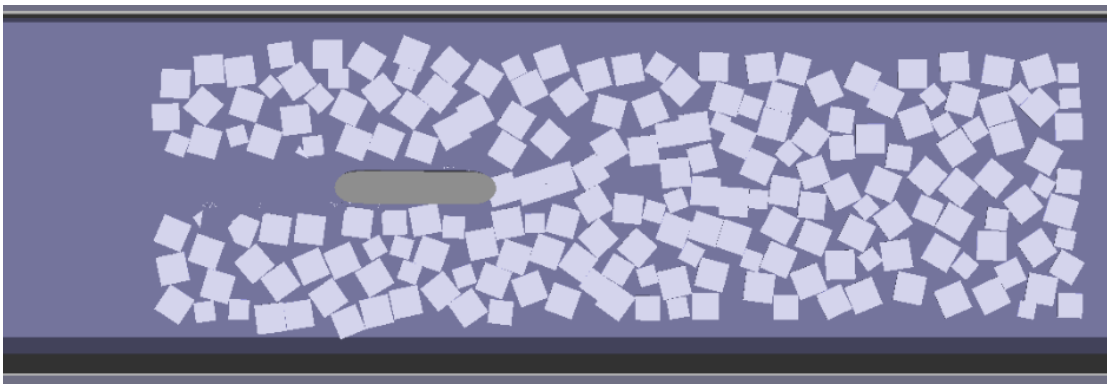

–

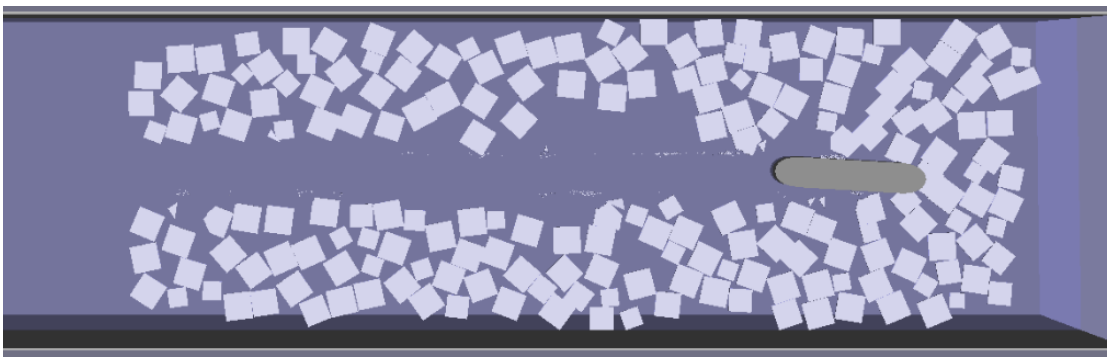

–

Figure 4.12: Scenario 1

Initially, the mooring system is tested with no thruster forces acting on the vessel. At the first simulation this is done by placing the vessel at 0 degrees yaw angle, meaning it is pointing towards the ice field. All controller gains are set to

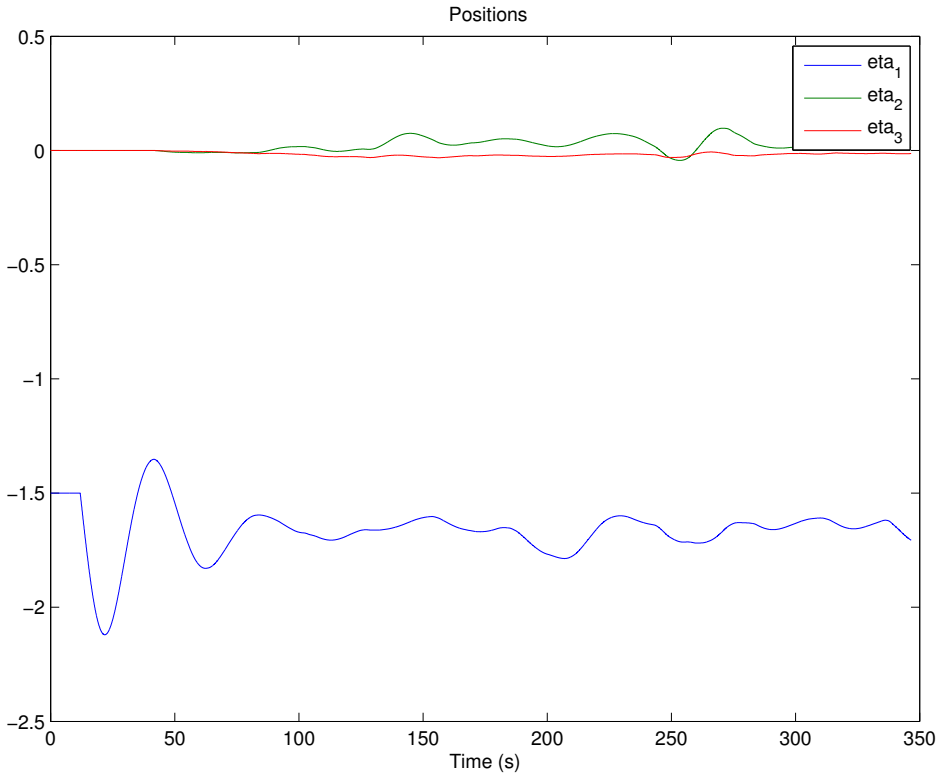

Figure 4.13: Position plot for the 0 degree heading simulation (Scenario 1).The reason that the x-position is lying at -1.5 is that this is where the mass center is, while the turret is at zero. This is described in Section 4.2.

zero, meaning the mooring system is the only thing that prevents the vessel from drifting. The ship is then run through the ice tank. The result of this simulation is displayed in Figure 4.12.

The vessel is keeping a relatively steady course through the ice. The loads in yaw are quite small due to the ship moving straight into the ice, so even though it does not have any yaw controller action, it keeps the heading quite well.

Figure 4.13 shows a position plot from this scenario. The sway position offset is lying around 0.2 meters, meaning about 6 meters full scale. In Section 3.1 it was shown that the mooring lines are close to being stretched out at 0.8 meters, so this seems to be a reasonable value.

It is easy to see the fluctuating characteristics of the ice load.

It is possible to see the contact network effect discussed in Section 1.1.5 in some of the images.

Scenario 2: 45 degrees, only mooring

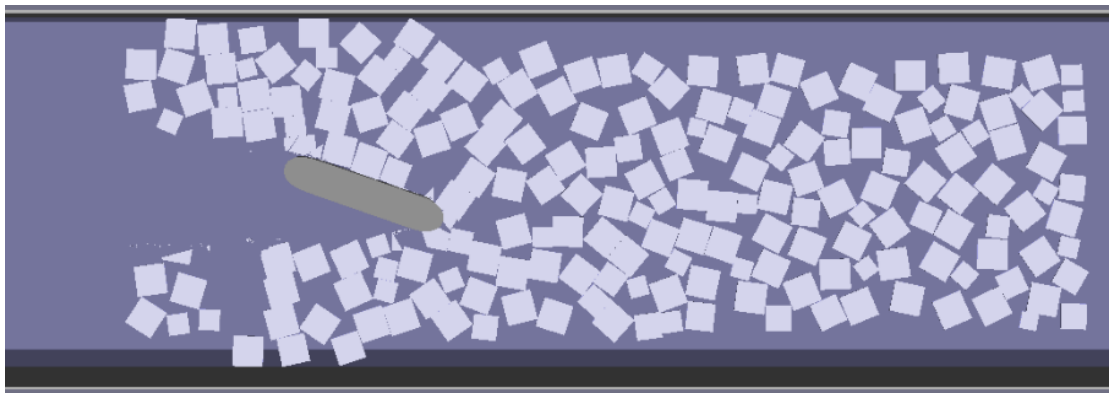

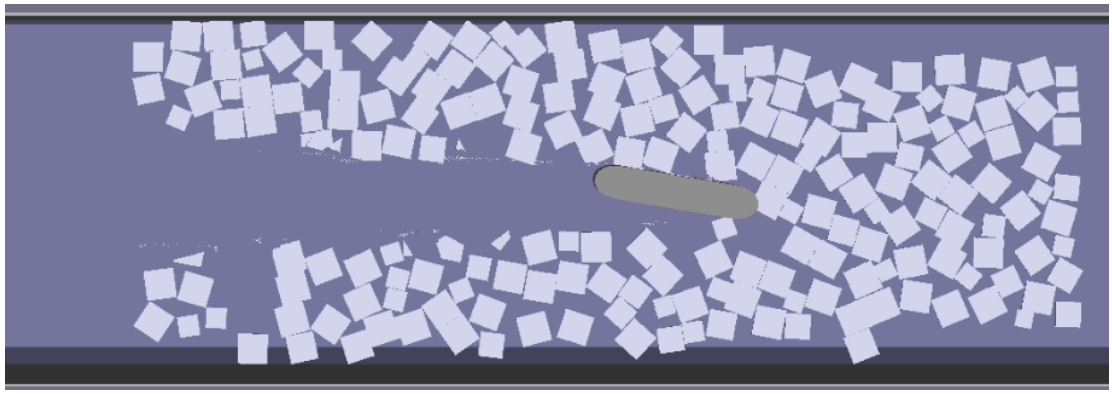

Figure 4.14: Scenario 2

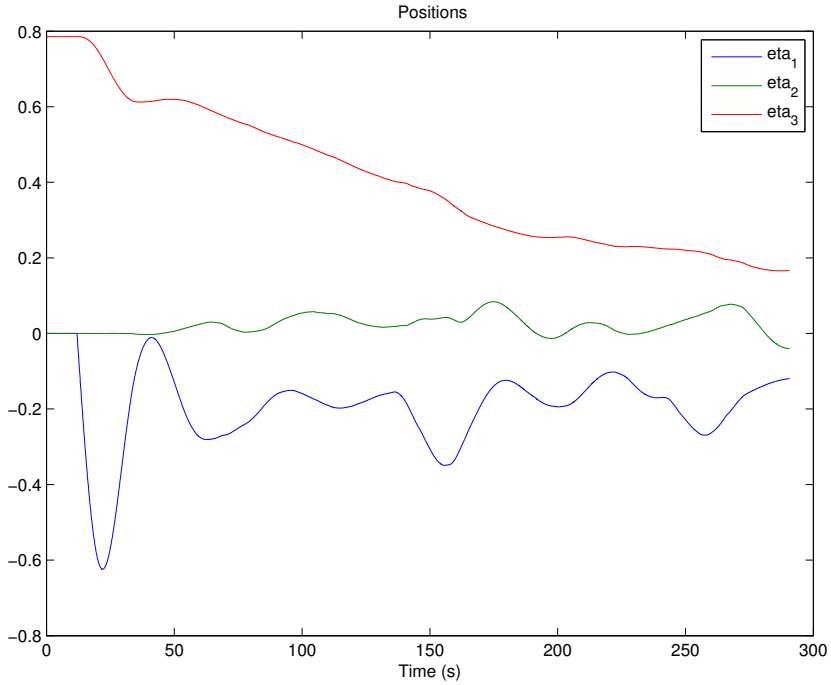

Figure 4.15: Position plot for the 45 degree heading simulation (Scenario 2).

This scenario is testing the effect of a turret placed in the front part of the vessel. Now the ship is still relying on its mooring only, while having an initial 45 degree yaw angle. The result in Figure 4.14 shows how the ship is changing angle towards 0 degrees since it is turning freely on the turret. This is also seen on the position plot in Figure 4.15. The force plot in Figure 4.16 shows how the mooring is creating a moment in yaw. The plot shows the total force applied to the vessel, meaning both mooring and control forces. Since there is no controller in this case all the forces are generated by the mooring.

Initially the ship is starting to turn even before hitting the ice, which is due to drag from the water. It is also seen from Figure 4.15 that the total offset is a bit bigger than in the previous scenario.

It is worth noting that the position plots are in NED frame, meaning they are not representing any direction on the ship like surge or sway.

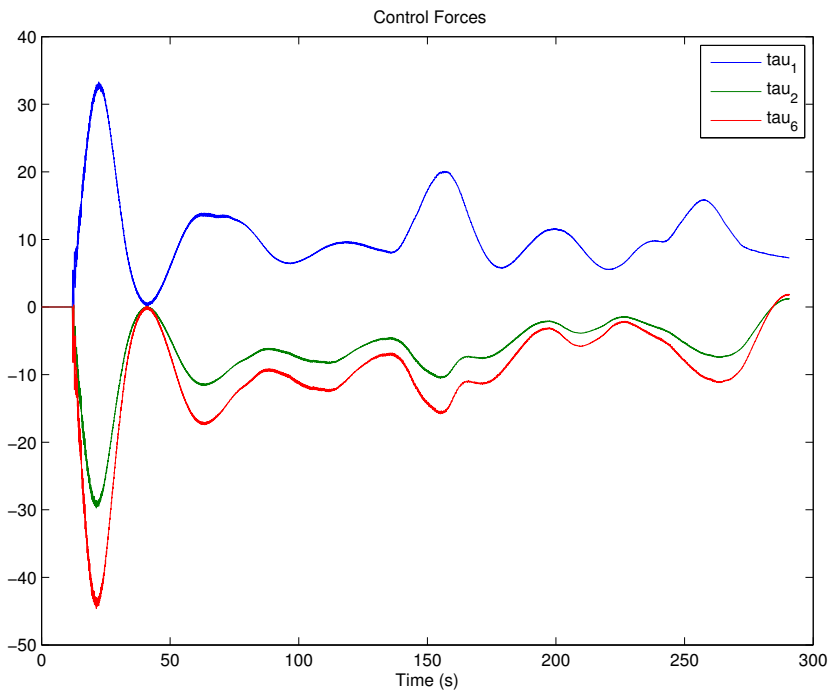

Figure 4.16: Force plot for the 45 degree heading simulation (Scenario 2).

Scenario 3: 0 degrees, damping action

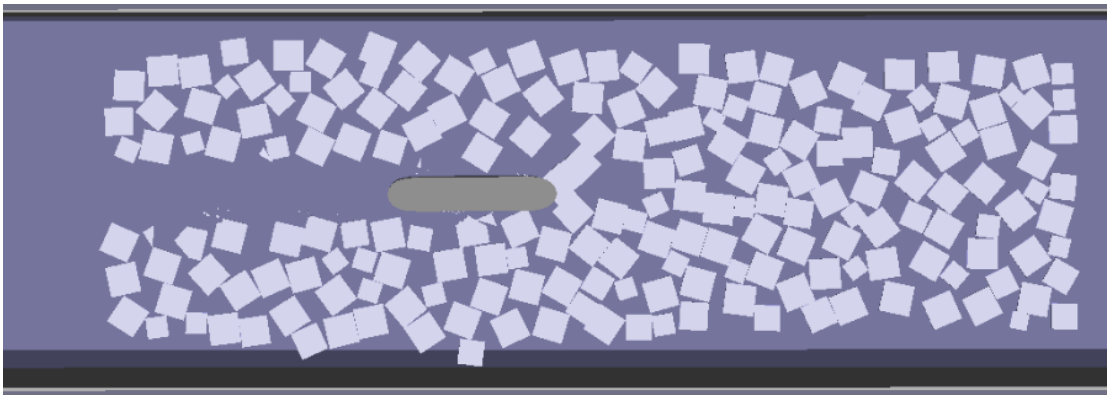

–

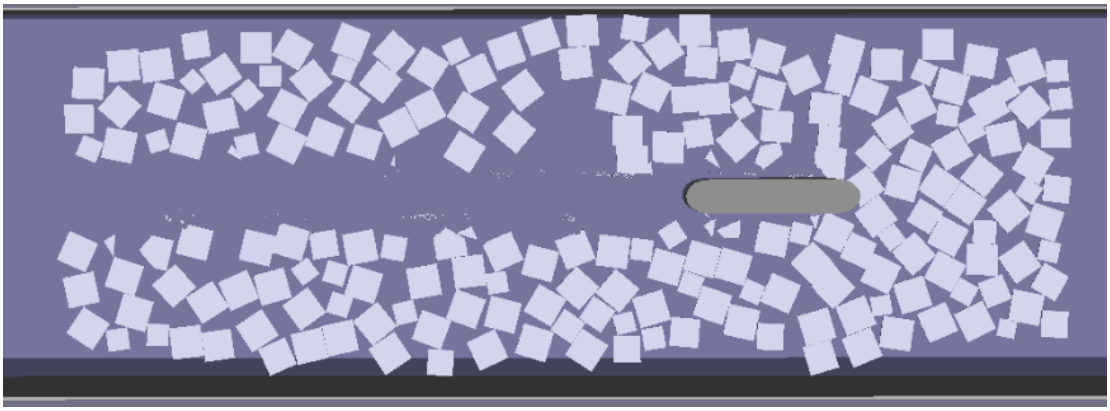

–

Figure 4.17: Scenario 3

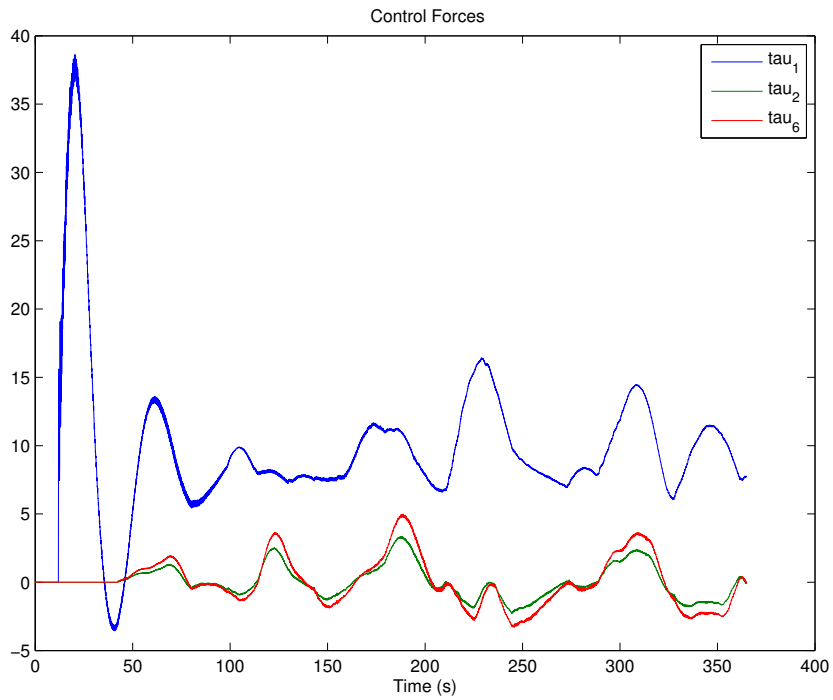

Figure 4.18: Force plot for the 0 degree heading simulation with active damping (Scenario 3).

This scenario looks about the same as scenario 1 from the simulator visualization, since the ship is still moving straight forward through the ice. It is however seen in the comparison plot in Figure 4.19 with the scenario without damping that the damped system has smaller peaks. It is not a huge difference though, so it might be considered to increase the damping gain.

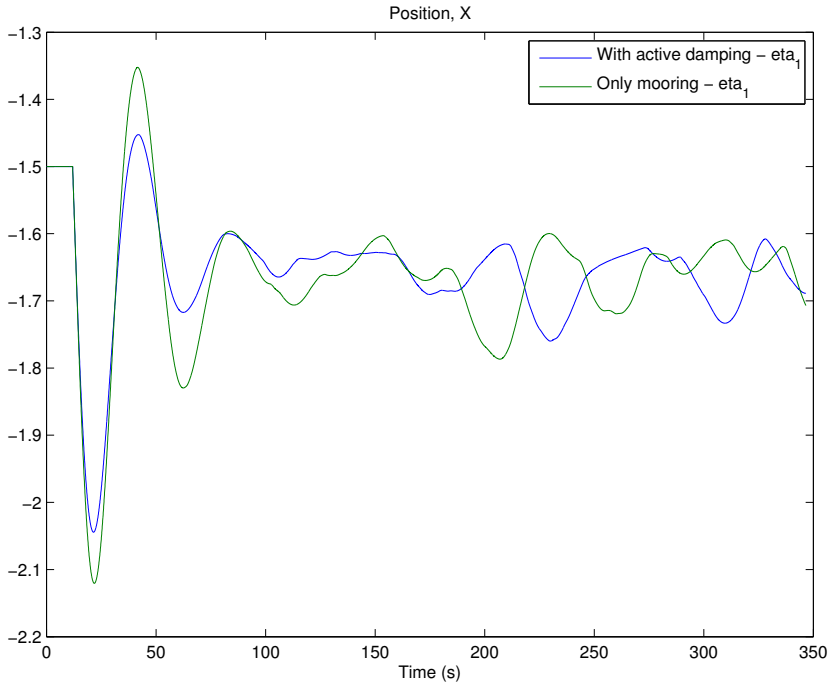

Figure 4.19: Plot comparing surge position for the 0 degree heading simulation with active damping (Scenario 3) and without any controller action (Scenario 1).

Scenario 4: 90 degrees, PID action

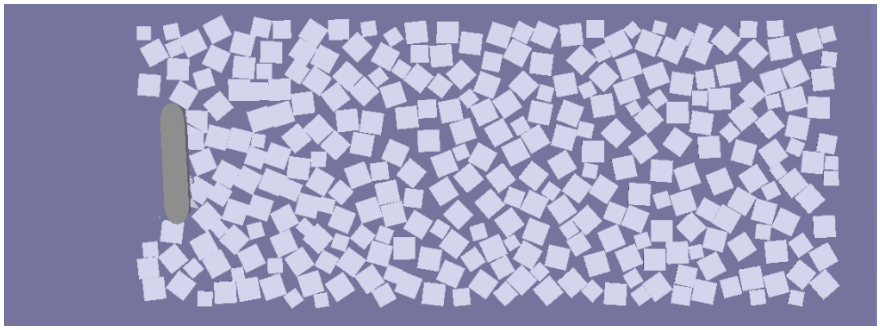

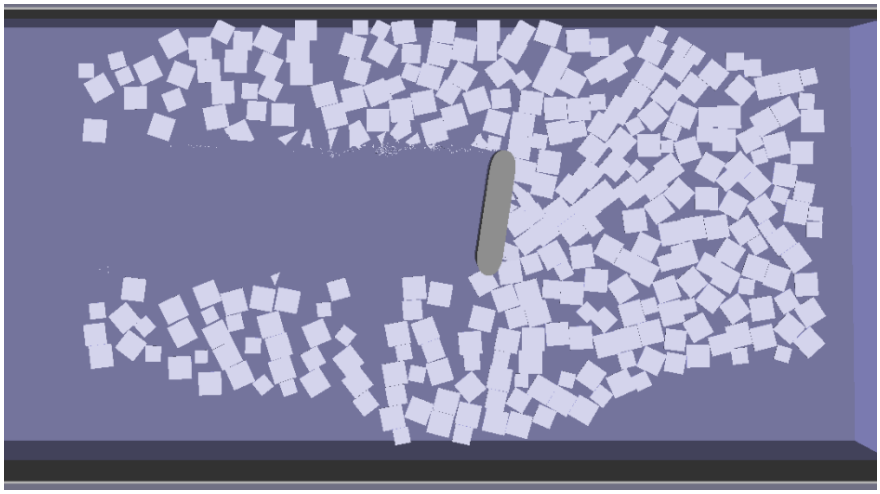

–

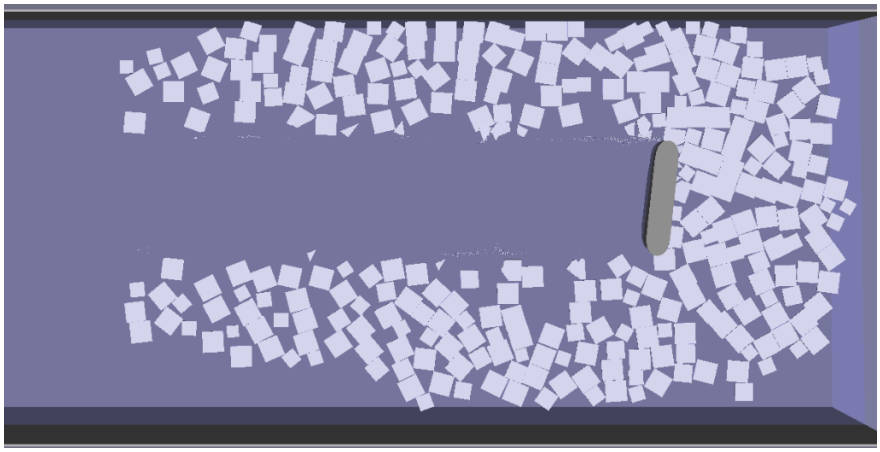

–

Figure 4.20: Scenario 4

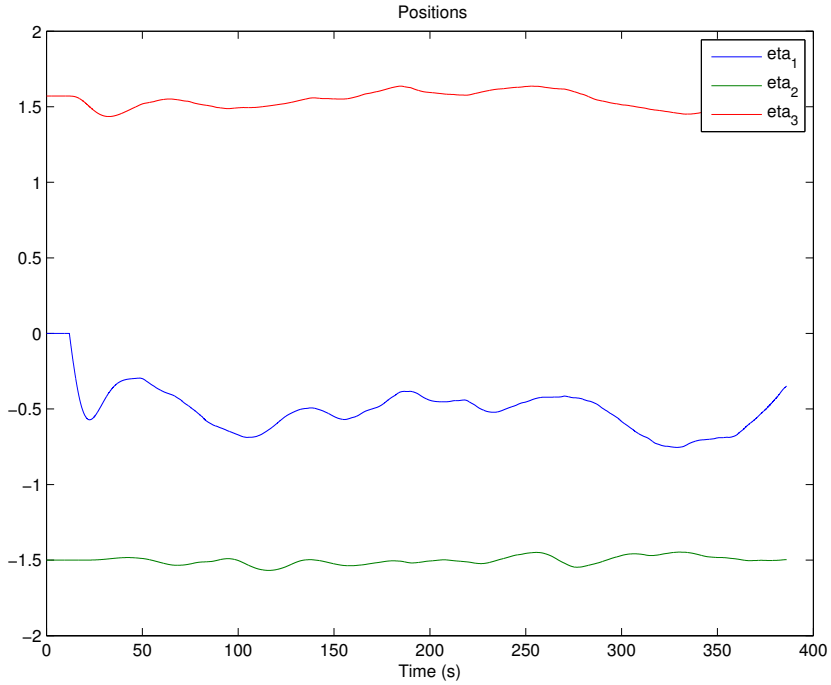

Figure 4.21: Positions for scenario 4. PID action in yaw.

Now the PID controller is applied in yaw, and we see that the ship is not turning along the stream as it did in scenario 2. It is actually turning a bit the opposite way towards the end. considering the turret is pointing down in the image. This might be due to integral windup followed by a sudden reduction of load. This is an example of why it can be an advantage to have some sort of hybrid control for switching or resetting the controller, as mentioned in Section 3.5.

The surge and sway restoring is still controlled by the mooring system only, with additional damping from the controller. It is seen that the position offset is significantly larger, around 0.5 m, than for the 0 degree simulation, where it was around 0.2. It also has larger fluctuations. Figure 4.20 shows that the ship is gathering a lot of ice in front, which is contributing to making large forces.

The force plot in Figure 4.22 shows some large fluctuations. The fact that the yaw moment force is on the opposite of the sway force (which generates the moment from the bow-part-positioned turret) is indicating that the controller is using quite a lot of effort, and has probably charged its integrator quite a bit.

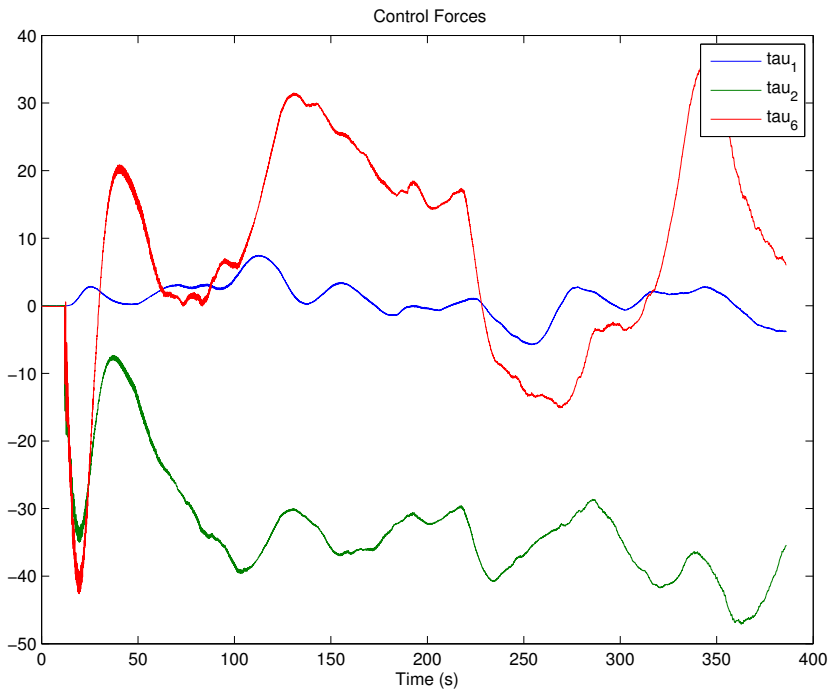

Figure 4.22: Forces for scenario 4. PID action in yaw.

Scenario 5: 90 degrees with setpoint chasing

For this test scenario, the system is run with only the low-pass setpoint generation and no limiting for the reasons mentioned in Section 4.3. The controller damping action is still in place together with PID in yaw.

Since the ship in this case behaved very similar as in scenario 4 the simulator visualization is not included.

It is seen from the plots in Figures 4.23 and 4.24 that the position in x-direction is moving a lot more than in y, but it is not so much as earlier, as can be seen in Figure 4.25. The sway force, which corresponds to x-direction (north) due to 90 degree heading, is significantly larger than in surge. The yaw force is having a quite large bump, which might be caused by some integrator wind up. It turns out quite moderately on the yaw angle though.

It is interesting to see the difference between with and without setpoint chasing. The oscillations are clearly smaller, but the stationary offset is maybe a bit too small, considering utilization of the mooring. The setpoint time constant might be a bit too high, that depends on how long time one is willing to let it take to balance out.

It is also worth to mention that due to the randomness of these simulations the results might differ from one time to another due to random events.

These setpoint chasing comparisons are done at 90 degree heading in order to get high loads to see how the setpoint behaves.

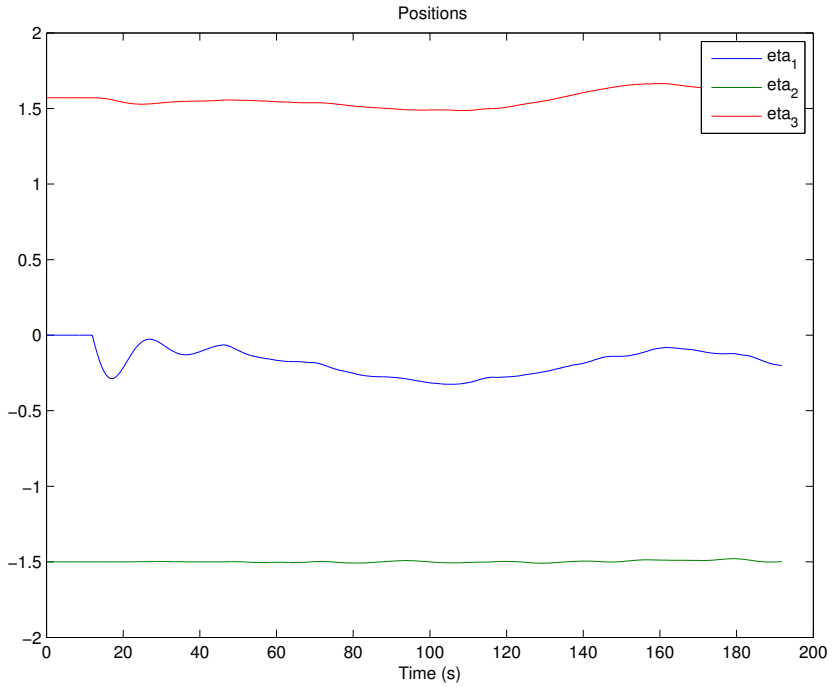

Figure 4.23: Positions for scenario 5. PID action in yaw and setpoint chasing.

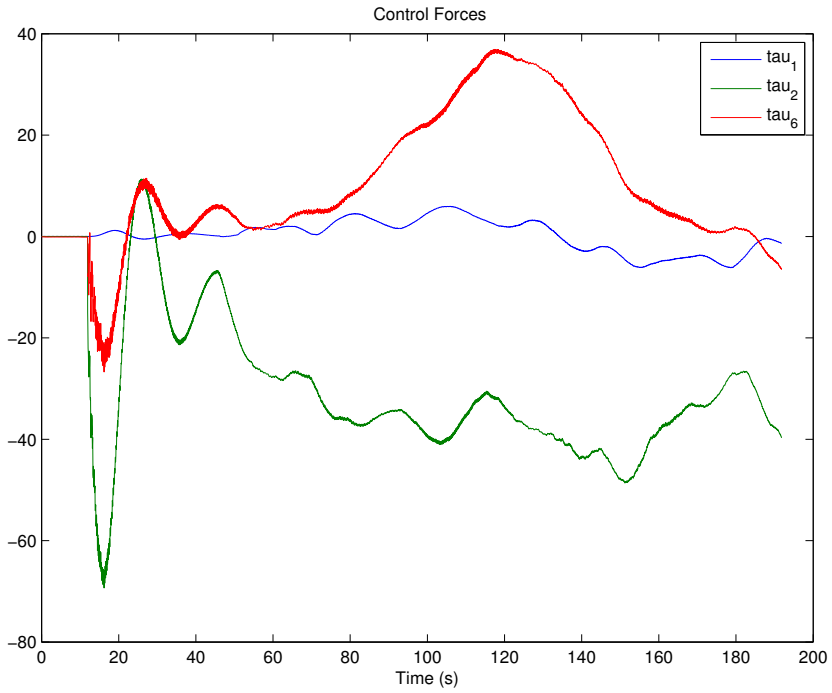

Figure 4.24: Forces for scenario 5. PID action in yaw and setpoint chasing.

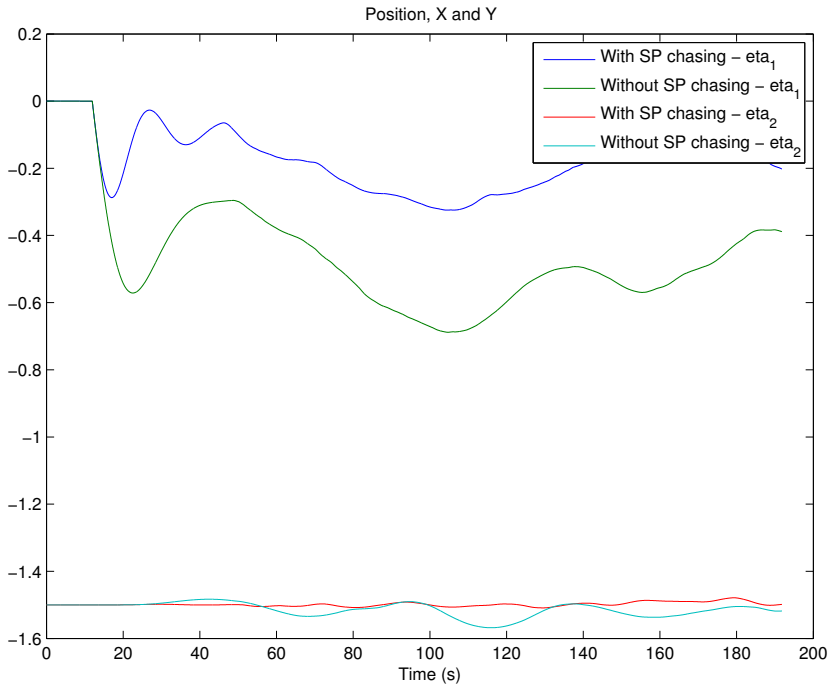

Figure 4.25: Comparison plot (Scenario 5) of positions with the low-pass setpoint chasing system compared to scenario 4 with only PID action in yaw and mooring system in surge and sway.

Scenario 6: 90 degrees with setpoint limiter

This is the same as scenario 5, but with the setpoint limiter instead of the low-pass setpoint generator. So still PID control, and proportional control from the setpoint, which should be free to wander around until it reaches the limit, which is set to 0,4 m radius. The controller damping action is still in place.

The position plot in Figure 4.26 is showing that the x-position is still moving below 0,4. It is however never especially far from it; it seems to never cross 0,6 or so. It is hard to tell exactly if it would go further without the setpoint limiter. An interesting observation is the force peak in sway on Figure 4.27 at around 260 seconds. When observing Figure 4.26 the same peak can be observed, but it is not that significantly larger than the other peak, which did not give an equally large force response. This could be explained by that since the position is close to the limit, small changes in this area will cause large forces. The same kind of variations does not cause the same force variation, so this might be due to the setpoint.

The comparison plot in Figure 4.28 is showing that the setpoint case is keeping the position a bit closer to zero.

In opposite to scenario 5 the y-positions are not very different here. This makes sense since the setpoint limiter is not influencing when the position is close to zero.

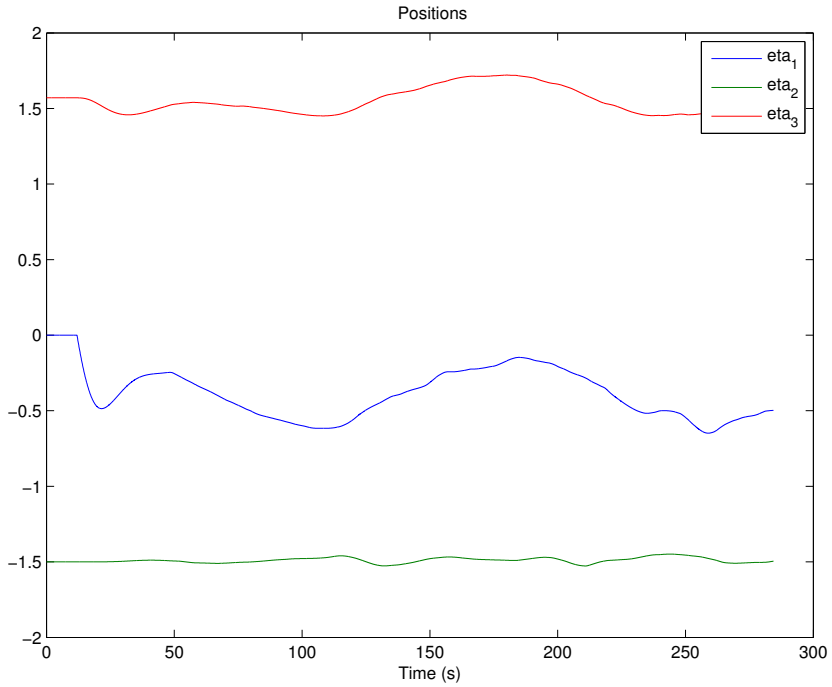

Figure 4.26: Positions for scenario 6. PID action in yaw and setpoint limiter.

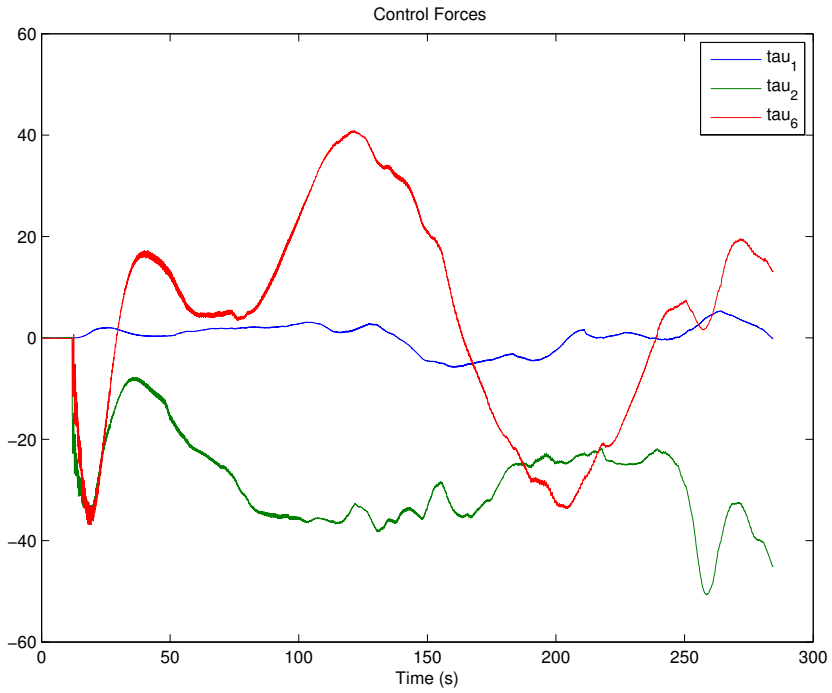

Figure 4.27: Forces for scenario 6. PID action in yaw and setpoint limiter.

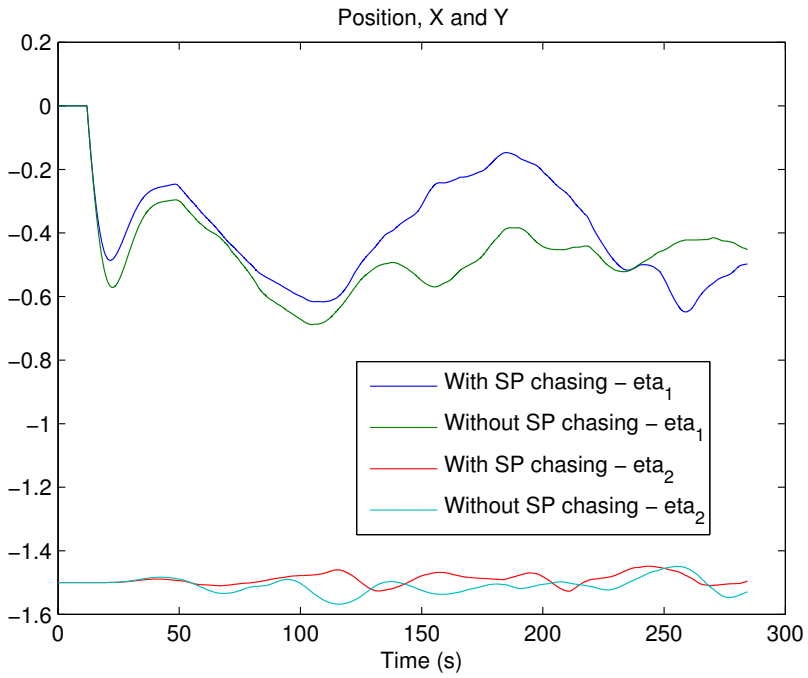

Figure 4.28: Comparison plot of positions with the setpoint limiting system (Scenario 6) compared to scenario 4 with only PID action in yaw and mooring system in surge and sway.

Scenario 7: 0 degrees, Linear and FEM comparison

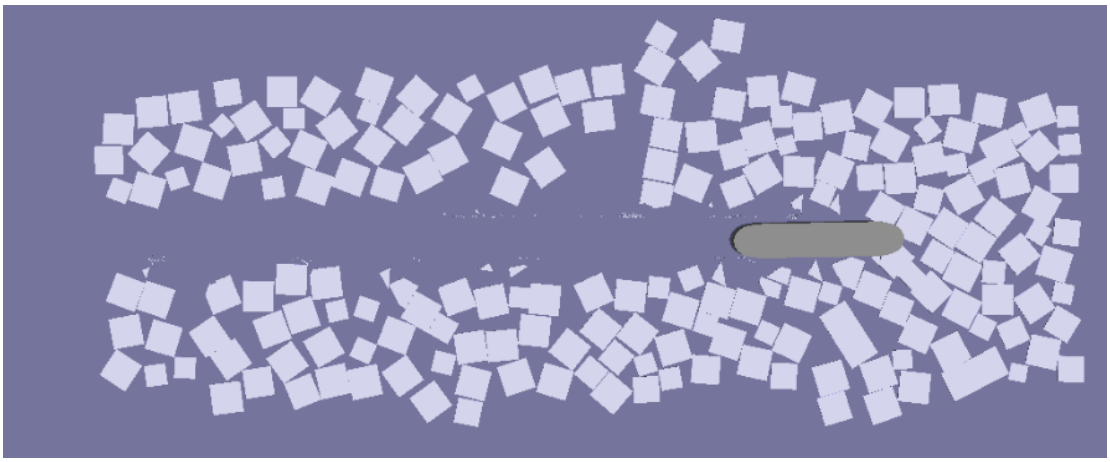

Figure 4.29: Scenario 7

This test is to see how the linear mooring model approximation from Section 3.1 is performing compared to the FEM mooring. This is done with no other forces than the mooring, as in scenario 1.

The linear mooring was incorporated by disconnecting the FEM mooring in the controller model and applying a controller gain to the PID (or, in this case PD) controller matching the linear coefficients obtained in Section 3.1.

Figure 4.30 shows the positions of the ship in the two scenarios. From this it seems that the linear mooring (blue) might have some more stiffness since it is lagging less behind in surge compared to the FEM (green). In sway it is hard to determine anything since it is so small loads anyway.

The force plots (Figure 4.31) show a greater degree of similarity. They are oscillating a bit differently (which is not unexpected since there is some randomness involved), but seem to stay around the same values.

The force plots being similar is however not surprising since this is the force amount required to pull the ship through this particular ice field. The fact that one mooring system has to stretch further in order to create that amount of force is the part of interest.

This shows that the linear mooring system behaves similar to the FEM mooring, but they are not equal.

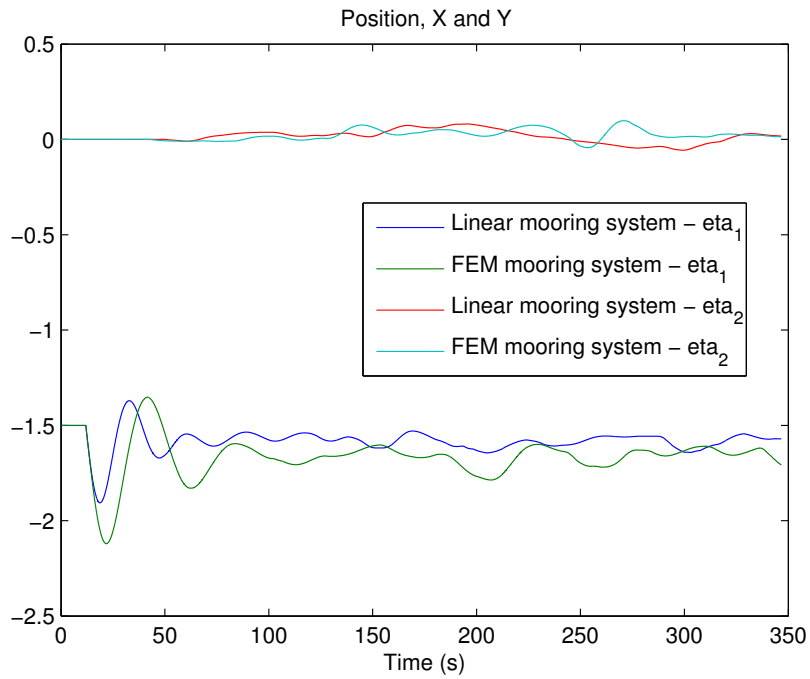

Figure 4.30: Positions comparison (Scenario 7) with scenario 1, comparing FEM mooring only with linear approximation mooring only.

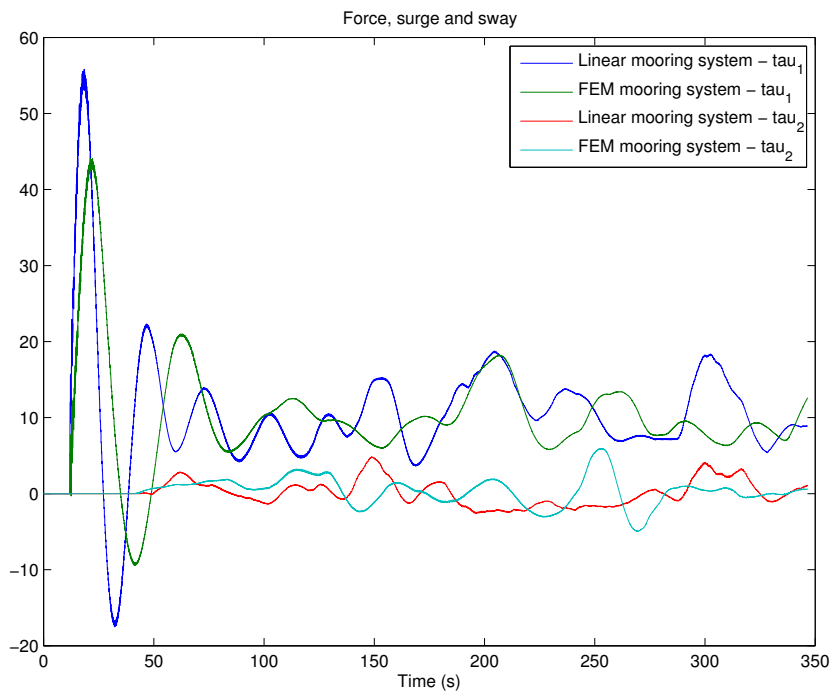

Figure 4.31: Force comparison (Scenario 7) with scenario 1, comparing FEM mooring only with linear approximation mooring only.

Chapter 5

Conclusion

Designing a mooring system based on a C program code, incorporated into a Simulink s-function, initialized with a Matlab script and then used to generate C++ code to work in a simulator seems link a process with a sufficient amount of potential failures. Still it turned out to be an achievable task, however still with a decent portion of debugging hours. Some of the major challenge with getting this many different technologies work together is that the error messages have a good variety of possible places to show up.

The mooring system is probably too weakly dimensioned. I got to know a bit too late to do something about it, that a mooring system for this kind of vessel in sea ice could have around 12-16 mooring lines, 1 000 to 1 500 meters long for the full scale 200 meters depth. This system would have been significantly stiffer than the system used here. However, this still shows that the modelling approach works, and this system can easily be adapted to the right size. Since mooring system design was not in the scope of this thesis, it will be left until later.

Apart from that the FEM mooring seems to perform satisfactory, giving reasonable force outputs. It seemed to have some high frequency disturbances, but these are not dominating when connecting the system with the NIT.

The setpoint generator performance was easier to identify when creating test scenarios in Simulink than when using it for setpoint chasing with the NIT simulator. It still made an improvement on the position recordings, it might however have been more clear if the simulation had been allowed to run for longer, due to the maybe a bit too high time constants in the setpoint generator. It would also have been nice to be able to run the entire setpoint generator within the NIT, and not each part separately.

The controller gains could probably also have been tuned up. From observing the force plots, they are having a lot left before the Arctic Drillship maximum

model scale thrust of 201 N. It is important to remember that these forces are including the mooring, but that should in most cases mean that the thrusters have even more to spare. In other words it is probably feasible having even smaller position offsets than what was happening in these simulations.

The testing of the linearized model has shown that it works as an approximation, but it has some clear differences from the FEM mooring system. The most obvious difference is the ability of the FEM to model motions traveling up and down the mooring lines, while the linear model will only treat it as a static system. This ability is likely to be extra important to model when operating in ice, since the sudden changes in ice loads may send significant wave motions down the mooring lines.

5.1 Recommendations for Further Work

One major limitation of this work has been that there has not been used much time on dimensioning the mooring system or the simulation scenarios to real life values. It has been tried to choose values as realistically as possible, given the amount of information available. Therefore, using some time to design a proper mooring system and run these through some realistic simulation scenarios should make it possible to achieve good results that can be applied to real life systems.

There is also still a number of improvements to do regarding the user friendliness of the simulator in terms of parameter settings and measurement readings. The parameters are now set in both the XML file, the C++ simulator code, the Matlab s-function initialization script and in different levels of the Simulink model. It should be possible to define all these from an input file, like the XML file.

The time steps should be included in this. If possible it would be good to only need to define the time step at one place. Now it is defines both in the mooring model, in Simulink and in the NIT.

Also, the forces from the mooring and the controller are now combined before sent to the simulator, meaning they can not be plotted separately. The mooring force should therefore be fed back separately.

Since the setpoint limiter does only work inside Simulink and not in the simulator, this is also something to investigate.

In order to get a better idea of whether the ship is able to handle the commanded thrusts, there should be implemented a thruster model with thrust allocation for the Arctic Drillship.

In short, to summarize:

- Perform a complete mooring system design
- Gather all parameters and settings at one place
- Feed back forces separately from the controller and mooring
- Get the setpoint chasing fully working within the simulator
- Make a thruster model with thrust allocation

Bibliography

Aamo, O.M., 1999. Adding Mooring Systems to the ABB Integrated Vessel Simulator Governing Equations. Technical Report. Department of Engineering Cybernetics, NTNU.

Aamo, O.M., Fossen, T.I. (Eds.), 2001. Finite Element Modelling of Moored Vessels, Mathematical and Computer Modelling of Dynamical Systems.

Balchen, J.G., Andresen, T., Foss, B.A., 2003. Reguleringsteknikk. 5 ed., Institutt for Teknisk Kybernetikk, NTNU.

Bushuyev, A., . Sea Ice Nomenclature. 1.0 ed. WMO.

Chen, C.T., 1999. Linear System Theory and Design. 3 ed., Oxford.

Deter, D., Doelling, W., Lembke-Jene, L., Wegener, A., 2009. Stationkeeping in solid drift ice, in: Dynamic Positioning Conference. Houston, TX: Marine Technology Society.

Faltinsen, O.M., 1990. Sea Loads on Ships and Offshore Structures. Cambridge.

Faÿ, H., 1990. Dynamic Positioning Systems. Éditions Technip.

Fossen, T.I., 2002. Marine Control Systems. Marine Cybernetics.

Fossen, T.I., 2011. Handbook of Marine Craft Hydrodynamics and Motion Control. Wiley.

Gjessing, I.A., 2014. Simulation of a Thruster-Assisted Position-Moored Vessel in Sea-Ice. Project thesis. Norwegian University of Science and Technology.

Gürtner, A., Baardson, B.H.H., Kaasa, G.O., Lundin, E., 2012. Aspects of importance related to arctic dp operations, in: Proceedings of the ASME 2012 31st International Conference on Ocean, Offshore and Arctic Engineering, OMAE2012.

Hals, T., Efraimsson, F., 2011. Dp ice model test of arctic drillship, in: Dynamic Positioning Conference. Houston, TX: Marine Technology Society.

Hals, T., Jenssen, N.A., 2012. Dp ice model test of arctic drillship and polar research vessel, in: OMAE2012, ASME 2012 31st International Conference on Ocean, Offshore and Arctic Engineering. Rio de Janeiro, Brazil: ASMEy.

International Organization for Standardization, 2010. ISO/FDIS 19906:2010(E): Petroleum and natural gas industries Arctic offshore structures. International standard. International Organization for Standardization.

Keinonen, A., Wells, H., Dunderdale, P., Pilkington, R., Miller, G., Brovin, A., 2000. Dynamic positioning operation in ice, offshore sakhalin, mayjune 1999, in: ISOPE-2000, 10th (2000) International Offshore and Polar Engineering Conference, pp. 683–90.

Keinonen, A.J., Shirley, M., Liljestrm, G., Pilkington, R., 2006. Transit and stationary coring operations in the central polar pack .

Kerkeni, S., Jochmann, P., Metrikin, I., Løset, S., 2013a. Experimental and numerical investigation of dynamic positioning in level ice, in: Proceedings of the ASME 2013 32nd International Conference on Ocean, Offshore and Arctic Engineering.

Kerkeni, S., Santo, X.D., Doucy, O., Jochmann, P., Haase, A., Metrikin, I., Løset, S., Jenssen, N.A., Hals, T., Grtner, A., Moslet, P.O., Støle-Hentschel, S., 2014. Dypic project: Technological and scientific progress opening new perspectives, in: OTC Arctic Technology Conference, 10-12 February, Houston, Texas, Offshore Technology Conference.

Kerkeni, S., Santo, X.D., Metrikin, I., 2013b. Dynamic positioning in ice comparison of control laws in open water and ice, in: Proceedings of the ASME 2013 32st International Conference on Ocean, Offshore and Arctic Engineering OMAE2013.

Kjerstad, Ø.K., Metrikin, I., Løset, S., Skjetne, R., 2014. Experimental and phenomenological investigation of dynamic positioning in managed ice. Cold Regions Science and Technology .

Kjerstad, Ø.K., Skjetne, R., 2014a. Modeling and control for dynamic positioned marine vessels in drifting managed sea ice. Modeling, Identification and Control , 1–14.

Kjerstad, Ø.K., Skjetne, R., 2014b. A resetting observer for dynamic positioning of marine vessels subject to severe disturbances .

Lane, K., Power, D., Youden, J., Randell, C., Flett, D. (Eds.), 2004. Validation of Synthetic Aperture Radar for Iceberg Detection in Sea Ice.

Løset, S., . Station keeping in ice. Lecture notes / presentation.

Løset, S., Onshuus, D. (Eds.), 1999. Analysis of speeds of drift ice in the Pechora Sea.

McClintock, J., McKenna, R., Woodworth-Lynas, C., 2007. Grand Banks Iceberg Management. Technical Report. PERD/CHC.

Metrikin, I., 2014. A software framework for simulating stationkeeping of a vessel in discontinuous ice. Modeling, Identification and Control 35, 1–38.

Metrikin, I., Løset, S., Jenssen, N.A., Kerkeni, S., 2013. Numerical simulation of dynamic positioning in ice. Marine Technology Society Journal 47, 14–30.

Moran, K., Backman, J., Farrell, J.W., 2006. Deepwater drilling in the arctic oceans permanent sea ice, in: Proceedings of the Integrated Ocean Drilling Program.

Nguyen, D.T., Sørensen, A.J., 2007. Setpoint chasing for thruster-assisted position mooring, in: The 26th International Conference on Offshore Mechanics and Arctic Engineering.

Nguyen, D.T., Sørensen, A.J., 2009a. Setpoint chasing for thruster-assisted position mooring. IEEE Journal of Oceanic Engineering 34, 548–558.

Nguyen, D.T., Sørensen, A.J., 2009b. Switching control for thruster-assisted position mooring. Control Engineering Practice 17, 985–994.

Nguyen, D.T., Sørensen, A.J., Quek, S.T., 2007. Design of hybrid controller for dynamic positioning from calm to extreme sea conditions. Automatica 43, 768–785.

oil-price.net, 2015. Oil price. URL: `http://www.oil-price.net`.

Orsten, A., 2013. Reliability-based control for towing of icebergs in open water. Project thesis. Norwegian University of Science and Technology.

Skjetne, R., 2014a. Arctic dp: The arctic offshore project on stationkeeping in ice, in: The IBC Maritime Ice Class Vessels Conference.

Skjetne, R., 2014b. Literature Survey on Position Mooring Control Systems. Technical Report. Kongsberg Maritime AS.

Sørensen, A.J., 2012. Marine Control Systems. Lecture notes. Norwegian University of Science and Technology.

Standards Norway, 2007. NORSOK Standard N-003.

Steen, S., 2011. Motstand og Propulsjon - Propell- og Foilteori. Marin Teknikk 3, Kompendium. Institutt for Marin Teknikk, NTNU.

Strand, J., Sørensen, A., Fossen, T.I., 1998. Design of automatic thruster assisted mooring systems for ships. Modeling, Identification and Control 19, 61–75.

Teknisk Ukeblad, 2015. Stor tvil om barents-oljen blir lønnsom. URL: http://www.tu.no/petroleum/2015/01/21/stor-tvil-om-barents-oljen-blir-lonnsom.

Tipler, P.A., Mosca, G., 2008. Physics for Scientists and Engineers. 6 ed., Freeman.

Triantafyllou, M., Yue, D., Tein, D. (Eds.), 1994. Damping of Moored Floating Structures, Offshore Technology Conference.

Wikipedia, 2015. Ultimate tensile strength. URL: http://en.wikipedia.org/wiki/Ultimate_tensile_strength.

Appendix 1

The Single Turret Line Simulink Model

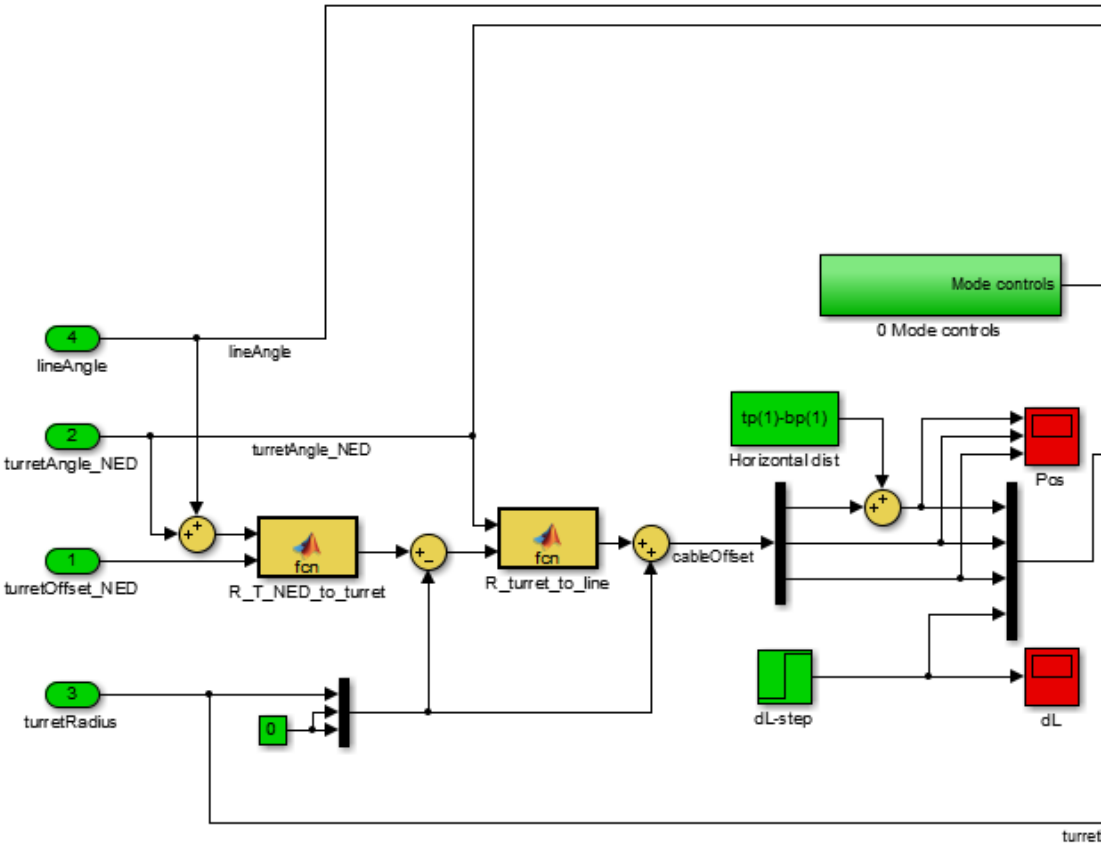

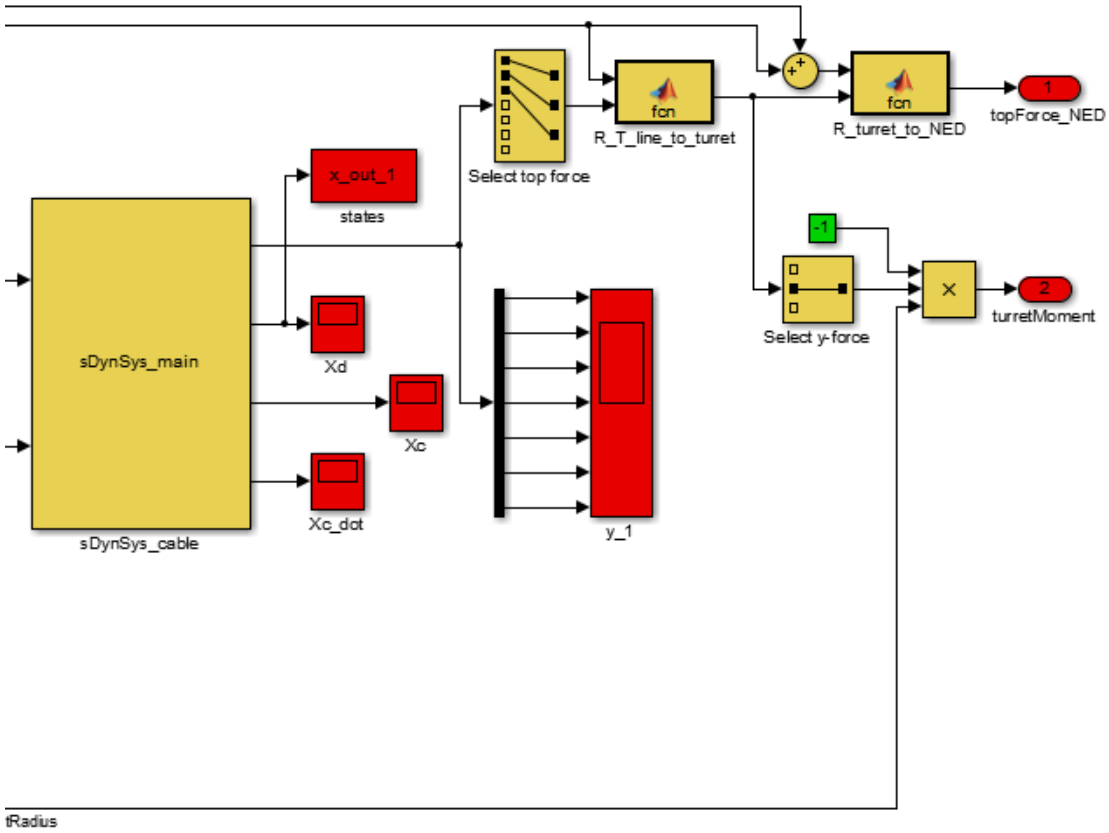
sDynSys_main
sDynSys_cable
x_out_1
states
Xd
Xc
Xc_dot
Select top force
fcn
R_T_line_to_turret
fcn
R_turret_to_NED
1
topForce_NED
-1
Select y-force
×
2
turretMoment
y_1
tRadius

Appendix 2

Changes made in the cable FEM model (cable.c)

- Line 621: The top force was fetched from `sn` (section after last section) instead of section `sn-1` (last section due to zero indexing). Changed `sn` to `sn-1`.
- Line 637-639: Removed minus sign from bottom forces output. The forces went in opposite direction from what is logical.
- Line 14 and 1012: Undefined `MATLAB_MEX_FILE` on top of the file and redefined it at the bottom, since it made problems for the compilation due to that the cable function is not run from Matlab but from sDynSys, so it does not use the MEX interface.

Appendix 3

Changes made in the s-function main code (sDynSys_main.c)

- Line 576, 714, 849 and 889: Changed `(real_T *)u1_U[0]` to `(real_T **)u1_U`, which solved the problem of not being able to fetch data from other than the first input port of the system.

Appendix 4

Known issues with the system

- Depending on the parameters of the mooring system in the mooring s-function model there is a upper limit for the number of elements in the cable sections. Exceeding this number will cause null-values in the calculations, resulting in missing force outputs and a very slow running simulation. This should be tested within Simulink before plugging the model into the controller of the numerical ice tank.
- The timesteps for the cable will for some values cause strange behavior like high-frequent noise or other random irregularities due to some numerical issues. Different timesteps should therefore be tried in order to see the effects of changing them, and finding the optimal values.
- For some reason the setpoint generator is not working in the NIT simulator when both the lowpass setpoint generator and the limiter are connected. One of them separately works, and the whole thing works in Simulink.